The Lease Polder

A parameter sensitivity analysis and feasibility study on the concept of the Lease Polder

D. M. Slagmoolen

Faculty of Civil Engineering
Hydraulic Engineering
October 2021

4392906

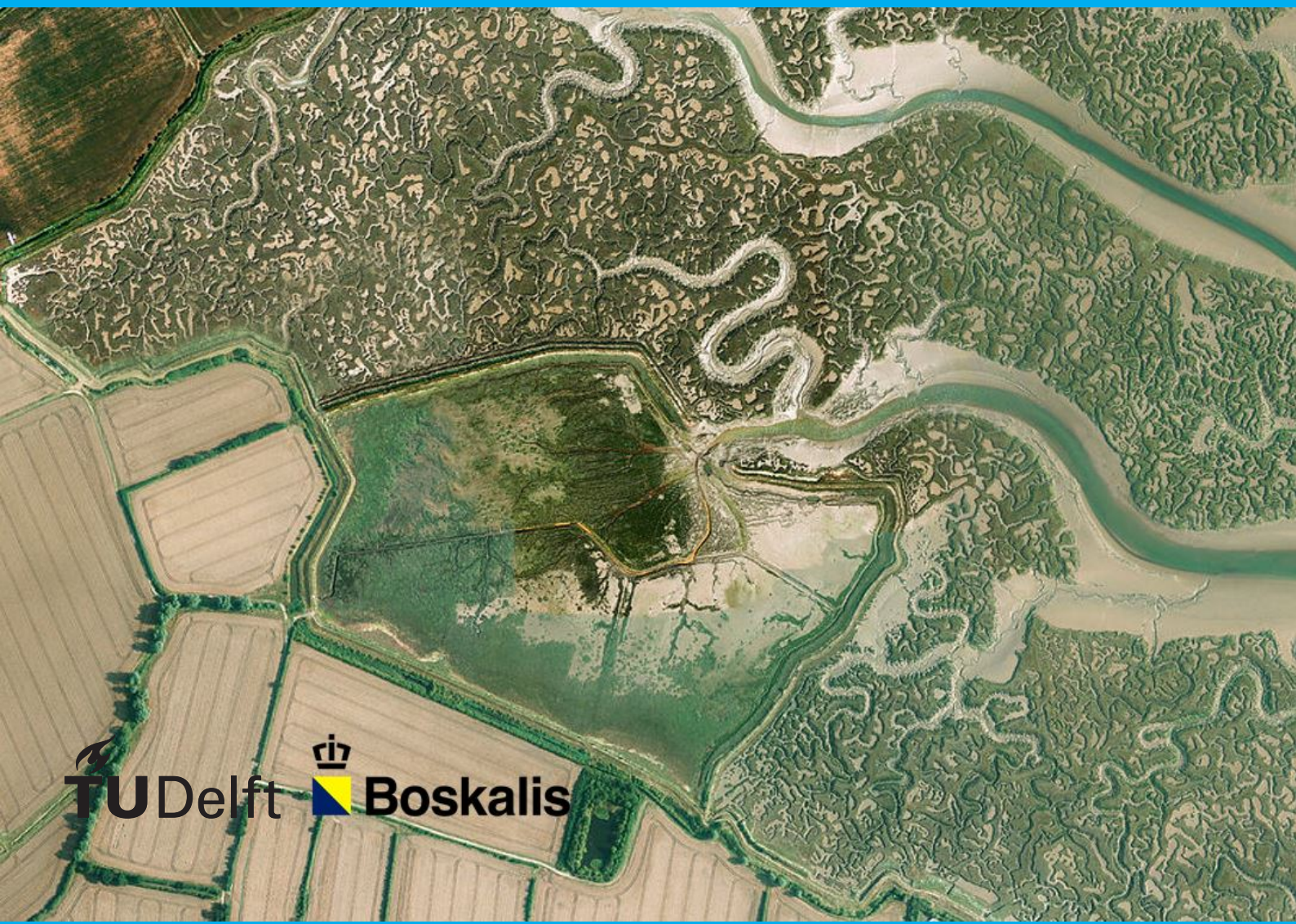

The Lease Polder

A parameter sensitivity analysis and feasibility study on the concept of the Lease Polder

by

D. M. Slagmoolen

To obtain the degree of Master of Science
at the Delft University of Technology,
to be defended publicly on Wednesday October 27, 2021 at 14:30 AM.

Student number:	4392906	
Project duration:	December 1, 2020 – October 27, 2021	
Thesis committee:	Prof. Dr. Ir. S.G.J. Aarninkhof,	TU Delft, supervisor
	Ir. G. G. Hendrickx,	TU Delft
	Dr. ir. M. Klein,	Royal Boskalis Westminster N.V.
	Dr. ir. B.C. van Prooijen,	TU Delft

An electronic version of this thesis is available at `http://repository.tudelft.nl`.

TU Delft Boskalis

Abstract

Ongoing sea level rise combined with significant levels of land subsidence cause the everlasting need for reinforcements of the current coastal protection measures to ensure a certain level of coastal safety. Developing countries in the Asian regions tend to suffer from even more severe levels of land subsidence and often lack the financial resources to fulfil these continuing needs for reinforcements, which put the coastal areas under the continuous tread for potential flood disasters. The Lease Polder is a new Building with Nature approach for the sustainable design of protective coastlines and can offer a durable solution to this current problem. The concept is built upon the principle of sharing a part of the land with the hydraulic system and thereby allowing the natural vertical growth of the area by siltation during in- and outgoing tide. The concept is, however, still in its infancy, causing numerous uncertainties regarding the feasibility. The critical design parameter that effects the feasibility is the Lease Polder period, denoting the duration for which the breach of the Lease Polder is kept open. This study aims to offer a quick assessment tool that can determine the optimal Lease Polder period and perform a feasibility analysis for arbitrary Lease Polder cases, based on a sensitivity analysis of influential parameters on the potential siltation process.

A simplified 2DH process-based Delft3D model was used to perform a sensitivity analysis on multiple sediment characteristics, hydraulic boundaries and dimensional parameters. The parameter sensitivity was determined by comparing the results from a set of parameter scenarios to a base-case model. This base-case model was a simplified version of the Tollesbury realignment site and was calibrated and validated on the available historical data sets. The base-case model was simplified to a square $430m$ by $430m$ basin area with a near-horizontal initial bed level $1m$ above average sea level and a $50m$ wide breach. The foreshore was assumed to be alongshore uniform with an offshore tidal boundary condition and an assigned level of suspended sediment concentration. A wave module was coupled to the flow module to include a constant input of wave forces.
Processing the results consisted of exponential curve fitting through the average change in bed level of each scenario, followed by the determination of the initial sedimentation rate and the average equilibrium bed level. These two characteristics were then transformed into parameter specific functions describing the dimensionless dependency for a given parameter value relative to the base-case scenario. A quick assessment tool called the WisLi-tool was created to predict the sedimentation curve for arbitrary Lease Polder cases, based on these parameter specific functions. It thereafter uses this curve to perform a cost-benefit analysis on the complete life cycle of a Lease Polder, resulting in a quantitative net profit or loss. Finally, the tool will enter an optimization process by determining the optimal Lease Polder period which results in the maximum financial benefit.

The simplified model based on the Tollesbury was able to accurately reproduce the morphological changes which followed from the historical data analysis. A summary of the sensitivity of the most significant parameters is listed below.
Suspended sediment concentration The suspended sediment concentration (SSC) at the boundary showed a positive linear relationship with the initial rate of sedimentation, where the increase in SSC was directly proportional to the increase in initial sedimentation rate. The average equilibrium bed level was however independent of the SSC.
Breach width The breach width showed to have a negative relationship for both the initial rate of sedimentation and the average equilibrium depth.
Polder length and width The dimensional length and width of the polder showed to have an insignificant effect on the initial sedimentation rate, with differences remaining within the 10% range. The average equilibrium bed decreased for increasing polder length and width.
Initial polder bed level The sensitivity analysis on the initial polder bed level showed a dichotomy into two regimes, where the 'shallow regime' was coherent to initial bed levels between $OD+1.0m$ and $OD-1.5m$ and the 'deep regime' to the bed levels between $OD-2.0m$ and $OD-4.0m$. The deep regime was characterized by the abrupt stop in sedimentation due to the high levels of wave energy entering the polder. Both regimes showed decreasing levels of initial sedimentation rate and average equilibrium bed level for increasing initial

polder bed levels.
Tidal amplitude The tidal amplitude showed to have a positive relationship with the initial sedimentation rate and the average equilibrium bed level for tidal amplitudes of 2.5m and lower. Higher tidal amplitudes caused high-velocity circular flow patterns within the polder, preventing further siltation.
The above-mentioned relationships were translated into functions describing the dimensionless dependency for a given parameter value relative to the base-case scenario.

The analysis on the effect of sea level rise on the sedimentation process of a Lease Polder concluded that the siltation process was able to produce a local bed level change following the exact rate of sea level rise, for an average rate of sea level rise of 4.2$mm/year$. The Lease Polder can, therefore, be seen as a partly self-sustaining system of coastal defence.
The quick assessment WisLi-tool was able to accurately predict the sedimentation curve based on case-specific input parameters using the dimensionless functions derived from the sensitivity analysis. By utilizing location-dependent financial input parameters, the tool was capable of performing an optimization process for the determination of the optimal Lease Polder period.

The final conclusion is that there is not a single uniform optimal duration for the Lease Polder period but that it may vary for each individual Lease Polder case. However, the WisLi-tool was able to assess arbitrary Lease Polder cases based on their parameter values and could determine the case-specific optimal duration of the Lease Polder period. Therefore, the WisLi-tool can act as a valuable resource during both the design and operational phases.

Preface

With the hard effort that was put into this thesis, I am officially completing my MSc degree in Hydraulic Engineering at the Delft University of Technology. The study was performed in collaboration with Royal Boskalis Westminster NV, a leading company in the world of dredging and marine engineering. During this period, I did research on a new Building with Nature concept called the Lease Polder, which introduced me to the world of numerical modelling.

I would like to grand special thanks to Boskalis for offering me the opportunity to do my thesis at the Hydronamic department at their office in Papendrecht and for providing the required tools for the model computations.

During the course of my thesis, Gijs Hendrickx has been of great value for me by guiding me through the whole process of my research. Despite the strange times during Covid-19, he was always there to have an online discussion and advise on certain project decisions. His enthusiasm for the profession of hydraulic engineering. I want to thank Mark Klein for introducing me to the department within Boskalis and for his excellent eye for detail. In combination with his expertise in numerical modelling, he was able to give valuable insights within the model and with showing the tricks of the trade of report writing. A special thanks to the chair of my committee, Stefan Aarninkhof, for first of all introducing me to the subject and for bringing me in contact with Boskalis. Your quality of pointing out the importance of certain subjects and the ability to ask critical questions helped me with following the right directions. Thank you Bram van Prooijen for helping with the physical derivation and for joining as the last member of the committee. Thanks to the whole Hydronamic team for showing me the good atmosphere at the office and a special thanks to Huub Rijper and Tim van der Biezen for helping along with the modelling questions. A final thanks to Thomas Vijverberg for overseeing the process. I am very grateful for sharing all your time and knowledge and I am extremely proud to share my dissertation with all of you.

D. M. Slagmoolen
Delft, October 2021

Contents

List of Figures

List of Tables

1 Introduction

1.1. Context

In recent centuries, the construction of dikes, dunes and revetments have been the main means of protecting coastal areas against flooding. Not only coastal areas but also estuarine areas have become highly valued land due to the attraction of industry and residential communities. Living and building along coastlines and estuaries provide great opportunities for economic growth due to the possibility of making a marine connection to other parts of the world through harbours and inland waterways (Crowell et al. 2007). Besides this advantage, it also offers a strong recreational factor for both residents and tourists (Ghermandi and Nunes 2013). However, this is not entirely without risk. Ongoing sea level rise and more extreme weather conditions, which are linked to recent climate change, continue to cause havoc on coastal lands (Camhis and Coccossis 1984). Countries like the Netherlands have become the precursor in counteracting these changes. They are able to ensure coastal protection with the help of sea dikes, revetments and other forms of coastal protection, whilst more than half of its land lays below mean sea level (Olsthoorn et al. 2008). In order to ensure low levels of risk with ongoing sea level rise, a high level of safety and regular inspection are mandatory, where reinforcements are often needed. In many cases, these reinforcements can become quite costly (Fu and Song 2017).

Not all coastal areas have the same resources to fulfil these needs of reinforcements. For example, coastal areas in the Asian region have to contend with sometimes much larger forms of subsidence as is shown by the map in figure 1.1 (Kaneko and Toyota 2011). In combination with far fewer resources to counter these problems, this leads to a future threat of ensuring coastal safety. A shortfall of financial resources being one of them. The budget of the Dutch Delta plans per meter of coastline is often a multiple of that from Asian regions (Wong 1998, Robert John Nicholls et al. 2019). Next to that, there is another shortcoming, which is sand. Some areas suffer from severe sand shortages, which causes the construction of soft reinforcements or reclamations not to be the most feasible solution and sometimes even unattainable (Charlier 2002).

The aforementioned cases are longing for a sustainable solution in order to bypass these obstacles. This is where the Lease Polder can be of service. The Lease Polder is a new concept that represents a specific elaboration of the principle of tidal restoration. It is a form of Building with Nature (BwN), where the forces of nature are harnessed to benefit the environment, economy and society, in order to create a new approach to hydraulic engineering (De Vriend and Van Koningsveld 2012). Tidal restoration is a form of alternative coastal defence that makes use of natural tidal dynamics and associated morphological processes. Low-lying, settled areas within a dike area are "given back" to nature so that tidal processes can take their natural course. These processes can lead to cyclic siltation and thereupon result in soil elevation. In addition to coastal defence, the concept offers opportunities for nature development and recreation, and possibly also opportunities for developing an economically profitable form of aquaculture (Belzen 2021).

The detail that sets a Lease Polder apart from regular tidal restoration (often called managed retreat) is the cyclic process after a certain level of ground elevation is reached. From that point on, the breach in the main dike will be closed so that the depoldered area can be used again for e.g. agriculture or eco-space. After a few decades, the ground will have subsided again and, together with the persistent relative sea level rise, will

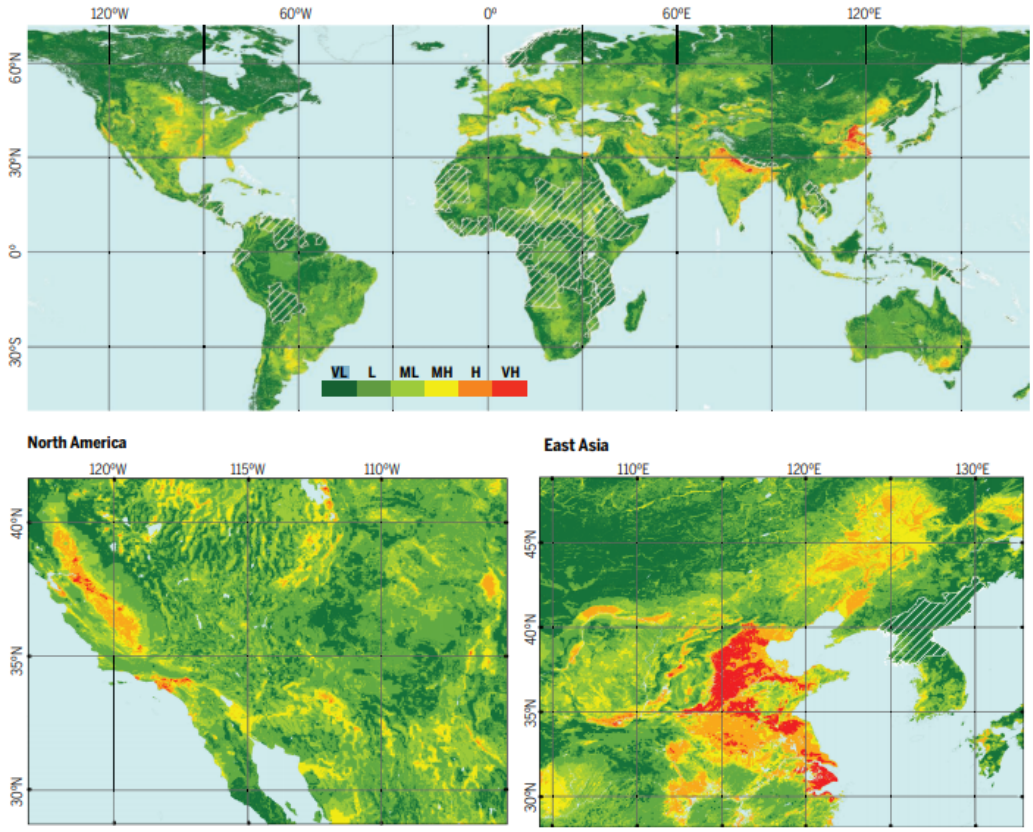

Figure 1.1: Map of global potential land subsidence. The color map indicates the probability of future land subsidence from VL (Very Low) to VH (Very High). Including two focused maps of the Northern American region and the East Asian region (Herrera-Garcıa et al. 2021).

lead to a demand for strengthening coastal protection. The cycle of the Lease Polder has now been completed and the process can repeat itself. The rate of sedimentation is therefore one of the most important properties of a Lease Polder that determines the cycle time of a Lease Polder, and therefore the rate of increasing coastal protection. The idea is that the two states of tidal restoration and normal land usage can be altered in a checkerboard pattern along an estuary. This way, the concept gives substance to a climate-proof space development along estuaries and aims to enhance spatial quality by linking both coastal protection and economical land usage, creating a sustainable win-win situation (Schelling, Steeg, and Leopold 2014).

1.2. Problem statement

Various regions within Asia, for example Jakarta and Manila, are heavily affected by land subsidence and relative sea level rise. Current coastal protection measures cannot meet these prospects and sand scarcity prevails, preventing direct reinforcements from being an economically favorable solution for a multitude of those areas. The Lease Polder can be a nature-based solution to counteract this problem in a sustainable manner. However, the absence of a clear, quantitative understanding of the effects of different parameters on the sedimentation rates within a Lease Polder makes it difficult to perform a proper feasibility study for Asian regions.

Pilot projects with the Lease Polder have been performed alongside the Dutch coast, the coast of Britain and the German coast, which seem to show favorable results in terms of sedimentation rates and enhancement of coastal protection. Examples of these projects are the Sieperdaschor(NL), Peazammerlannen (NL) and the Tollesbury retreat (UK), with most of them being only opened as a managed retreat. Nevertheless, hydraulic and environmental boundary conditions can differ significantly from the prior pilot cases. In addition, a number of concepts exist that can possibly enhance the sediment catchment rate of the Lease Polder, which lack practical proof of concept. Examples of these sediment enhancement concepts are the application of

tidal retention and sediment injection. Attaining a better understanding of these influential parameters and enhancement concepts are essential for evaluating the feasibility.

1.3. Research question and objectives

In response to the problem statement, a research question is formulated. The main objective is to determine the sensitivity of different drivers and parameters on sediment accretion within a Lease Polder. Furthermore, the question was raised whether certain modifications to a Lease Polder could result in higher sedimentation rates and thus making the Building with Nature concept economically more attractive. With the results from this main objective, an insightful cost-benefit analysis could be drawn, which would eventually lead to the requirements of a viable project. It is therefore needed to deduce the extent to which a Lease Polder is capable of increasing coastal protection. Besides a protective measure, a Lease Polder can have supplementary values from both a cultural and an ecological perspective, by offering protected natural habitat. The complete objective is described by the following research question:

How can a sensitivity analysis of influential Lease Polder parameters on the siltation rate improve the design feasibility for arbitrary Lease Polder cases.

In pursuance of obtaining a comprehensive answer, a set of sub-questions is formulated and listed below.

- What type of numerical modelling can simulate siltation processes observed in former Lease Polder cases?
- How can such a model help with the determination of the sensitivity of different parameters on the rate of siltation within the polder?
- To which extent can the siltation in a Lease Polder counteract the impact of a certain rate of sea level rise on coastal protection?
- To what degree can the parameter sensitivity be utilized to predict siltation rates for arbitrary Lease Polder cases with the help of a quick assessment tool?
- What are the main design parameters and how can these design parameters be improved to optimize the efficiency of a Lease Polder by enhancing the sedimentation rate?

The aim of the study is to asses the parameter sensitivity on polder siltation by creating a simplified numerical model in Delft3D based on an existing Lease Polder case, which can simulate the main hydrodynamic processes in order to reproduce similar sedimentation rates within the Lease Polder. After these processes are validated, numerous scenarios will be created to identify the effect and sensitivity of each individual parameter or boundary condition.

1.4. Research approach

To ensure a structured approach, the study follows a four-phase setup. In the first phase of the study the focus is on the currently existing literature around Lease Polders, as well as the research documents and literature around the former and ongoing pilot projects. Results of these research documents are compared to obtain a broader understanding of the empirical and scientific correlations between parameters and sedimentation rates.

The second phase of the study is focused on the development of a Delft3D Lease Polder model and the validation of this model. This model is used as a base-case model for the comparison of different scenario models. In preparation for this, a pilot case has to be found on which the simplified numerical model can be based upon. This pilot case ideally has an extensive collection of measurements and datasets in order to validate the numerical model. The pilot case that is used during this study is the Tollesbury realignment site in the UK.

When the numerical base-case model is validated, phase three of the study is entered. The main objective of this phase is the determination of the sensitivity and the effects of a set of influential parameters and

boundary conditions on sedimentation rates. All these parameters and boundary conditions are evaluated separately in different scenarios. This phase will also be dedicated to the ascertainment of the effect of enhancement concepts on sedimentation rates.

The fourth and final phase is dedicated to the feasibility study of the Lease Polder concept. Here, the results from the third phase are used to create a tool that can shape a rough indication of sedimentation rates for individual cases. These sedimentation rates, as mentioned earlier, are on their own the main indicator for the feasibility of the Lease Polder. The tool will help with a quick assessment on the improvement of the main design parameters in order to optimize the feasibility of a Lease Polder project in an early phase of the design process.

1.5. Thesis outline

As was discussed in the previous section, this research document will be following the four phases that were used as guidelines throughout the report. The first phase of the research can be entered following the brief introduction on the Lease Polder topic and the research approach that were discussed in Chapter 1. Chapter 2 will be devoted to this first phase by establishing a theoretical base originating from former literature. The second phase, where the case study on the base-case scenario in Tollesbury is performed and summarized, will be discussed in Chapter 3. Chapter 4 will be dedicated to the first part of the third phase, where the complete model setup and calibration and validation of the base-case model will be evaluated and the setup for for the different parameter scenarios will be discussed. The results of the individual parameter scenarios, which consist of the second part of the third phase, will be assessed in Chapter 5. Chapter 6 will be completely dedicated to the fourth and final phase of the study where the feasibility analysis will be performed and the quick-assessment tool will be elaborated. The final discussion on the method and the results will be touched upon in Chapter 8, after which the conclusion and recommendations will follow in the last chapter, Chapter 8. A schematized stream diagram of the various study phases is displayed by figure 1.2.

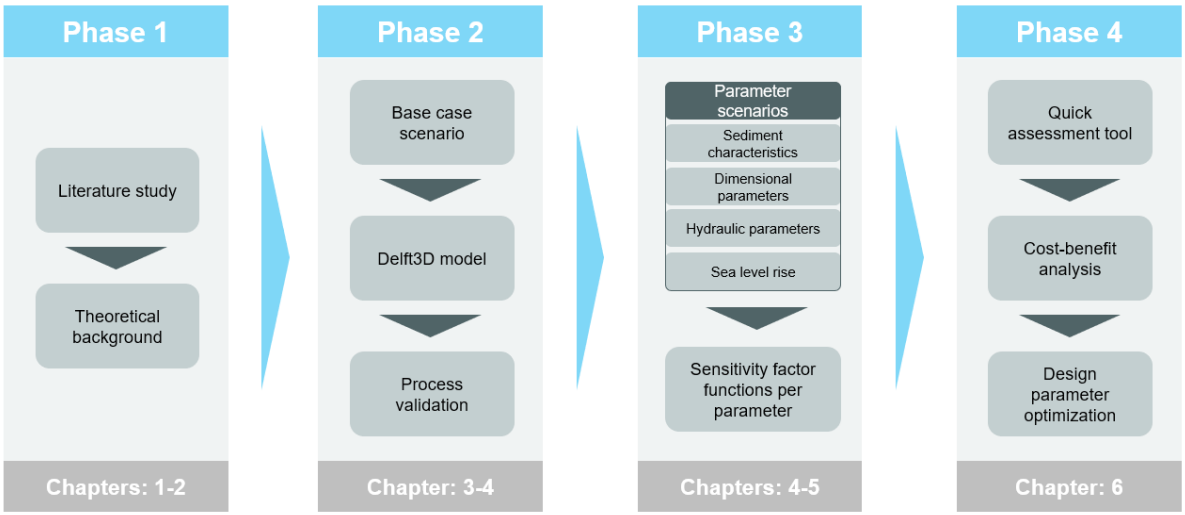

Figure 1.2: Stream diagram of the various study phases with their accompanying chapters

2

Theoretical background of the Lease Polder

This chapter provides a comprehensive description of the concept of the Lease Polder based on the existing literature. First, the motivation behind the usage of a Lease Polder in certain areas will be explained in Section 2.1. The process of sedimentation and how this can benefit the coastline and enhance coastal protection will be discussed in more detail in Subsection 2.1.3. In order to answer the main research question, one needs to have a proper understanding of the main hydraulic and morphological processes that take place in a Lease Polder and how these develop under various circumstances. In an effort to predict the scale of sedimentation and give a broad estimation of sedimentation rates for separate cases, a selection of parameters must be made that are expected to have an effect on sedimentation rates within the polder. This selection will be based on the theoretical background found in existing literature and is discussed in Section 2.2.

2.1. The Lease Polder

Global population demographics are continuously changing, as well as the spatial planning of residential areas. In the past two centuries, the total world population has risen from 1 billion to 7.7 billion people (Khan, Hou, and Le 2021, Roser, Ritchie, and Ortiz-Ospina 2013). Population densification and urbanization is a process that is expected to continue till in the far future (Simon 2019), with some areas being more favorable for growth than others. Coastal areas have been shown to experience accelerated rates of population density growth in comparison to inland regions (Small and Robert J Nicholls 2003). Asian countries like Bangladesh and China have shown a factor larger than two in population growth in low lying coastal areas in the past decade in comparison to national population growth (McGranahan, Balk, and Anderson 2007). This trend in coastal migration is mainly caused by the favorable economic growth potentials of regions connected to water (Neumann et al. 2015). Not only coastal areas but also estuarine areas have become highly valued land due to the attraction of industry and residential communities. The possibilities of making a marine connection to other parts of the world by means of harbours and inland waterways have provided living and building along coastlines and estuaries with great opportunities for economical growth (Henderson, Storeygard, and Weil 2011). Next to that, it also offers a strong recreational factor for both residents and tourists (Wong 1993).

This ongoing trend of increase in coastal urbanisation also brings some significant inconveniences. Global climate change has shown that living in coastal areas can be a high-risk choice, considering its vulnerability to marine hazards (Robert J Nicholls, Wong, et al. 2007). Examples of coastal erosion, flooding and saltwater intrusion have been shown to severely impact coastal environments (Robert J Nicholls and Cazenave 2010). Furthermore, tsunamis and storm surges can have even more devastating consequences, causing extreme forms of economical damages and high levels of causalities (Kanoğlu et al. 2015). For this reason, there is an ever-increasing demand for better coastal protection. Most of the coastal regions are protected by some form of coastal barrier, ranging from a dam of wooden sticks to complete breakwaters and dikes (Dillenburg and Hesp 2009) (Masria, Iskander, and Negm 2015). These types of coastal protection are nearly always a static form of protection. Ongoing effects of sea level rise will therefore cause a continuous increase in dimensional requirements. High costs are associated with these reinforcements of dykes and their further maintenance, which often cannot be realized by less developed countries in for example Asia (Sovacool et al. 2012).

Several recent studies from for example Ecoshape have suggested that flood defences based on ecosystem-based solutions (Building with Nature or Nature-Based Solutions) could offer an interesting opportunity to develop more robust safety systems. The Building with Nature approach can provide a solution to the problems faced by conventional dikes due to ongoing sea level rise, without compromising the level of coastal safety. The philosophy of building with nature is based on the principle of using the forces of nature, instead of counteracting them, in order to create a sustainable system that can gradually follow the changes in sea level, whilst also adding socio-economic functions and ecosystem services (Van Slobbe et al. 2013). New types of coastal defence based on a building with nature approach ("Innovative Dike Concepts") are seen as a possible measure for optimizing the current safety strategy, the Lease Polder being one of them (Schelling, Steeg, and Leopold 2014). The following sections will analyse and asses the exact processes within the Lease Polder based on the existing literature.

2.1.1. Concept explanation

A Lease Polder is a form of tidal wetland enclosed within a system of double dikes, meaning that there is both a dike at the front of the wetland in between the sea and the tidal wetland (primary dike) and one at the back dividing the wetland and the hinterland (secondary dike). The key principle behind the Lease Polder is the process of sediment catchment, which naturally raises the bed level of the tidal wetland. The tidal wetland in between the two dikes is what from now on will be called the 'polder'. A breach will be made in the primary dike in order to connect the polder in between the two dikes with the sea or estuary making it a tidal wetland. The complete anatomy of a Lease Polder is shown by figure 2.1. Water from the estuary or sea can now flow freely in and out of the polder during each tidal cycle. By replacing the conventional single dike with this double dike system, a coastal protection strip is created instead of a single line of defence. During storm conditions, this double dike system ensures that the height of the two individual dikes can be lower than the single dike in case of a conventional solution, due to a reduction in wave energy on the tidal wetland, known as wave dissipation (will be further elaborated in section 2.1.3 'Coastal safety').

During conventional conditions, wave dissipation is occurring as well, only on a lower scale. When wave energy is dissipated, suspended sediments in the water column will be allowed to settle inside the polder, slowly increasing the bed level in the polder. The bed level will keep on rising in the coming years or decades until a certain state of bed elevation is reached, after which the breach can be closed again. This specific state of bed elevation can either be depended on the required level of coastal safety, or on the rate of sedimentation, which is expected to decrease over time. The land can now be rehabilitated as agricultural land. The complete description of this cycle will be given in the next section.

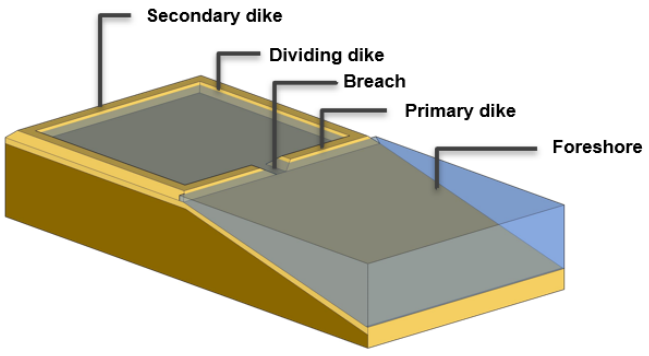

Figure 2.1: The anatomy of a Lease Polder

2.1.2. Life-cycle of a Lease Polder

The complete life-cycle of the Lease Polder can be separated in the initiation phase and in the cycling phase. The initiation phase is the period from which the decision is made for the construction of a Lease Polder until the moment that the breach is made in the primary dike (phase 1). From that moment the cycling phase is entered which will be repeated indefinitely (phase 2, phase 3 and phase 4). The name 'Lease Polder' originates from the fact that the polder is not permanently enclosed, but is shared with the estuary on a cycling basis.

The life cycle of a Lease Polder is schematized by figure 2.2. These four phases are further elaborated on below.

Phase 1 The initiation phase starts with the decision to implement a Lease Polder for a predetermined stretch of coastline. This coastline can either separate a sea, an ocean or estuaries from the mainland, called the hinterland. In the period prior to the initiation phase, that land could be either used for agricultural purposes, natural areas or minor residential areas. During that period, the land has continuously subsided due to bottom settling whilst the sea level continued to rise. When these timelines of land subsidence and sea level rise are extrapolated, it can be noted that current protection measures will not meet the safety requirements in the near future without extra reinforcements. At this point, the agreement can be made to transform the single line dike defence into a Lease Polder. The considerations that determine whether the construction of a Lease Polder is economically more favorable than regular dike reinforcements will be further elaborated on in the feasibility study in Chapter 6. As already stated, the main physical components of a Lease Polder consist of the following three parts: the primary dike, the polder area and the secondary dike. Usually, the primary dike is already in existence. However, the secondary dike is not always present. The Netherlands is known for having a large quantity of these secondary dikes already in the preexistence, called 'slaperdijken' (Huitema 1947). Possible locations for the construction of a Lease Polder are more favorable when such secondary dikes are already present due to lower investment costs, but not mandatory since the cost of the construction of a smaller secondary dike can be lower than initial reinforcements of the primary dike in the long-term (Belzen 2021). Next to these main components, divisional dikes are needed perpendicular to the coastline to separate one Lease Polder from the other. Now a fully enclosed polder is established, primed for implementation as a Lease Polder.

Phase 2 This phase is the beginning of the cycle phase. With the purpose of connecting the polder to the water body, a breach is made in the primary dike of the Lease Polder. Water will now flow freely into the polder as high tide comes and will flow out of the polder with low tide going out. The bottom surface will be relatively low in the beginning phase, making the inundation time comparatively long. No aquaculture lifeforms are established yet in this initiation phase of the Lease Polder cycle, but the habitats are made favorable. The water from the water body has a relatively high amount of sediment in suspension due to higher levels of wave energy, hydraulic currents and sediment supply from nearby rivers (Oevelen et al. 2000). These hydraulic forces diminish when the water enters the polder, causing the suspended sediment to settle inside the polder making the bed level rise over time.

Phase 3 The polder will continue to stay hydraulically connected to the water for an indefinite period of time so that the tidal current continues to flow in and out of the polder. The bed level continues to rise as the process of sedimentation inside the polder advances. Tidal channels start to form on the inside and on the outside of the polder (Oevelen et al. 2000). Over time, a tidal wetland is formed providing a favorable habitat for ecological growth and aquaculture. As the bed level keeps rising, the rate of the rise in bed level diminishes. At a specific point, not all of the polder will be inundated with each tide due to the higher bed level. The rate of sedimentation and thus the rate of bed level rise is far from optimal at that point and the system seems to reach for a sort of morphological equilibrium (Esteves 2019).

Phase 4 Whenever the system reaches a level of insufficiency in the catchment of sediment, the decision can be made to close the breach in the primary dike. The bed level of the polder has now reached a certain height that can guarantee the desired level of coastal safety (Belzen 2021). When the breach is sufficiently small it can be closed in one time on low tide with the help of a simple excavator. Any remaining water can be either left to dry and infiltrate into the ground or can be pumped out. The fully dried and closed-off polder can now be used for agricultural purposes while remaining to provide the required level of safety for the hinterland. Depending on the rate of land subsidence and sea level rise, the polder can be used for agricultural purposes for decades, whilst retaining its level of coastal protection. When, at some point in the future, the level of coastal protection has became insufficient, phase 2 can once more be initiated. The system of the Lease Polder now consists of a closed cycle.

The complete cycle of phase 2, phase 3 and phase 4 can now be repeated indefinitely. The original name of the Lease Polder is wisselpolder. The term 'wissel' in 'wisselpolder' is a Dutch term for 'change' or 'switch' and arises from the principle of switching between the two states where the polder is either used for agriculture or be used as a tidal wetland. The former, when there is no opening in the primary dike, will from now on be called the closed state. The latter, when there is an opening in the primary dike and water is allowed to flow in and out of the polder, is what from now on will be called the open state.

The aim is to have an extended strip of adjacent Lease Polders along a coastline, where the cycles of these polders are out of sync. This way a checkerboard pattern is created along the coast of polders that are used as wetland and are rising in bed level, and polders that are used for agriculture and are lowering in bed level due to subsidence. The agricultural activities can simply be switched back and forth between two adjacent Lease Polders when switching from the open to the closed state.

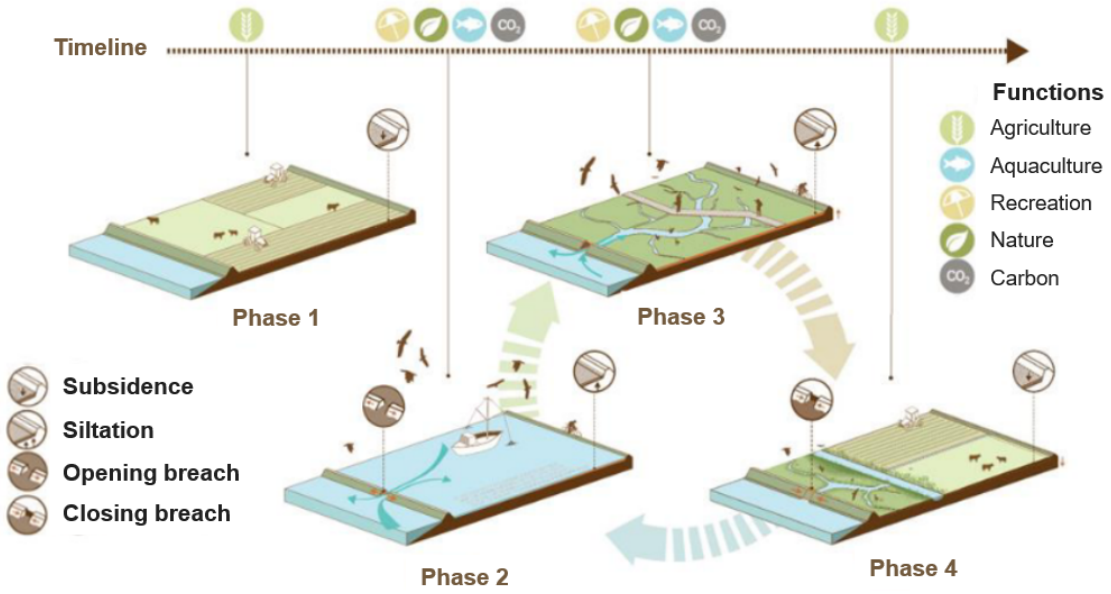

Figure 2.2: The life-cycle of a Lease Polder (Adjusted from Belzen 2021)

2.1.3. Coastal safety

Two well-known forms of conventional coastal protection are the standard sea dike and an overtopping resistant dike. Conventional sea dikes have been the primary form of coastal defence in the Netherlands and allow in most cases for a maximum overtopping rate of 0.1 l/m/s for a probability not greater than 1/10.000 per year (Rijkswaterstaat 1999). Overtopping resistant dikes allow for far greater rates of overtopping and allowance probability, provided that the consequences are low (Verhagen et al. 2005). The essence of making coastal safety more efficient with a Lease Polder lies in the fact that the height of a seaward dike (primary dike) in a Lease Polder system can be lower than that of an overtopping resistant dike, and that the height of a secondary dyke within a Lease Polder system can be lower than that of a flood-retaining conventional sea dyke, provided the system can silt up with sea level rise and the distance between the two dikes is chosen sufficiently (Bakker 2003). This is mainly due to the fact that wave energy is dissipated inside the polder area, as will be explained below.

Principle functions of the primary and secondary dike

Figure 2.3 shows the main principle of how a Lease Polder system provides coastal safety while in an open state and how a reduction in hydraulic forces causes the height of the primary dike and the secondary dike to be lower than for a normal sea dike. The fact that the polder area is connected to the estuary or ocean causes the primary dike to actually not be the main body of coastal defence and will not have the primary water-retaining function. In fact, the smaller secondary dike is now the main water retaining dike, so that the primary dike will not need extra height to prevent wave overtopping. After all, as soon as the polder between the two dikes is connected to the estuary by a breach or means of passage, wave overtopping of the primary dike is of less importance, because there is already high water on the other side of the dike. However, the height of the secondary dike must be maintained to compensate for sea level rise. Due to its sheltered location, this secondary dike will take over the flood defence function from the moment of construction. Due to the development of a high-lying foreland between the two dykes, the green dyke will become increasingly

robust over time. From the moment of construction of the green secondary dike, the safety requirements that apply to the primary dike will be lowered.

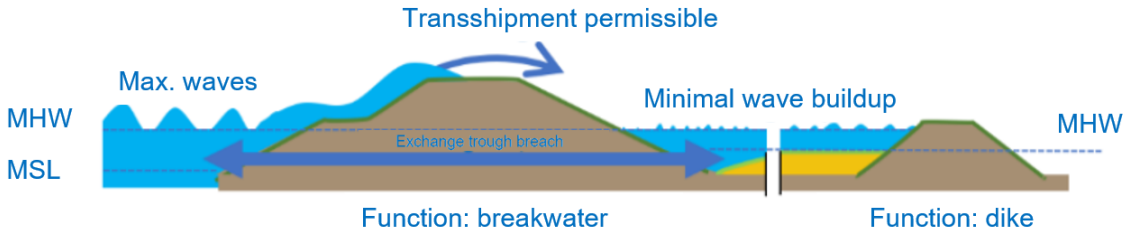

Figure 2.3: The principle of a Lease Polder providing coastal safety, in the phase where the main water body is connected to the polder. The Lease Polder is in its open state (Belzen 2021).

Wave dissipation on the tidal wetland.

On the tidal wetland in the polder area, wave energy will be limited due to two reasons, namely, wave diffraction and wave breaking. First of all, after the penetration of wave energy from the open water into the polder, wave energy will be reduced due to diffracted by the main parts of the primary dike. The phenomenon of wave diffraction implicates that sudden variations in wave energy along the crest cause wave energy to transfer along the wave crest. This is often due to a blockage in the wave direction by for example a breakwater or other hydraulic structure. The wave will bend around into the so-called shadow zone as shown in figure 2.4. The diffracted part of the wave will form a circular wave with the edge of the dike as its centre point. Wave energy and thus wave height decreases along each crest (Bosboom and Stive 2012). For that reason, waves reaching the secondary dike would theoretically, following linear wave theory, measure around 50% of the incident wave height given an equal bottom depth (Bosboom and Stive 2012).

However, the second argument of lowering wave energy, i.e., wave breaking, implicates that the bottom depth is not constant. The most substantial part of the Lease Polders will already have a sloped polder area. Wave shoaling occurs when waves travel over decreasing bed levels, which will only be amplified when the bed level further rises due to accretion (Kiesel et al. 2020). The dispersion relationship therefore yields a decrease in wave celerity and wavelength (Bosboom and Stive 2012). Following the formula for the relationship of shoaling and wave height, wave height should theoretically increase when entering shallower waters. However, this is limited due to wave dissipation by wave breaking (Bosboom and Stive 2012). The two previously stated reasons for lowering wave energy cause the incident waves at the primary dike to only contain a fraction of their wave energy left when reaching the secondary dike.

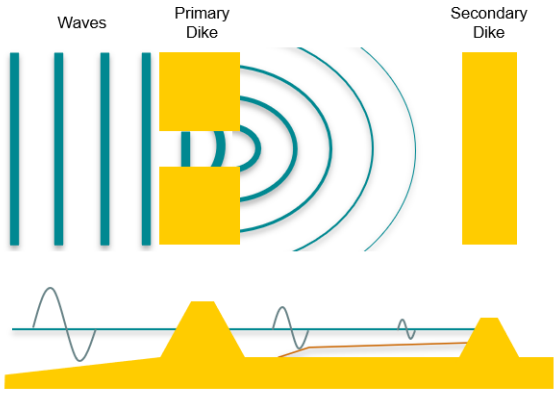

Figure 2.4: The reduction of wave energy in an open Lease Polder system by wave breaking on the elevated part of the tidal wetland inside the polder, and due to wave diffraction through the breach of the primary dike

Crest height of the primary and secondary dike.
First, the differences in crest height for the primary dike are elaborated, considering a conventional sea dike and a Lease Polder. The height of a standard seawall (crest height) is determined on the basis of a number of criteria. These criteria are shown in figure 2.5 and consist of the following parts:

(a) Normative high water (based on a certain probability of exceedance);

(b) Surcharge for high water rise (including subsidence);

(c) Setting and latch;

(d) Oscillations, gusts, seiches and local upheaval;

(e) Local subsidence in the plan period;

(f) Wave run-up and wave overtopping.

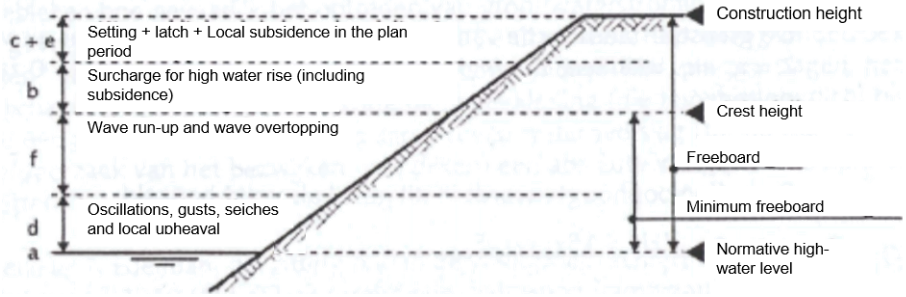

Figure 2.5: Contributions for sea dike crest height. Edited from Rijkswaterstaat 1999

These contributions change when the choice is made for the construction of a Lease Polder system. The main criterion that is resolved is the absence of wave run-up and wave overtopping, which is often the most substantial part of the design crest height. Higher rates of overtopping are allowed - assuming that the inner dike can withstand the increase in runoff forces of the overtopped water - since the polder area in between the primary and secondary dike has a low level of consequence when flooded. After all, the secondary dike will still be there to act as the main body of coastal defence. In most cases, the primary dike will already be in existence before the decision was made to construct a Lease Polder system. In some cases, this former sea dike would approach the period where its present crest height would not meet the safety requirements for being a sea dike. The moment the secondary dike is constructed, the crest height criterion for wave run-up and wave overtopping will not be obligatory, often giving the former sea dike the opportunity to suffice as a primary dike in a Lease Polder system without any extra reinforcements needed. This can be a financial benefit for the Lease Polder.

This same reasoning holds for the secondary dike. Only in this case, it is not the fact that the wave overtopping volume can be neglected, but the fact that wave height reaching the secondary dike will be several factors lower. The exact factor can be obtained from the numerical model in Delft3D. One other thing that needs to be taken into account is the presence of wind-generated waves in the polder. Studies have shown that a maximal width of a Lease Polder can be around 2000m in order to avoid large wind generated waves (Williams, Associates, and Faber 2004). Following this criterion ensures that a freeboard of the secondary dike of 0.5m will suffice for counteracting wind-wave overtopping (Belzen 2021).

2.1.4. Ecological advantages

The inter-tidal wetland area that is created within a Lease Polder will not only improve coastal safety but will also enrich the intrinsic natural value of the landscape. This area might create a favorable habitat for several types of vegetation, leading to the migration of different types of fish and bird species. Next to that, the sedimentation process can play an important role in the captivity of carbon. These ecological advantages will be further elaborated below.

Vegetation development
The historic development of salt marches caused by accidental dike breaches has proven to offer a dynamic natural habitat (Verbeek and C. Storm 2001, Wolters, Garbutt, and J. P. Bakker 2005). Pilot projects of the Lease Polder have shown that the intertidal wetland area provides the same excellent habitat for the development of new vegetation species (French 1999). Vegetation growth is an important factor in several processes around the development of a healthy and self-sustaining tidal wetland. By damping the wave energy, vegetation accelerates sediment catchment inside the polder. Besides the catchment of sediment, it also creates a safe and favorable breeding ground and habitat for fish and birds (Schelling, Steeg, and Leopold 2014). The growth of vegetation stimulates a positive feedback loop. The plants create microhabitats and modify their environment so that the marsh formation evolves (Onaindia, Albizu, and Amezaga 2001).

The initial growth of plant species seemed to be hardly dependent on the initial existence of vegetation on the former polder, since saline plant species need to replace the former species (J. Bakker et al. 2002). The essential aspect in landing new species turned out to be a supply of seeds from neighbouring salt marches by the tide. The three most dominant plant species that were observed in the restored salt marches were the Salicornia, the Spartina and the Puccinellia (Sánchez Leal, K. Storm, and Verbeek 1998). An important factor in improving the establishment of vegetation is drainage. Areas that lack proper drainage of water after high tide cause water-saturated soils which prevent settlement of new plants (Zedler and Callaway 1999).

Fauna
Besides natural habitat for different types of vegetation, the Lease Polder also provides a good environment for several types of fauna. The intertidal wetland area in between the two dikes creates the perfect maternity environment for different types of fish and birds due to its sheltered characteristics. Several cases of tidal wetland recovering show similar paces of fauna colonisation compared to natural originating tidal wetlands (Oevelen et al. 2000). Although the time that fauna needs to establish itself in the wetlands is longer than that from the vegetation, it will often follow indefinitely depending on external environmental characteristics. Pilot cases like the Sierperdaschor in the Netherlands for example showed migration of different types of fauna already five years after commissioning of the Lease Polder (B. Kornman 2000, C T A Moermond 1994). This can possibly take longer for different environments. For example, fish have shown cases of three years to 25 years for proper establishment.

The move-in of fish species are thought to be linked to the existence of a system of tidal channels (Schelling, Steeg, and Leopold 2014). A proper channel system provides additional wave shelter and overhanging vegetation which serve as refuge and residence for the fish population. Other studies also showed that square-shaped polder areas are more favorable than narrow and elongated polders (Oevelen et al. 2000). In order to maintain a proper fish habitat, the area requires continuous inundation. A mounded surface with creeks and channels makes sure that puddles of water remain present with low tide since most of the tidal wetlands are on average above mean sea level. Bird migration is mainly dependent on the evolution of vegetation in the polder. As soon as reeds and other types of vegetation grow relatively tall, birds will come in for their breeding season (Oevelen et al. 2000).

CO_2 captivity.
Another important ecosystem service that is provided by the new intertidal wetland within a Lease Polder is the potential captivity of carbon by sedimentation (Boerema, Van Passel, and Meire 2018). Carbon sequestration by sediment burial has a positive effect on climate regulation. Intertidal salt marches have been shown to store more carbon than they release in comparison to normal agricultural activities per square meter and have even been shown to be able to sequestrate equal or more carbon than the average Dutch forest (J. V. Belzen, T. J. Bouma, and Ysebaert 2020). Dutch salt marches are estimated to capture over 60.000 tonnes of CO_2 each year (Tamis and Foekema 2015). The capture of carbon in slat marches is also known as 'Blue Carbon' projects. Other examples of Blue Carbon projects are mangrove forests and salt swamps (Macreadie et al. 2019). The capture of carbon does not instantly show its economical benefit, but will in the long term show its financial prosperity.

2.1.5. Social economical advantages
Besides ecological advantages, several social-economical advantages can be introduced with the commissioning of a Lease Polder system, including the reduction of flood damages in case of a dike breach and the

opportunity of saline agriculture. Above that, the intertidal area will create several possibilities for attracting tourism and leisure. All will be covered below.

Agriculture of tidal wetland plants and shellfish farming
The intertidal wetland area of a Lease Polder can bring the perfect opportunity for saline agriculture during the open period of the Lease Polder. Sowing these saline crops in advance can lead to the development of extended saline crop fields in the tidal wetland area. Sea aster, sea lavender and Salicornia have been shown to be the perfect saline crops to cultivate in intertidal wetlands located in regions with a maritime climate(Huiskes 1996). Growing and harvesting these crops have proved to be a very lucrative business, providing an on average higher revenue per square meter than conventional agriculture (J. v. Belzen, Rienstra, and T. Bouma 2021).

Flood damage reduction
Besides attenuating storm waves, the tidal wetland in a Lease Polder induces a significant reduction in not only the chance of a breach in the secondary dike, but also in the size of the impact followed by a breach in the secondary dike. Studies that analysed historic flood disaster data from 1717 until 1953 indicate that natural tidal wetlands in front of dikes led to a significant reduction in damages (Zhu et al. 2020). Due to the confinement of the breach area, the magnitude of flooding discharge is significantly lowered. When the flood discharges are significantly lower, not only the impact of the damage will be lower but it also provides more time for evacuation, lowering the potential causality rate of a flood disaster. The confinement of a potential breach area is caused by the bed elevation of the tidal wetland, reducing the frontal area of the secondary dike as shown in figure 2.6. In the case of a conventional dike in combination with sea level rise, this area would only grow, making the potential breach area larger. Whereas the growing wetland will grow together with sea level rise, keeping the potential breach area consistently small over time. Therefore, the growing wetland in a Lease Polder will cause a reduction in potential flood risk.

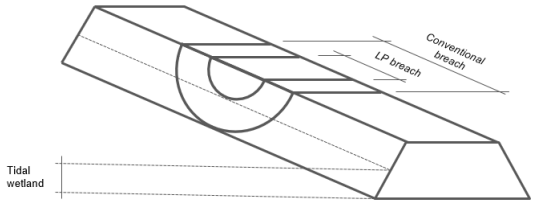

Figure 2.6: Damage reduction due to smaller breach area for both a conventional dike and a Lease Polder

Attraction of tourism and leisure
The presence of a diverse collection of flora and fauna in the intertidal area of a Lease Polder provides a considerable attractive force for leisure and tourism. When the wetland areas are made accessible for the people, in a way that the ecosystems are preserved and not disturbed, they can strengthen and expand social aspects within the area with local economical growth as its result (Schelling, Steeg, and Leopold 2014, J. v. Belzen, Rienstra, and T. Bouma 2021).

2.2. Influential parameters on the siltation rate

Former studies have tried to both empirically and physically determine the effect of individual parameters on the siltation within managed retreats. However, many of those studies failed in finding direct effects, since the measured historical data is scarce and the effect of single parameters is difficult to isolate. The sections below summarize the found and expected relations between certain influential parameters and the siltation rate.

2.2.1. Suspended Sediment Concentration

The sediment availability in the estuary and its supply to the depoldered area significantly influences the net sedimentation balance. Prior research regarding sedimentation patterns of depoldered areas showed that, if

the necessary sediment supply is present, accretion will always occur regardless of bed elevation (Miller et al. 2008). When sediment supply is inadequate, regardless of the elevation, there will be no accretion and the area may even erode away (Haltiner et al. 1996). Exact data sets for the suspended sediment concentrations around the location of a breach are difficult to find. Suspended sediment concentration in estuaries varies strongly over time and this variation is predominantly depending on seasonality and the moment in the tidal cycle (Temmerman et al. 2003). Especially the difference in wind regimes and biological activities can effect the seasonality (Schelling, Steeg, and Leopold 2014). Besides this non-steady aspect, the suspended sediment concentration is also non-uniform and can differ over the complete length of an estuary. Maximum values in the suspended sediment concentration have been found around the mixing point of saline and fresh water (Schuttelaars 2002). Overall, a positive relation is expected between the suspended sediment concentration and average rate of sedimentation as is shown by figure A.1. A more quantifiable relation will be assessed during this study.

2.2.2. Tidal range

The tidal range is one of the main components determining the tidal prism. A higher tidal ranges means a larger tidal prism, which could possibly suggest a higher sediment exchange (Williams, Associates, and Faber 2004). Besides the tidal prism, tidal range also effects the location of intertidal habitat as shown in figure A.2 (Esteves 2019). A case study of depolderd sites in the UK observed tidal ranges from 2m to 7.6m (Oevelen et al. 2000). However, a distinct correlation between tidal range and sedimentation rates was not found in that particular study.

2.2.3. Polder area size

Area sizes of different similar realignment schemes differ from 1 ha (Rother, Scott n.d.) to nearly 450 ha in Tiengemeten, Hoeksche Waard (Boo 2007). Together with the bed elevation and tidal range, the area size influences the tidal prism (Lakhan 2003) (assuming the breach area is in equilibrium). The total net imported sediment is expected to enlarge with a larger tidal prism. However, the net vertical sedimentation rate is not expected to grow since the amount of sediment per square meter stays at maximum constant. On the other hand, area size plays a significant role in the fetch length for wind waves (Rohweder et al. 2008). Larger fetch lengths increase the wind wave height and thus the internal wave energy (Marani et al. 2011). Consequently, Fetch length has a direct impact on the resuspension of sediment (Mariotti et al. 2010). This mechanism, in combination with incoming and outgoing tidal fluxes, determines the erosion or accretion rates over time (Chauhan 2009). All matter combined, it is expected that larger area size has a negative relation with the sedimentation rate. This study will quantify this relation for both the individual width and length of a polder.

2.2.4. Initial polder bed level relative to MSL

The tidal prism is indirectly affected by the bed elevation, relative to the mean sea level (MSL) of the initial polder. Lowering the bed elevation can potentially increase the tidal prism, assuming there is no tidal damping and the bed level is above mean low water (MLW) (Jarrett 1976). Increasing the tidal prism suggests that the net volume of sediment that is brought in with the flood tide will increase as well, resulting in a larger net volume available for accretion (Williams, Associates, and Faber 2004). However, different cases in the UK (Horsey Island, Stone Marsh, Canvey Point) have suggested that there is a minimum to the relative bed elevation in order to result in sufficient sedimentation rates (Oevelen et al. 2000). An extensive case analysis gave the impression that there is an optimal relative bed elevation around mean high water level (MHW) (Oevelen et al. 2000). These are however all impressions based on former cases and direct relations still have to be proven.

2.2.5. Polder area shape

Area shapes can differ in numerous ways, with a near square rectangle as the most simple form. Cases of more round, triangular, elongated or completely irregular shapes are also in existence. A distinctive effect of the shape on sedimentation rates is not expected (Oevelen et al. 2000). However, cases of strongly elongated basins showed a significant difference in sedimentation patterns. The Sieperdaschor is a very narrow (300m) polder but extends inland for a considerable length (3.600m) (C. Moermond et al. 1994). Sedimentation patterns differed strongly across the profile. In the first 4 years, sedimentation rates were at an average of 5 cm/year right after the breach but dropped to around 0 to 1 cm/year at the most landward point (B. A. Kornman and Van Doorn 1997). No clear statement has been made on why sedimentation differs over the

profile, but the hypothesis is the early deposition of suspended sediment at the most seaward side of the polder. This can cause the tidal water supply to lack suspended sediment at the most landward side of the polder (Oevelen et al. 2000). During this study, the shape of the different polder scenarios will be limited to rectangular shapes.

2.2.6. Polder slope

A seaward slope (surface elevation increasing in landward direction) improves the drainage of the area between two floods and thus contributes to a good dry-wet cycle. However, no distinctive correlations between polder slope and sedimentation rate have been found in previous cases (Oevelen et al. 2000). This study will look at the difference in sedimentation rates for sloped polders and horizontal polders.

2.2.7. Breach dimensions

The absolute dimensions of a breach can have an effect on the tidal prism and on the quantity of external wave energy entering the polder. The dimensions of a tidal inlet are not static parameters but tend to evolve dynamically to an equilibrium state (Escoffier 1977). Escoffier found a relation between the cross-sectional area of the inlet and the cross-sectional averaged velocity in the entrance channel u_e (shown as V in figure 2.7). Point 'c' represents an unstable equilibrium, which suggests that a breach smaller than the unstable equilibrium dimensions will silt up over time and eventually close. On the other hand, breaches with slightly larger breach dimensions will erode over time and become wider. Point 'b' represents a stable equilibrium. Breaches larger than the unstable equilibrium will tend to reach the stable equilibrium dimensions (Bosboom and Stive 2012). The absolute maximum of the closure curve indicates the point where the tidal prism is at a maximum. From that point on the tidal prism will no longer be damped and stays constant at its maximum for wider breaches.

Till this point, there are four main variation types of Lease Polder breaches (Kiesel et al. 2020):

- Single breach projects;
- Multiple breach projects;
- Complete removal of the existing flood protection;
- regulated tidal exchange.

Reasons for choosing one over the other depends on various aspects, such as dimensions of the polder, the scale of the hydrodynamic processes and the current state of protection. Besides these aspects there are also the final goals that play a role, e.g. the promotion of biodiversity, enhancing the flood defence and the creation of natural shoreline (Ledoux et al. 2005). However, a significant knowledge gap is still in existence regarding the effect of different types and dimensions of breaches on sedimentation rates. This study will look at the potential of multiple breaches and the exact effect of the breach width on the morphological changes.

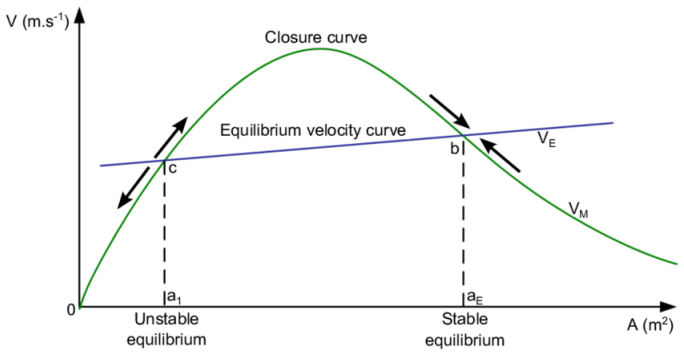

Figure 2.7: Escoffier diagram for tidal inlet stability adapted from Escoffier in 1940 (Dodet 2013)

To conclude, both hydraulic and dimensional parameters are expected to have a significant influence on the the morphological development within the polder. However, a quantifiable effect of the individual parameter on the rate of sedimentation lacks for almost all parameters. The next chapters in this study will focus on

assessing this exact relationship for each individual parameter by means of simulating several parameter scenarios with a numerical model.

3

Base-case scenario - Tollesbury Lease Polder case

As explained, a base-case model of a Lease Polder will be made in Delft3D. In order to validate and calibrate the model, a certain case study is needed with sufficient available data regarding the polder characteristics, the boundary conditions and the measured morphological changes over time. This chapter will discuss all the above mentioned for the Tollesbury case, which is used as the foundation of the base-case model.

3.1. Case study location

The Tollesbury saltmarsh is located as a side-estuary along the Blackwater Estuary in the area of Essex, United Kingdom (figure 3.1). The Blackwater Estuary forms the mouth of the Blackwater River between Maldon and West Mearsea and currently is the main site for salt marsh restoration research in England (R. Emmerson et al. 1997). Next to the Blackwater River, the estuary connects the Chelmer River (near Maldon), to the North Sea. With an area size of 55.38 square kilometres, it is one of the largest Sites of Special Scientific Interest (SSSI) (Spash and Simpson 1993). The estuary geology mainly consists of clay with low levels of sand and gravel (Hazelden and Boorman 2001).

There are little to no variations in salinity due to its well-mixed characteristics (R. Emmerson et al. 1997). The discharges of both the Blackwater River and the Chelmer River combine to a total of $3.3 m^3 s^{-1}$, which is negligible compared to the tidal prism of the Blackwater estuary (Price 2016). An average tidal range of $4.5 m$ during spring tide makes tidal forcing the main forcing component in the estuary (Chang et al. 2001).

A large extent of tidal mudflats and salt marshes, around $6.84 km^2$, were created over the past centuries due to the high concentration of suspended of fine silts and the large tidal range (R H C Emmerson et al. 1997, (N. J. Cooper, T. Cooper, and Burd 2001). However, in the past century, more than $2 km^2$ of the salt marches have been eroded by wave action(N. J. Cooper, T. Cooper, and Burd 2001). In order to preserve the remaining salt marshes, the SSSI has turned several areas into research sites. Abbotts Hall, Orplands, Northey Island and Tollesbury, among others, are now used for numerous research projects with the goal of obtaining a better understanding of the processes in these salt marshes. A better understanding of the physical and natural processes will help with preserving what is left and with restoring what was lost. These sites are now called managed restoration sites and have a total area of around 90 hectares (Shepherd et al. 2007). On these sites measurements are performed on a regular basis, creating an extensive set of historical data.

The existence of these historical datasets makes that these research sites are well suited for the foundation of numerical models. Therefore, the Tollesbury site has been selected as the base-case scenario for this research.

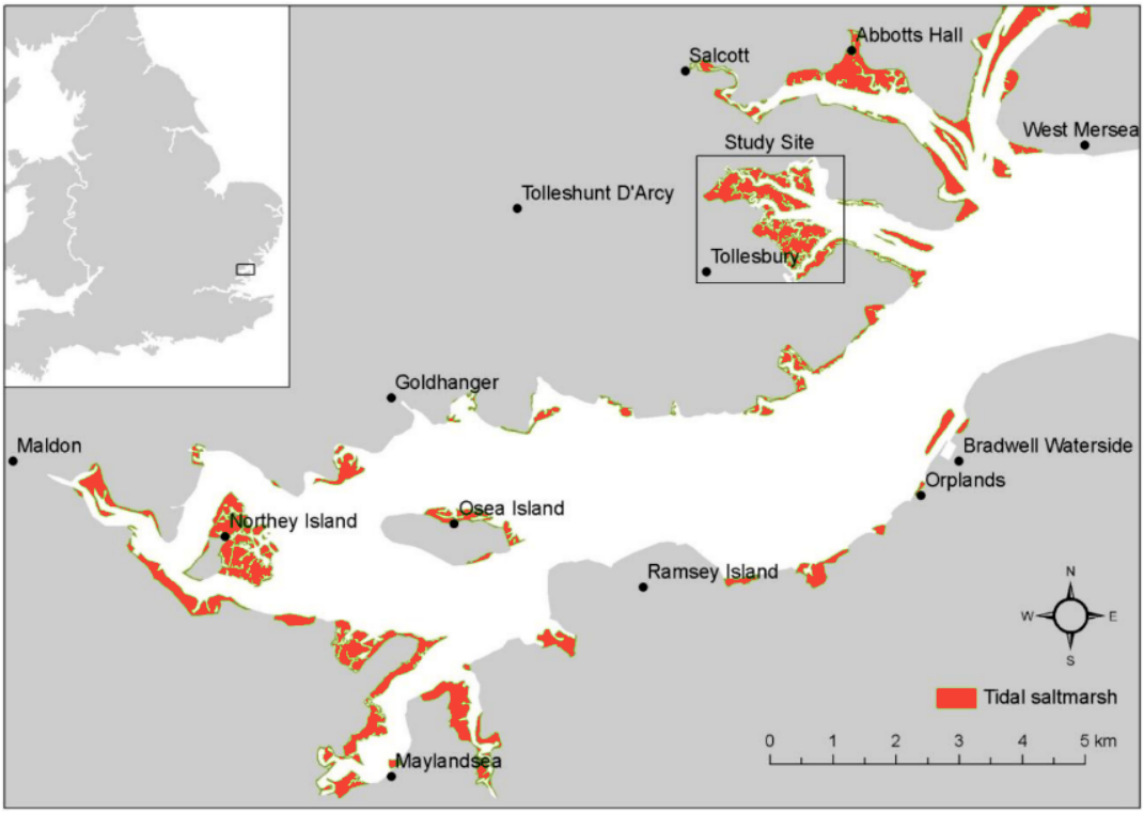

Figure 3.1: Map of the UK, Blackwater Estuary. Saltmarsh areas are depicted in red on the map. (edited from Price 2016)

3.2. Tollesbury salt marsh

On the northern side of the Blackwater Estuary, the Tollesbury Estuary is located. The estuary has a total area of 240 hectares of which 130 hectares are covered by active salt marshes which are inundated on a daily basis (see figure 3.2). The upper part of the salt marshes is called the Old Hall Marshes and the lower part is called the Tollesbury Marshes. At the beginning of 1993, the planning started for a managed realignment site at the South-Western part of the Tollesbury marsh, which was completed in late 1995 (Meadowcroft et al. 1996). The managed realignment area was enclosed several decades before with a dike going all around the northern part of the realignment site, connected to the mainland in the southwest. The polder area was used for agricultural purposes for decades and had a lower bed level in comparison to surrounding marshes. At the beginning of august 1995, a breach with a width of 50m was made in the northern part of the dike. It connected the polder to the Tollesbury Estuary, making it the largest managed realignment site of its time in the United Kingdom (Meadowcroft et al. 1996).

In the first stages research was mainly focused on hydrology and vegetation, which later developed into studies monitoring sedimentation and soil structure. These sedimentation studies showed rapid sedimentation rates in the first few years after which it started to slow down. The first average sedimentation rates were measured to be 31.6mm/y in the first year after which it started to diminish to an average of 14.3mm/y during the period between 2000 and 2007 (Goudie 2008). During this time a large quantity of new vegetation species was colonizing the growing mudflats.

Figure 3.2: Map of the Tollesbury Estuary, Essex, UK. In green is the area selected that is used by the SSSI as a research area. It is an enclosed area by dikes, with a breach that connects the area to the Tollesbury Estuary.

3.3. Historic data analysis

As was explained in Chapter 1, a numerical model will be made based on the base-case scenario. In order to validate such a numerical model, a proper understanding is needed of the local data such as bathymetry and parameters like sediment characteristics. Historical data regarding different forcing types is also required. For example, average values for wave forcing, wind forcing and tidal forcing are studied. The next subsections will further elaborate on these subjects.

3.3.1. Tidal forces

The Tollesbury estuary is has a semi-diurnal tidal system (Elsner 2009). During a recent study, pressure sensors were installed to measure water levels during several periods. The main pressure sensors were located in the main tidal channel running through the breach of the realignment site, right in front of the breach where the bed level is around $OD+0m$ (OD means Ordnance Datum, vertical datum used in the UK representing the MSL). Measurements were performed during two weeks in the months May, August, November of 2011 and February 2012. The results of these measurements are shown in figure A.3 of Appendix A. Figure 3.3 shows the measured water level during two weeks in May (black line). The tide does not make a complete sinusoidal wave but instead flattens out around $OD+0m$. This is due to the fact that the area has completely dried out during low tide. The red line depicts the observed tidal surge measured by a gauge from the National Oceanographic Data Center near Harwich, located around $35km$ north-east of Tollesbury. These local tidal surges are deviations in the measured tide and the predicted tide at Harwich and are thought to have an effect on the measured tide at Tollesbury (Price 2016).

Studies from Pye et al. 1993 measured more averaged water levels in the Blackwater estuary over longer periods of time and deducted tidal ranges. Here, the full tidal cycles could be observed without drying out. The mean tidal range was measured to be $4.7m$ during spring tide and $3.0m$ during neap tide. Mean high water spring tides (MHWS) were measured to be $OD+2.35m$ and the mean high water neaps (MHWN) were measured around $OD+1.5m$ (see figure 3.1).

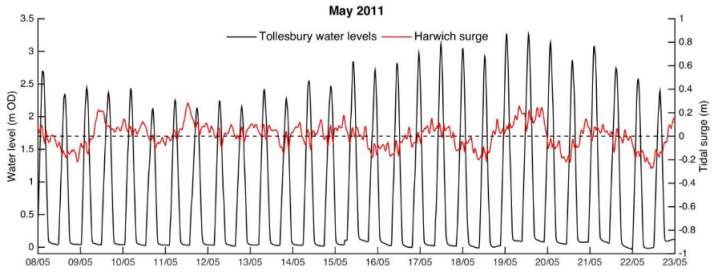

Figure 3.3: Water level measured in Tollesbury (Black line) and tidal surge measured in Harwich (Red line) during the month May 2011 (Price 2016)

Table 3.1: Waterlevels observed at Tollesbury (Pye et al. 1993)

	MHWS	MHW	MHWN	MSL	MLWN	MLW	MLWS
Water level	OD +2.35m	OD +1.925m	OD +1.5m	OD +0m	OD -1.5m	OD -1.925m	OD -2.35m

3.3.2. Wind forces

During the same study of Price 2016, data was used from the archive MIDAS to obtain historic wind speeds and from the Walton-on-the-Naze weather station ($32km$ north-east of Tollesbury) to collect gust speeds (Watson, Kritharas, and Hodgson 2015). Table 3.2 shows the average measured wind speeds, average gust speeds and peak gust speeds for different months. The numbers are derived from a two-week data set (history plots are presented in Figure A.4). Based on wind roses, one can conclude that the dominant wind direction is southwest (see Figure A.5).

Table 3.2: Measured average wind speeds, gust speeds and peak gust speeds for the months May, August November 2011 and February 2012. Measured at the Walton-on-the-Naze weather station and the MIDAS archive

Period	**Mean wind speeds [m/s]**	**Mean gust speed [m/s]**	**Peak gust speed [m/s]**
May 2011	4.88	7.74	15.695
August 2011	4.96	8.18	14.15
November 2011	5.90	8.14	11.83
February 2012	5.12	8.33	15.95
Average	5.21	8.09	14.40

3.3.3. Wave forces

Waves that arise at the Tollesbury estuary are mainly generated by wind. Furthermore, the magnitude of the wind waves is highly dependent on the wind speed and wind direction. No data is available on measured wave height at the Tollesbury estuary. Therefore, an average wave height and period had to be calculated for which the following empirical formulae that hold up for shallow water wind waves are used respectively (Demerbilek 2008):

$$\frac{gH_{m_0}}{u_f^2} = 4.13 \cdot 10^{-2} \cdot \left(\frac{gX}{u_f^2}\right)^{\frac{1}{2}} \tag{3.1}$$

$$\frac{gT_p}{u_f} = 0.751 \cdot \left(\frac{gX}{u_f^2}\right)^{\frac{1}{3}} \tag{3.2}$$

With an average wind speed of $u_f = 5.21 m/s$ and a maximum fetch length of $X = 5km$ wind waves with an average height of $H_{m0} = 0.2m$ are obtained. These wind waves will have a wave period of $T_p = 2s$.

3.3.4. Sediment characteristics

Acquiring a single uniform value for the local suspended sediment concentration (SSC) is an arduous process, since it is highly dependent on local varying circumstances. Hydraulic forces such as waves and currents have

a significant impact on the local level of SSC. Moreover, local levels of SSC are not only varying over time and area but also vary over the depth. Studies from Price 2016 and Elsner 2009 found values for SSC to be between $70 mg/l$ and $150 mg/l$. Sheldon 1968 measured an average suspended particle diameter range between 4 and 32 microns with the highest concentration around 8-10 microns. A more detailed description of these studies can be found in Appendix A.3.

A study by Watts et al. 2003 measured a dry bulk density for the soil within the polder bed ranging between $460 kg/m^3$ for younger soil and $660 kg/m^3$ for consolidated soil. The consolidated soil was located in an area right behind the breach and partly contained the original polder soil without undergoing sedimentation or erosion. This area appeared to be a non-accreeding area with higher values for the critical shear stress for erosion. a complete table and description of the measured critical shear stresses can be found in Appendix A.3

3.3.5. Bathymetry

The bathymetry of the Tollesbury research site in 1995 is shown by figure 3.4, right after the breach was made in the primary dike. The bed level starts at $OD + 1.0m$ at the side of the breach and gradually increases to $OD + 2.25m$ at the land side of the research site. Figure A.13 displays the bathymetry map of the research site at Tollesbury including the bathymetry of the Tollesbury marsh in front of the research site. The map gives a clear view of the tidal channels inside the Tollesbury Hall estuary. Depths of the main tidal channel which connects the research site to the Blackwater estuary range from $OD - 5.0m$ at the connection point to the Blackwater Estuary to $OD + 1.0$ at the breach of the research site.

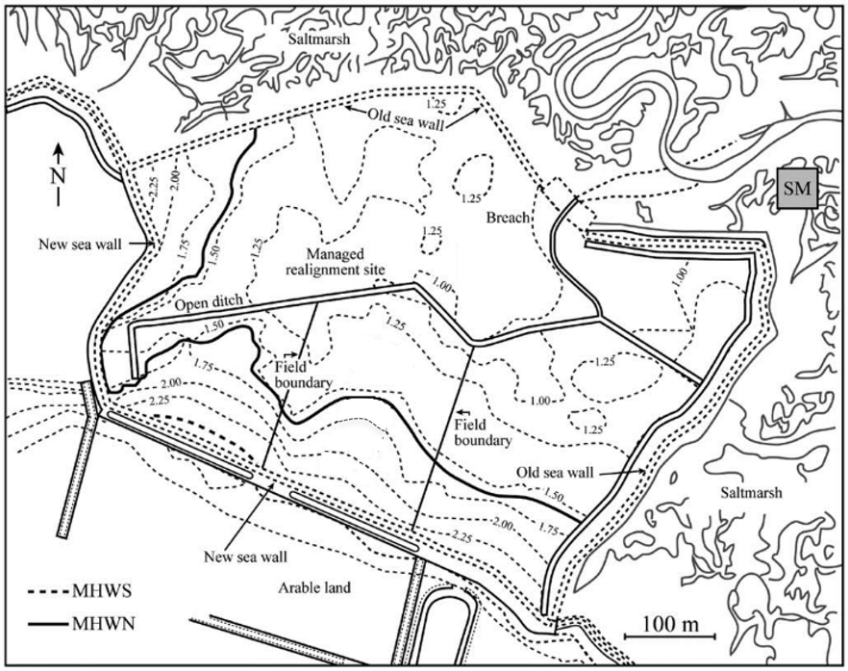

Figure 3.4: Map of the bathymetry of the Tollesbury research site in 1995, right after the breach was made in the primary dike. The dashed line shows the border of the MHWS frontier. The solid line shows the MHWN frontier (Goudie 2008)

3.3.6. Bathymetry development

In the field of the Tollesbury marsh, a total of 25 bathymetry transects were made in order to measure the daily accumulation of sediment (Garbutt and Wolters, 1995). The transacts were scattered around the polder area and throughout the surrounding tidal marshes as shown in figure A.6. The recordings of these transects already started two years prior to the commissioning of the Tollesbury research site and lasted till 2007. The surrounding Tollesbury Marsh turned out to have a constant sedimentation rate of around $3 mm year^{-1}$ throughout the years. This sedimentation rate did not change after the breach was made in the research area (Goudie 2008). Figure A.15 shows a history plot of the average values of bed level change over the years 1994 until the year 2008.

The first average sedimentation rates were measured to be $31.6 mm/y$ in the first year (1995) after which it started to decrease to an average of $14.3 mm/y$ during the period between 2000 and 2007. The complete data set of average measured bed level changes per year from 1995 to 2007 are shown in table 3.3. The values are obtained by taking the mean sedimentation rate of all sediment transects over each year. Figure 3.5 shows the average sedimentation values on a more detailed level. Comparing the different transects with each other show that the majority of sedimentation occurs between the outer parts of the polder area and the centre. Data from tranches 24 and 25 shows that there is hardly any sedimentation over time right behind the breach and that the surface soil remains as the initial surface soil of the polder. Initial sedimentation rates are measured to be optimal at the lowest initial bed levels, located at the seaward side of the polder on both sides of the breach. Lower rates of sedimentation are observed at the landward side of the polder area, assumed to be mainly caused by lower inundation periods (Price 2016). These processes result in the slow transformation of the sloped polder bed into a more horizontal and elevated bed with a ditch in the area surrounding the breach. The polder bed seems to develop and reach for a uniform equilibrium bed level (Watts et al. 2003).

Table 3.3: Average annual bed level change at the Tollesbury research site during the years 1995 until 2006. Values are the averages of all sediment transacts (Goudie 2008)

Year	'95	'96	'97	'98	'99	'00	'01	'02	'03	'04	'05	'06
Bed level change [mm/year]	31.6	25.6	23.9	22.3	20.7	19.1	17.5	15.4	14.8	12.7	11.2	9.6

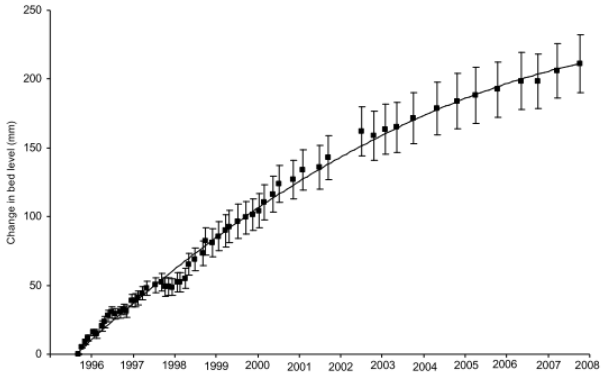

Figure 3.5: Average annual bed level change at the Tollesbury research site during the years 1995 until 2006. Values are the averages of all sediment transacts (Goudie 2008)

3.3.7. Vegetation development

With the purpose of detecting vegetation growth, several aerial photographs were taken of the Tollesbury realignment site from 1997 until 2011 by the Environmental Agency (see figures A.16 and A.17). Deducted from these pictures were maps that made a distinction between areas that were vegetated and areas that were not vegetated, so-called bare areas (figures A.18 and A.19). The map dated from 1997 shows that around two and a half years after breaching the primary dike, 7.1% of the total research area was vegetated. The most common species was Samphire (*Salicornia*, "Zeekraal" in Dutch) and was mainly established around the secondary dike where the bed level was relatively high and inundation times low. In 2011, nearly half of the research area was vegetated by different species. The aerial map shows that 8.4 hectares or 45.0% of the total area were vegetated. During the period between 1997 and 2011, Common Cordgrass (*Spartina anglica*, "Slijkgras" in Dutch) has become the dominant vegetation cover. The rate in growth of vegetation peaked in the period between 2001 and 2008 with a growth rate of $0.63 ha/year$. This growth rate eventually slowed down to $0.49 ha/year$ in 2013. It is likely that this decrease in growth rate will continue for the coming years until a plateau is reached (Price 2016).

Besides the development in vegetation, the aerial photographs also show a clear evolution of small channel systems within the research area. In the first couple of years, small channels start to form connected to the main channel and the human-made channels coming from the main channel (The human-made channels

were already in existence prior to the commissioning of the area). These newly formed small channels are formed naturally and help with draining the polder area.

All the information and parameter data regarding the Tollesbury case study that were presented in this chapter will be used to create a numerical model of a Lease Polder. The next chapter will elaborate on the simplifications and transformation of the parameter data that were needed to create a simplified numerical model.

4

Lease Polder Model Setup

The following chapter will elaborately describe the complete process of setting up and acquiring a stable and usable morphodynamic model of a Lease Polder, with the aim of attaining the sensitivity of influential parameters on sedimentation rates within a Lease Polder. Section 4.1 will cover all the subjects around the numerical model and its origins, ranging from grid setup to the parameter settings. Section 4.2 will describe the entire process of validating the base-case model based on the Tollesbury case. In section 4.4, all the scenarios that are used for the sensitivity analysis will be introduced.

4.1. Delft3D Morphodynamic model - Base Case model

With the purpose of determining the effect of influential parameters on the Lease Polder, a single base-case model is required with which the sensitivity of all different parameters can be modelled and benchmarked. Obtaining a workable numerical model requires data with which the model can be validated and calibrated. This particular base-case model is based on the Tollesbury research site, the Tollesbury Lease Polder.

The numerical base-case model will not be a one-on-one realization of the Tollesbury case but will resemble a fictive simulation where dimensional characteristics and certain forcing parameters will be simplified. These simplifications are needed to consequently change and compare a specific parameter, without undermining the essence of a one-on-one benchmark. For example, a sloped polder bed will lead to the change in multiple parameters when the horizontal dimensions are changed. Due to these simplifications, the model will not be directly calibrated, but will rather be validated in a three-step validation process on the incorporation of the processes. This three-step validation process uses three individual models.

The main calibration will be performed on the first model, called the 'Tollesbury Calibration' model. This model resembles the bathymetry of the Tollesbury case the closest, including the incorporation of the sloped polder bed, the tidal channel and tidal flats in the bathymetry and will be calibrated to resemble the historic sedimentation rates.

After the processes and sedimentation rates are calibrated and validated for the 'Tollesbury Calibration' model, the second model can be validated in this model, which neglects the tidal channel and the tidal flats and replaces it with a uniform foreshore (more details for this simplification will be further explained in subsection 4.1.3). This model is called the 'Uniform Foreshore Validation' model. From here, the final 'Base-case' model will arise by replacing the sloped polder bed with a horizontal bed. The bathymetry maps of the three models are shown by figure 4.4. The thought behind this simplification is further explained in subsection 4.1.5. By dividing the validation process into three individual steps, a better understanding of the effect of the simplifications is ensured. Figure 4.1 shows a complete overview of the validation and simplification process that will be further elaborated in the following subsections.

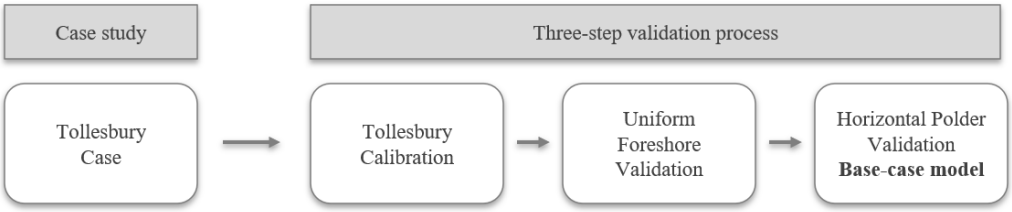

Figure 4.1: Overview of the three-step validation process used to calibrate and validate the Tollesbury model and the simplifications to the final Base-case model

The remainder of this section will describe the complete setup of the numerical base-case model. It will include all the individual components of the model, for example, the bathymetry, the boundary conditions and parameter settings will be explained.

4.1.1. Processes

In order to create reliable and usable model results, the proper processes need to be incorporated into the numerical model. Sedimentation within a Lease Polder is reliant on the interplay of separate processes. Leaving out one of these processes can result in an irreliable model making the results futile. This particular model includes three different processes: Flow, waves and sediment morphodynamics. The process of wind is deliberately left out and indirectly incorporated in the wave process. This incorporation will be further elaborated on in subsection 4.1.6. The main reason for leaving the process of wind out of the base-case model is remaining simplicity and to lower computational time.

4.1.2. Sediment fractions

The process of sediment morphodynamics will be incorporated into the model via two separate sediment fractions. One of these sediment fractions will represent the sediment layer that is already present in the polder bed layer (called the 'Mud Bed' fraction). Typically, this bed layer has been there for several years and has had time to fully consolidate, making it significantly more resistant to erosion in comparison to newly settled sediment. The other sediment fraction will represent the suspended sediment that is present in the water at the seaward boundary (called the 'Mud Suspended' fraction). This is the sediment that would normally be present in the estuary due to the supply from rivers and erosion further seaward in the estuary. When the sediment has settled due to for example a decrease in local flow speeds, the bed shear stress that is needed to re-suspend this sediment is significantly lower than for the sediment that has been consolidating for a long period. These aspects of the individual sediment fractions will be taken into account by means of differentiating the sediment characteristics, as will be further elaborated in subsection 4.1.7.

4.1.3. Dimensional Simplifications

As was stated earlier, the numerical base-case model will be a fictional approximation of the Tollesbury managed realignment. Making dimensional simplifications will allow for better and easier parameter adjustments and will make the comparison between certain scenarios more distinct. The slightly rectangular Tollesbury polder will be projected as a perfectly square polder in the model with the dimensions of $430m$ by $430m$. The bathymetry map of the Tollesbury foreshore indicates the distinct presence of a tidal channel connecting the Tollesbury Marsh to the research site, called the Tollesbury Creek (see figure A.13). The sides of the channel are occupied by higher-lying tidal flats that are only inundated during high tide.

In the final base-case model, the assumption is made that the foreshore does not consist of a tidal channel and tidal flats, but will have a uniform sloped foreshore retaining the same slope angle as the original tidal channel. The reason for this is, again, to remain the one-on-one benchmark criterion while making the different scenarios. Normally, when the tidal amplitude is changed, the tidal prism would change accordingly, resulting in a shift in the dimensions of the tidal channel and tidal flats (Bosboom and Stive 2012). This would mean that the dimensions of the channel and flat in the model would also have to be changed when simulating such a model, which would violate the one-on-one criterion making the models non-comparable. By neglecting the existence of a tidal channel and tidal flats, one is able to properly compare two different models with varying dimensions.

This study will, however, incorporate the tidal channel and tidal flat during the calibration process. These results will be compared to the results of the simplified base-case model with the uniform sloped foreshore. The differences in processes and sedimentation that arise will be evaluated in order to justify this simplification. A 3D schematization of the fictional polder that will be used as the base-case model is depicted in figure 4.2.

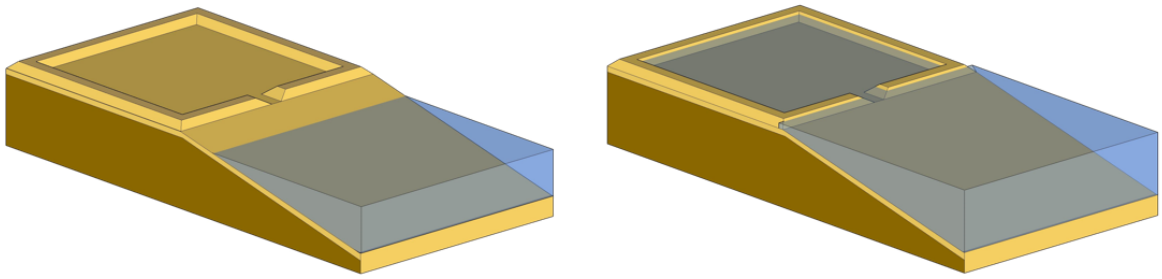

Figure 4.2: The 3D schematization of the base-case model with different tides. Left: Lease Polder model with low tide. Right: Lease Polder model with high tide

4.1.4. Computational Grid

In order for a Delft3D model to perform numerical computations to compute the spatial development of hydraulic and morphological processes, a system of connected grid cells is required. Such a system of grid cells is called a computational grid. The finer the grid, the more detailed the processes can be computed and stored. Knowing that the flow gets confined near the breach and that the flow speeds will increase in the breach, it is a necessity to refine the grid around that area. By refining the grid around the breach, computational errors and insecurities can be avoided. However, more grid cells mean a longer computational time. Therefore the grid is only refined locally and not throughout the complete domain.

Both the Flow module and the Wave module need their own individual computational grids. Figure 4.3 shows the Flow grid on the left and the Wave grid on the right. The grid refinements are clearly visible near the breach. The flow grid consists of a $430m$ by $430m$ polder area at the top and a foreshore of $430m$ by $540m$. The grid cell size at the boundary of the polder area is $6.5m$ by $14.0m$ and is refined to $2.5m$ by $4.0m$ at the breach. The wave grid requires a larger domain since the waves need their necessary space to develop in shallower water and to avoid inaccuracies at the boundaries. The inner part of the wave grid consists of the same grid as the flow grid, only the outer part is extended by extra grid cells. The upper part of the wave grid behind the primary dike has a size of $850m$ by $430m$. The foreshore of the wave grid measures a width of $850m$ and a length of $1140m$ (see figure 4.3).

4.1.5. Bathymetry

The bathymetry of the base-case model is a simplification based on the original bathymetry map of the Tollesbury research site recorded in 1995, right after the breach was made (see figure 3.4). According to the map, the bed level at the breach is around $OD + 1.0m$ and progressively increases to $OD + 2.25m$ near the back of the polder. For the Tollesbury calibration of the base-case model, this data will be linearly projected to the model bathymetry, meaning that the bed level will have a uniform slope from $OD + 1.0m$ at the breach to $OD + 2.25m$ at the back.

However, the polder bed in the to be used base-case model, after the calibration process, will have a near-horizontal bed. A near-horizontal bed will allow for better comparisons when altering certain parameters. When for example the mean water level would be linearly increased in combination with the sloped polder bed, the tidal prism would not increase linearly, which could lead to foul conclusions. For this reason, the bed of the base-case model will be near-horizontal. The polder bed cannot be completely horizontal due to numerical issues with flooding and drying of horizontal cells. When large numbers of horizontal grid cells would

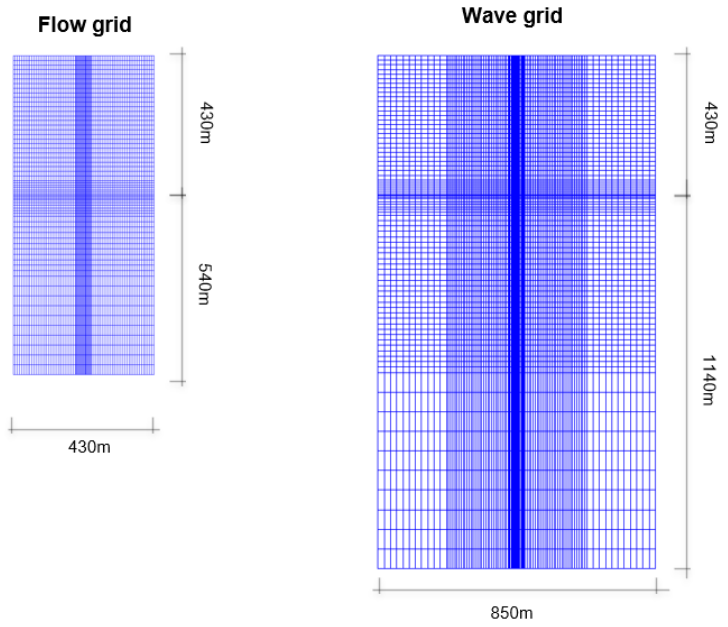

Figure 4.3: Computational grids that are used by the FLOW and WAVE module of Delft3D. On the left: the flow grid. On the right: Wave grid

instantaneously flood or dry in Delft3D, numerical instabilities are of frequent occurrence. Incorporating a very mild slope in the polder bed (an offset of $0.1m$ over the total length of the polder basin) will evade this problem and allows for a smooth run-off, hence the near-horizontal polder bed level.

The bathymetry of the foreshore of the base-case model is based on the slope of the original tidal channel. The tidal channel in front of the breach reaches a depth of $OD-2.0m$ at a distance of $540m$ from the breach, as is shown by figure A.13. As stated earlier, the base-case model would adhere to a uniform sloped foreshore with a similar slope to the tidal channel found at the Tollesbury case. All three bathymetries for the separate models of the three-step validation process are depicted in figure 4.4. The bathymetry for the wave grids will copy the bathymetry of the flow grids, only with an extended horizontal foreshore and an elongated primary dike. Figure 4.5 shows all the dimensions of the modelled bathymetry for the flow and wave grids of the final base-case model.

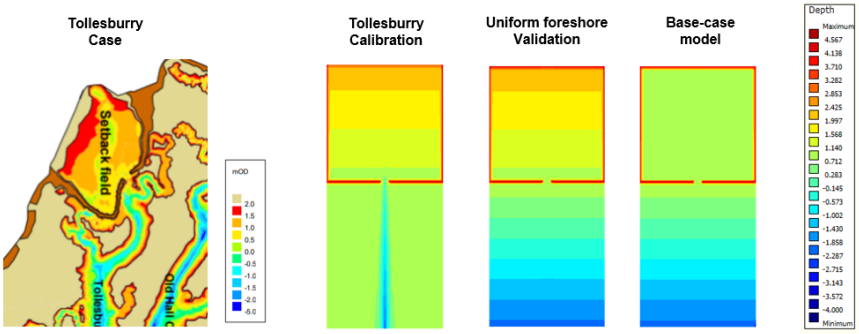

Figure 4.4: All three bathymetries of the flow grids for the three-step validation process in comparison to the bathymetry of the Tollesbury case

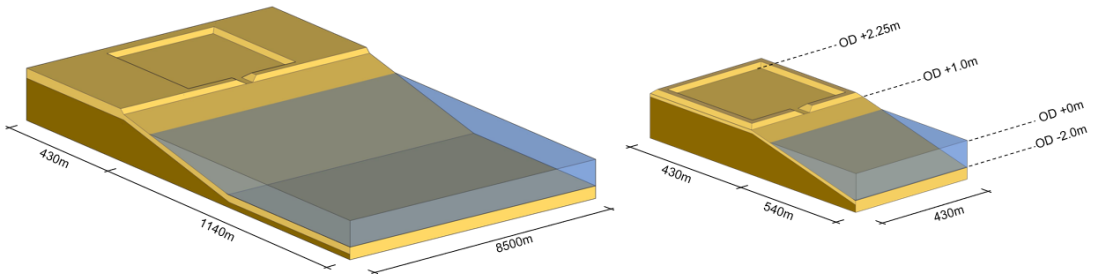

Figure 4.5: 3D schematization of the base-case bathymetry for the wave grid (left) and for the flow grid (right)

4.1.6. Boundary conditions

In order to simulate the forcing parameters that are present at the Tollesbury case, a group of boundary conditions have to be set along the western side of the model. These boundary conditions and their prescribed magnitudes and parameter settings will be discussed in this section.

Tide

In subsection 3.3.1 the tidal forces present in the Tollesbury estuary are discussed. The measurements from Pye et al. 1993 indicate a mean tidal range to be $4.7m$ during spring tide and $3.0m$ during neap tide. This data can be transformed into a tidal signal represented by two tidal constituents. By only using two tidal constituents, the tidal signal will be simplified to the most basic level, including spring tide and neap tide for a semi-diurnal tide. The two tidal constituents that were incorporated in the model are the principal lunar semi-diurnal constituent (M2) and the principal solar semi-diurnal constituent (S2). The amplitudes of the two tidal constituents can be computed separately as is done via calculations 4.1 and 4.2, resulting in a lunar component of $M2 = 1.925m$ and a solar component of $S2 = 0.425m$. Figure 4.6 shows the tidal input signal of the two constituents combined.

$$\text{Amp M2} = (4.7/2–3.0/2)/2 + 3.0/2 = 1.925m \tag{4.1}$$

$$\text{Amp S2} = (4.7/2–3.0/2)/2 = 0.425m \tag{4.2}$$

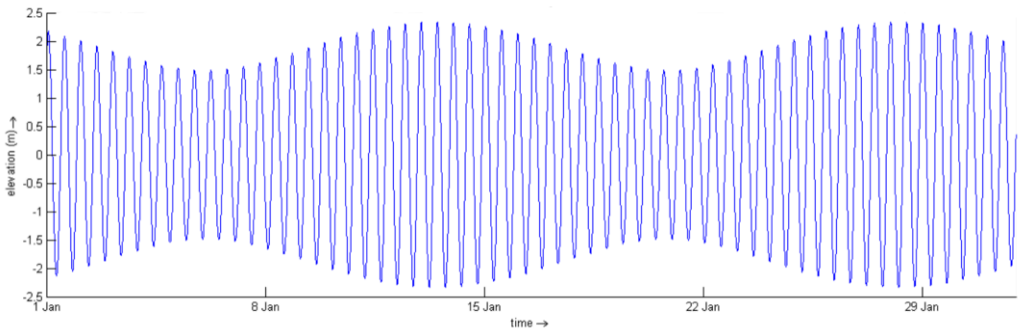

Figure 4.6: Model tidal boundary signal during two months. Consisting of a lunar component of $M2 = 1.925m$ and a solar component of $S2 = 0.425m$

Waves

Waves that occur at the Tollesbury research site nearly all consist of wind created waves, since the estuary is nearly completely sheltered from large ocean waves or swell waves. Following the findings from subsection 3.3.3, the dominant wave forcing consists of wind waves with a significant wave height of $0.2m$ and wave period of $T = 2s$. These values are found under the assumption that there is a constant wind force of $u_f = 5.21m/s$. In reality, these wind forces and thus the found wave characteristics vary continuously over

time. Simulating a realistic and continuously varying wave field would give more truthful results, but will make it less useful for proper comparisons between different scenarios. In order to keep the scenarios simple and thus comparable, a single wave field is used. By making the angle of incidence equal to zero degrees (perpendicular waves relative to the coastline) all hydraulic processes inside and outside the polder will be symmetrical, given that the dimensions are symmetrical and there are no extra lateral forces. Incorporating this in the base-case model will further improve the comparability.

The communication file between the Flow and Wave module has an interval of 120 minutes, meaning that every two hours a computation is made that creates a wave field based on the bathymetry and water level at that exact moment. A shorter communication interval would lead to more accurate computations for shorter simulated periods. Test simulations, however, showed that the results of relatively large communication intervals (120 minutes) are similar to the results of simulations with smaller communication interval times, given that the simulation period is sufficiently long.

Suspended sediment concentration

As was explained in subsection 4.1.2 two individual sediment fractions will be present in the model: the 'Mud Suspended' fraction and the 'Mud Bed' fraction. A constant sediment input will be imposed on the seaward boundary by the 'Mud Suspended' fraction. The three separate studies cited in subsection 3.3.4 measured three different suspended sediment concentrations ranging from an average of $150 mg/l$ to $70 mg/l$. Given that the higher levels of SSC were measured closer to the bed where the concentration is higher, an SSC of $100 mg/l$ was assumed to be a representative value for the 'Mud Suspended' fraction. This fraction will, however, only be assigned as an SSC at the boundary and will not be initially present in the bed layer. The 'Mud Bed' fraction on the other hand will be present as the initial bed layer but will have a zero input at the boundary. Making this distinction ensures a more true to nature model by differentiating in the difference between the already existing bed layer and the suspended sediment. Table 4.1 gives a summary of the assigned SSC values per sediment fraction.

Table 4.1: Suspended sediment concentration at the seaward boundary for both sediment fractions, including initial bed layer thickness

Sediment fraction	Begin concentration [kg/m3]	End concentration [kg/m3]	Initial bed layer thickness [m]
Mud Suspended	0.1	0.1	0
Mud Bed	0	0	3

4.1.7. Parameter settings

This chapter will discuss all the individual parameter settings that are adjusted according to the Tollesbury case. All parameter settings will be deducted from historic data covered in subsecton 3.3. Parameter settings that are not discussed in this section are assumed to remain their default settings following from the Delft3D manual (Deltares 2014).

Time frame

All simulations used in this research will start from a '01-01-2021' reference date. The runs will have a simulation stop time depending on the purpose of each simulation and will be clearly stated for each individual run. The time step that is used for each simulation is set to nine seconds. The validation of this particular time step will be evaluated in subsection B.5.1 based on the Courant number.

Initial conditions

The initial conditions of the base-case model indicate the starting values for the water level and the initial suspended sediment concentrations that are present in the water for the individual sediment fractions. The initial water level is set to be at Mean Sea Level (MSL). Both the initial conditions of the sediment fractions for SSC are assumed to be $0 mg/l$ in order to avoid immediate sedimentation in the polder. Test simulations showed that the suspended sediment concentrations reach their equilibrium values over the model area after three tidal cycles. The water in the model is adjusted to represent saltwater by setting the water density to $1025 kg/m^3$.

Sediment Characteristics

As mentioned before, the two individual sediment fractions have been appointed to simulate the more erosion-resistant consolidated bed material that is already present in the initial polder bed and the lighter, more susceptible for erosion, suspended sediment. Each of these sediment fractions has its own sediment characteristics. Both the 'Mud suspended' and the 'Mud Bed' fraction are appointed cohesive sediment. Table A.1 indicates that the sediment found at the Tollesbury case consists of three different sediment types: Clay, silt and sand. The weight ratio of clay and silt in the soil is around half-half, with approximately 6% sand. Per individual sediment fraction, these three different sediment types have been processed into a single overarching type with the purpose of remaining simplicity. The specific density of a mixture of clay, silt and sand can range from $2536 kg/m^3$ to $2716 kg/m^3$ (Schjønning et al. 2017). An average specific density of $2650 kg/m^3$ is assumed for both fractions.

The dry bulk density of the sediment at Tollesbury has been measured Watts et al. 2003 at several different locations within and around the Tollesbury research site (see table A.1). The dry bulk density of a soil sample from the original and consolidated polder soil (area FL in figure A.12) is found to be $660 kg/m^3$. Other samples in and around the polder showed dry bulk densities between $460 kg/m^3$ and $640 kg/m^3$. To be on the conservative side, the dry bulk density of the 'Mud Suspended' fraction is assumed to equal the 'Mud Bed' fraction. Having a slightly higher dry bulk density for the suspended fraction implicates that the computed bed levels in the model will be a fraction lower than in reality. However, these values will lead to more realistic bed levels once the polder is closed off and the ground is fully consolidated.

Both the freshwater settling velocity and the saline settling velocity are assumed to be equal for both sediment fractions. The settling velocity of silt and clay particles is very dynamic due to the varying range in shapes and due to the process of fluctuation (Van Rijn 2020). The settling velocity that is used in the model is based on the particle size-frequency distribution found near Tollesbury (figure A.11) and is estimated to be $0.15 mm/s$, based on several settling velocity calculations (Cheng 1997).

The critical shear stress for sedimentation indicates the critical shear stress above which sedimentation does not occur. In order to always allow for a sedimentation calculation, the value is kept at its default value of $1000 N/m^2$. The critical shear stress for erosion indicates the critical shear stress below which erosion does not occur. Measuring the critical shear stress for erosion is an arduous process, making the determination of a single value a difficult task. Measurements by Watts et al. 2003 indicate that the original soil at the Tollesbury polder has a critical shear stress for erosion several factors larger that the freshly settled sediment. Van Rijn 2020 performed several studies on determining critical shear stresses for different soil types and states that fresh muddy sediment has a critical shear stress for erosion much lower than what was found at the Tollesbury site. This substantiates the fact that determining the critical shear stress for erosion remains an arbitrary process. For this particular base-case model a critical shear stress for erosion for the suspended fraction is assumed to be $0.05 N/m^2$ and for the bed fraction $2.0 N/m^2$, both within the limits of Van Rijn 2020 and Watts et al. 2003. Lastly, the Erosion parameter is set to be $0.001 kg/m^2/s$ for the suspended fraction and $0.00001 kg/m^2/s$ for the bed fraction. These values are typical for a two fraction cohesive sediment model (Winterwerp et al. 2012). All used parameters for the base-case model are summarized in tables 4.2 and 4.3.

Table 4.2: Sediment characteristic values used for the base-case model for both sediment fractions: Specific density, Dry bed density, Fresh settling velocity and Saline settling velocity

Sediment fraction	Specific density $[kg/m^3]$	Dry bed density $[kg/m^3]$	Fresh settling velocity $[mm/s]$	Saline settling velocity $[mm/s]$
Mud suspended	2650	660	0.15	0.15
Mud bed	2650	660	0.15	0.15

Table 4.3: Sediment characteristic values used for the base-case model for both sediment fractions: Critical shear stress for sedimentation, Critical shear stress for erosion, Erosion parameter and Initial layer thickness

Sediment fraction	Crit shear stress for sedimentation $[N/m^2]$	Crit shear stress for erosion $[N/m^2]$	Erosion parameter $[kg/m^2/s]$	Initial layer thickness $[m]$
Mud suspended	1000	0.05	0.001	0
Mud bed	1000	2	0.00001	3

Morphology

Where hydrodynamics vary over relatively short periods of hours and minutes, morphodynamic changes develop over much longer time scales. Slight changes of a couple of millimetres in bed level can take months or sometimes even years. Modelling the morphological changes in the bed level can therefore become extremely computationally expensive. In order to curtail the computation times, a so-called morphological time scale factor (MorFac or MF) can be implemented. This factor multiplies the deposition and erosion fluxes between flow and bed and thereby accelerating the morphological changes and reducing the computational costs. Although a high morphological factor can significantly shorten run times, there are limitations to the magnitude of the factor. These are not fixed limitations but are depended on the type of simulation. By performing certain checks one can find a suitably large MorfFac without disturbing the overall hydro- and morphodynamics. This specific base-case model makes use of a MorFac of 24, meaning that every simulated month in the model translates to two years of real-time morphodynamic changes. Section B.5.2 will go further into the validation process of the MorFac used in this study. The monitoring details are further elaborated on in Section B.1.

4.2. Base-case model validation

This section will elaborate on the complete three-step validation process that will result in the final base-case model. First, the Tollesbury calibration model will be compared to the historic sedimentation data from the Tollesbury case study to which it is calibrated. Following that, the first simplification step of assuming a uniform foreshore, called the Uniform Foreshore Validation model, will be compared to the Tollesbury Calibration model. The last step of the validation process will consist of comparing the final base-case model (with the near-horizontal polder bed simplification) to the Uniform Foreshore Validation model.

4.2.1. Tollesbury Calibration

The main process on which the model is calibrated is the average bed level change in the polder. This change in bed level is predominantly caused by sedimentation processes of fine cohesive sediments in the polder. The Tollesbury calibration model is simulated for a real-time period of 12, 24 and 48 years. First, the results for the simulation period of 12 years are evaluated, since the observed data of the Tollesbury case also represent 12 years of operation. Figure 4.7(a) shows both the initial bed level at the start of the simulation and the bed level after 12 years of real-time simulation. Figure 4.7(b) displays the net bed level change of the simulated period. The same model is simulated for a real-time period of 24 years which is depicted likewise in figure B.3.

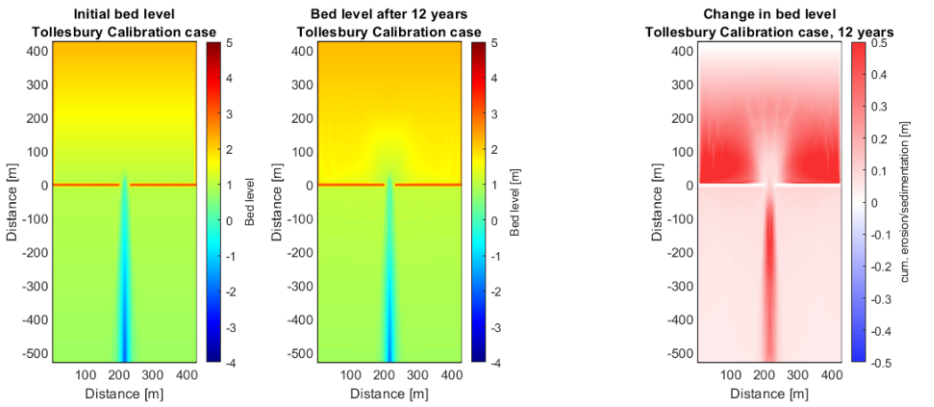

(a) Both the initial bed level on the left and the bed level after 12 real-time years.

(b) Change in bed level plotted by cumulative sedimentation/erosion.

Figure 4.7: Bed level change of the Tollesbury calibration model after a real-time period of 12 years.

The occurring pattern in sedimentation resembles the sedimentation described in the Tollesbury historical data. E.g., The landward area of the polder accretes at the slowest rate, but remains the highest in bed level overall due to its higher initial bed level and thus shorter inundation period. The seaward polder area on both sides of the breach shows the highest sedimentation rates. Price 2016 showed that the vegetation line slowly shifted from the landward side of the polder to the center part of the polder during the 12 years of monitoring. This advancement of the vegetation line is mainly caused by the rise in bed level which leads to reaching the threshold depth for vegetation growth. The resemblance is found in the fact that the initially sloped polder is rising to a rather horizontal equilibrium profile. This process is clearly noticeable when taking a closer look at the different cross-sections of the model over time, which are presented in figure 4.8. The figure also shows the development of two small tidal channels near the breach that help with the drainage of the polder. The tidal flats in front of the polder only undergo minor sedimentation, as was also measured at the Tollesbury case study.

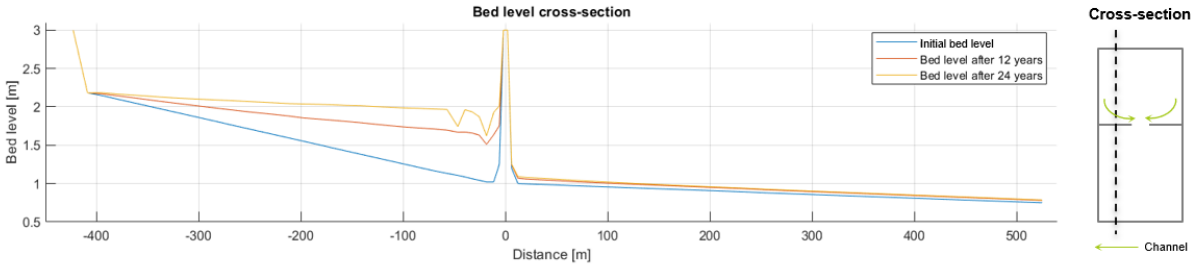

Figure 4.8: Bed level cross-sections perpendicular to the coastline, With the secondary dike at the left side and the seaward boundary on the right. The location of the cross-section is depicted in the right schematization. Bed levels are plotted for year 0, year 12 and year 24

The main tidal channel on the foreshore shows slight initial sedimentation, but reaches an equilibrium state which is shown by figure B.4. The historical data of the average change in bed level at the Tollesbury research site is plotted with the average change in bed level resulting from the Tollesbury calibration model in figure 4.9. The average rate of bed level change from the historical data was deduced from 25 measurement locations throughout the polder area, whereas the average bed level change from the numerical model has been determined by the change in bed level averaged over each grid cell. The parameter settings deducted from the Tollesbury case study that were described in the previous section result in an average bed level change following a similar trend as the historical observed data set. Not only the trend, but also the magnitude shows a significant resemblance, being only slightly lower than the observed data. The large scale 'wiggles' that can be observed in the sedimentation rate of the model displayed in figure 4.9 are caused by the effect of neap tide and spring tide in combination with a morphological factor of 48.

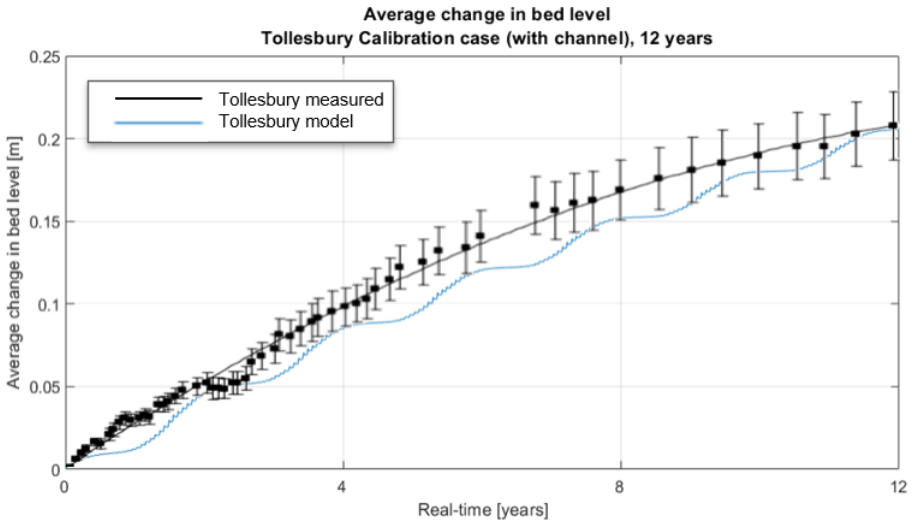

The a

Figure 4.9: Average change in bed level for both the Tollesbury calibration model and the Tollesbury case study from 1995 to 2008

The same run for the Tollesbury calibration model is also performed for a real-time period of 48 years. The average rate in bed level change during this period is displayed in figure 4.10. The data shows a distinct reduction in sedimentation rate where the average bed level change reaches for an equilibrium state, where the change in bed level is zero. This state is extrapolated to an equilibrium around $0.45m$ of total average bed level change.

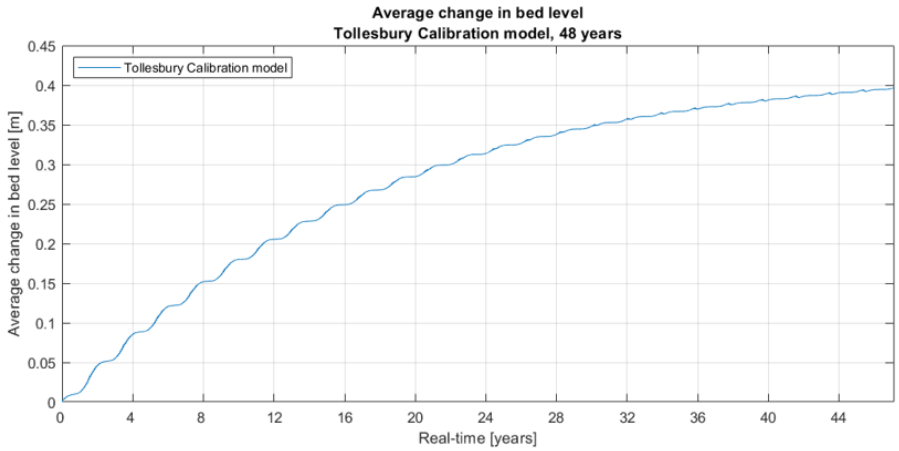

Figure 4.10: The average change in bed level for both the Tollesbury calibration model for a real-time period of 48 years

4.2.2. Uniform Foreshore Validation

This subsection will compare the results of the Tollesbury calibration model to the simplified Uniform Foreshore validation model, where tidal channels and tidal flats are neglected and replaced by an alongshore uniform foreshore. Both models are simulated for a longer real-time period of 24 years in order to observe the future trend. Figure 4.11(a) shows both the initial bed level at the start of the simulation and the bed level after 24 years of real-time simulation. Figure 4.11(b) displays the net bed level change of the simulated period.

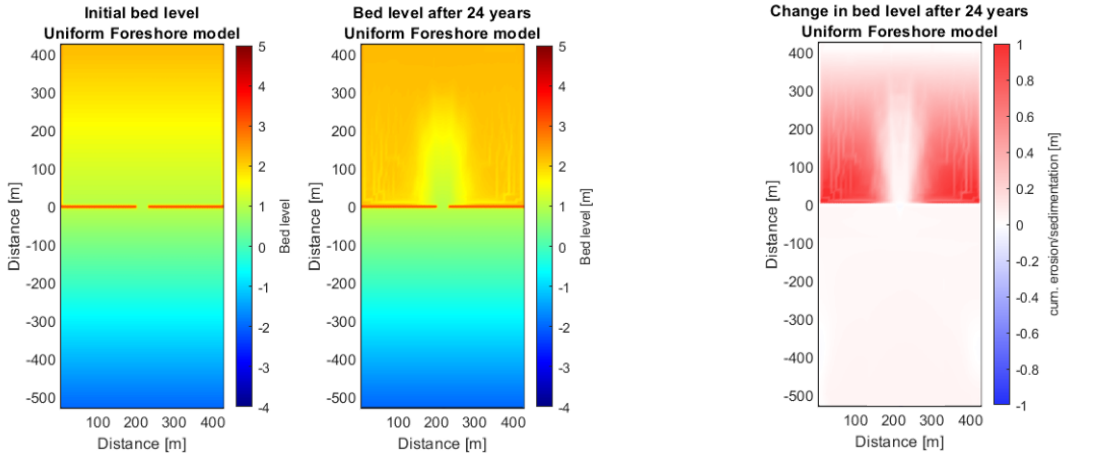

(a) Both the initial bed level on the left and the bed level after 24 real-time years on the right.

(b) Change in bed level plotted by cumulative sedimentation/erosion.

Figure 4.11: Bed level change of the Uniform Foreshore model after a real-time period of 24 years.

The average change in bed level is plotted for both the models and is compared with the Tollesbury historical data in figure 4.12. The initial rate of sedimentation is higher for the Uniform Foreshore model, with an average total bed level change being $3.5cm$ higher after 12 years. Both models appear to converge again to the same line after 24 years. The higher initial rate of sedimentation for the uniform foreshore is predominantly caused due to higher levels of SSC for the incoming tide. The higher level of incoming SSC is caused by the absence of wave breaking on the removed tidal flats. Figure B.5 shows the significant wave height right in front of the breach for both models. The observed significant wave height is more than a factor two higher for the uniform foreshore in comparison to the foreshore with tidal flats of the Tollesbury calibration model. Since the incoming waves have a certain level of directional spreading, some waves have to travel across the tidal flats before they reach the breach for the Tollesbury calibration model, causing the waves to lose their energy. Since this is not the case for the uniform foreshore, significant wave height is higher at the breach, making the incoming SSC higher and thus the initial rate of sedimentation higher (see figure B.6).

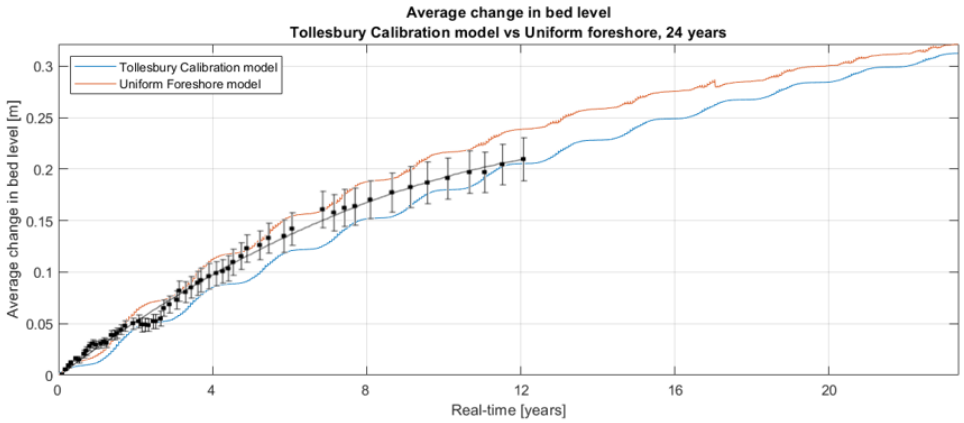

Figure 4.12: Comparison between the average bed level change of the Tollesbury Calibration model, the Uniform Foreshore validation model and the Tollesbury historical data. Both with the same real-time period of 24 years.

The waves immediately start to diminish when entering the shallow polder. Since the significant wave height is higher at the breach for the uniform foreshore, less sedimentation is observed right after the breach due to this dissipation in wave energy. Figure 4.13 shows this effect by comparing the bed level change of the Tollesbury calibration model with the Uniform Foreshore model. The Uniform Foreshore model clearly shows less sedimentation in the area behind the breach. The so to say 'pit' that arises is larger in diameter compared

to the Tollesbury calibration model. However, more sediment is being trapped at the sides of the polder making the net sediment import of the Uniform Foreshore model more efficient.

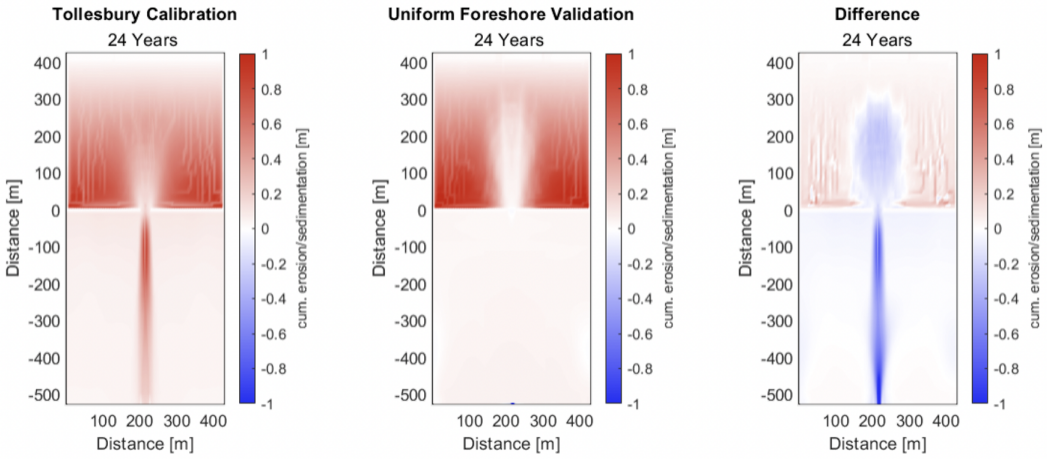

Figure 4.13: Comparison between the bed level change of the Tollesbury Calibration model and the Uniform Foreshore validation model. Both with the same real-time period of 24 years. Left: Tollesbury Calibration model. Middle: Uniform Foreshore validation model. Right figure: Difference in sedimentation and erosion between the two models

4.2.3. Near-horizontal polder Validation - Final Base-case model

This subsection will discuss the results of the final simplification of replacing the sloped polder bed used at the Uniform Foreshore model with a near-horizontal polder bed. The results will be compared to the results of the Tollesbury calibration model and the Uniform Foreshore model. The model will have a real-time simulation period of 24 years. Figure 4.14(a) shows both the initial bed level at the start of the simulation and the bed level after 24 years of real-time simulation. Figure 4.14(b) displays the net bed level change of the simulated period. Various processes change with the implementation of the simplification to a near-horizontal polder bed.

The foremost reason for this is the increase in the tidal prism. By changing the sloped polder bed to a horizontal bed at the bed level of the seaward side of the polder, the total water volume that is exchanged during each tidal cycle is nearly doubled. Figure B.7 shows a plot of the total water volume inside the polder during each tide for both models. The effect of the rise in bed level is directly visible in the decrease of tidal prism over time. Due to the higher levels of sediment import and the larger volume of water that is transported throughout the polder, the formation of tidal channels within the polder area is promoted. The arising tidal channels are very well distinguished in the bed level after 24 years shown in figure 4.14. The figure also shows that the increase in tidal prism, and thus the increase in maximum instantaneous discharge through the breach, causes higher erosive force in the breach which deepens the bed level at the breach area.

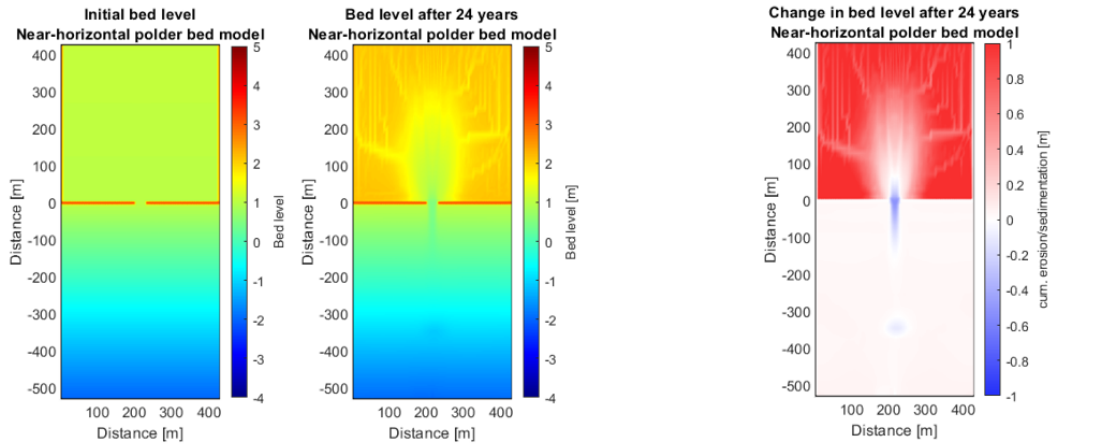

(a) Both the initial bed level on the left and the bed level after 24 real-time years on the right.

(b) Change in bed level plotted by cumulative sedimentation/erosion.

Figure 4.14: Bed level change of the Near-horizontal model (Base-case model) after a real-time period of 24 years.

Comparing the average change in bed level for the near-horizontal polder bed model to the other two validation models shows the effect of the increase in tidal prism (see figure 4.15). Not only the initial sedimentation rate is higher, but also the equilibrium bed level is higher. The average change in bed level for the Near-horizontal polder bed model is $0.58m$ after 24 years, making it a factor 1.8 higher than the $0.32m$ of average bed level change for the Uniform Foreshore model. The difference in initial tidal prism between these two models result in exactly the same factor suggesting the distinct correlation between the tidal prism and average bed level change ($240 * 10^{-5}/135 * 10^{-5} \approx 1.8$).

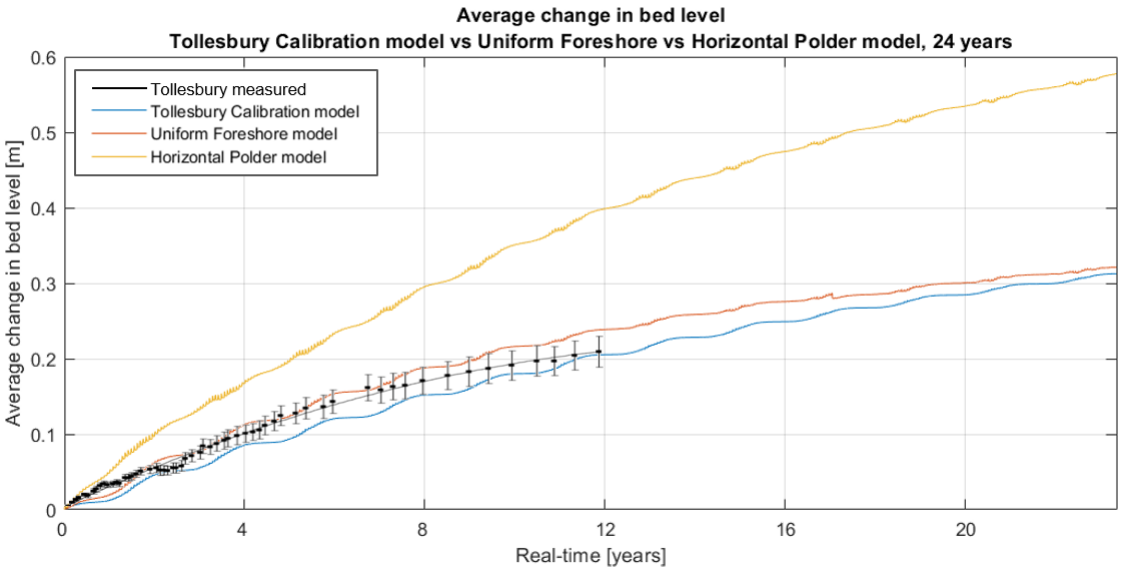

Figure 4.15: Comparison between the bed level change of the Tollesbury Calibration model, the Uniform Foreshore validation model, and the near-horizontal polder bed model. All with the same real-time period of 24 years. The historical data from the Tollesbury case study is overlaid in black

Figure 4.16 shows the comparison between the bed level change of the Uniform Foreshore validation model and the Near-horizontal polder bed model (base-case model) after a real-time period of 24 years. The comparison indicates the more distinct formation of tidal channels in the polder for the Near-horizontal polder bed model.

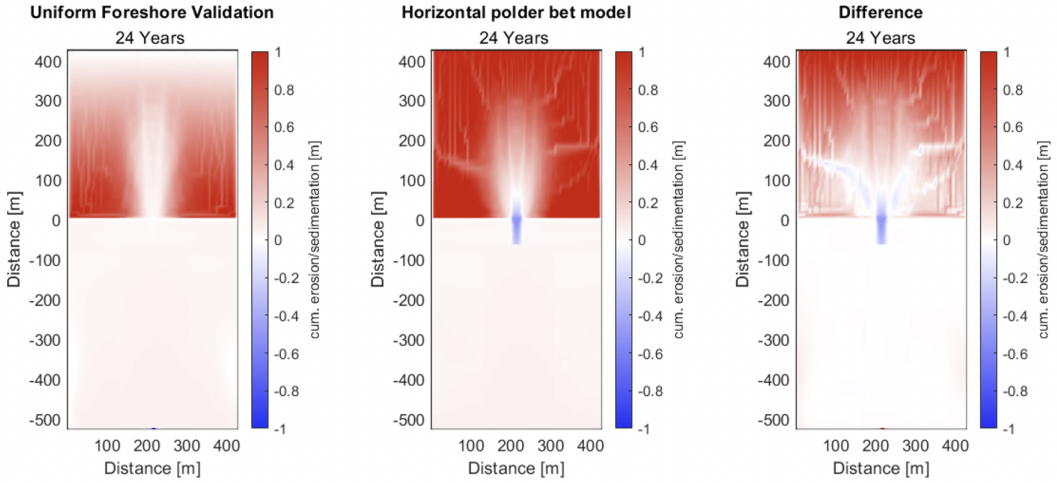

Figure 4.16: Comparison between the bed level change of the Uniform Foreshore validation model and the Near-horizontal polder bed model (base-case model). Both with the same real-time period of 24 years. Left: Uniform Foreshore validation model. Middle: Near-horizontal polder bed model. Right figure: Difference in sedimentation and erosion between the two models

In conclusion to this section, three separate models were compared in order to assess the effect of a set of simplifications, which would lead to the base-case model. The first model, the Tollesbury Calibration model, showed that it was possible to recreate the morphological changes that were observed at the Tollesbury research site with a numerical model in Delft3D. The second model, the Uniform Foreshore model, showed that the assumption of an alongshore uniform foreshore resulted in a slightly higher initial rate of sedimentation due to the higher levels of wave energy entering the polder. The third model, the Horizontal Polder model, resulted in a strong increase in equilibrium bed level and initial rate of sedimentation due to the increase in tidal prism. This model will be used in the next chapter as the base-case model for the parameter scenario comparisons.

4.3. Numerical validation

The remainder of this section will discuss the validation of the morphological factor and the appropriate time step for the final base-case model. A morphological factor of 48 was proven to be the maximum factor without causing instabilities or deviations in comparison to models with lower morphological factors. The maximum time step was validated by the CFL condition and by comparing the results of a model with a time step twice as small. A time step of $\Delta t = 9s$ was found to be the sufficient time step. A complete description of both validation processes can be found in Appendix B.5.

4.4. Delft3D Morphodynamic model - Scenarios

The sensitivity analysis of the individual parameters is based on different scenarios for each parameter. This section will go over the setup of all the scenarios for the different sediment characteristics, dimensional parameters and hydraulic parameters.

4.4.1. Sediment characteristics

Suspended sediment concentration - SSC

The sensitivity to the suspended sediment concentration will be determined by comparison of the base-case with four other scenarios with varying levels of suspended sediment concentrations at the boundary assigned within the 'Mud suspended' sediment fraction. All other parameters will remain equal to the base-case model. The four separate scenarios for SSC will consist of suspended sediment concentrations both lower and higher than the base-case value of 100mg/l. All the assigned values of the scenarios are displayed in table 4.4.

Table 4.4: All five scenarios that were used for the determination of the sensitivity of the SSC on sedimentation rates with their assigned values of SSC at the seaward boundary.

Scenario	SSC = 25mg/l	SSC = 50mg/l	SSC = 100mg/l	SSC = 150mg/l	SSC = 200mg/l
SSC	25mg/l	50mg/l	100mg/l	150mg/l	200mg/l

Critical shear stress for erosion Suspended fraction

Based on the validation process handled in the previous section, the critical shear stress for erosion of the suspended sediment fraction was determined to be $0.05 N/m^2$. Since the value of this specific parameter can have significant influences on the processes of sedimentation and erosion within the polder. Strongly flocculated particles or larger and heavier particles would lead to larger values of critical shear stress for erosion and would therefore be tested on its sensitivity to change. A total of four scenarios, under which the base-case, will be compared. The values of critical shear stress for erosion will range from $0.05 N/m^2$ to $0.20 N/m^2$. All the separate scenarios and their values are summarized in table A.2.

Table 4.5: All four scenarios that were used for the determination of the sensitivity of the value of critical shear stress for erosion on sedimentation rates with their assigned values for critical shear stress for erosion of the suspended fraction.

Scenario	$\tau_e = 0.05 N/m^2$	$\tau_e = 0.10 N/m^2$	$\tau_e = 0.15 N/m^2$	$\tau_e = 0.20 N/m^2$
Critical shear stress for erosion	$0.05 N/m^2$	$0.10 N/m^2$	$0.15 N/m^2$	$0.20 N/m^2$

Critical shear stress for erosion Bed fraction - non-erodible bed

Two scenarios for the critical shear stress for erosion of the bed fraction will be compared to determine the effect of a non-erodible bed layer, with the main reason for this being the creation of a benchmark model for scenarios with a non-erodible bed. A select group of parameter scenarios require a non-erodible bed in order to remain one-on-one comparable, since the variation of the parameter would result in an increase in tidal prism and therefore significantly affect the depth of the breach. For this, the comparison is made between the base-case with and without an erodible bed. The bed layer is made non-erodible by setting the critical shear stress of erosion of the bed fraction to $100 N/m^2$. The two scenarios are summarized in table 4.6.

Table 4.6: Values for the critical shear stress for erosion of the bed layer for the base-case scenario with an erodible bed and the base-case scenario without an erodible bed

Scenario	Erodible bed	Non-erodible bed
Critical shear stress for erosion - bed layer	$2.0 N/m^2$	$100.0 N/m^2$

4.4.2. Dimensional characteristics

Breach width

The sensitivity of the dimensions of the breach is determined by simulating three separate scenarios with varying breach dimensions. The variation in breach dimension will be realized by the adjustment of one single parameter: the breach width. The depth of the initial breach will be kept constant to the initial bed level of the polder at the breach, which is at $OD + 1m$. The base-case with a breach width of 50m will be compared to an identical polder with a breach width of $100m$ and an identical polder with a breach width of $150m$. The effect on sediment import of narrowing the breach will also be evaluated by a scenario with a breach width of $25m$. All the scenarios for the effect of the width of the breach are summarized in table 4.7.

Table 4.7: All four scenarios that were used for the determination of the sensitivity of the breach width on sedimentation rates with their assigned dimensions of the breach width.

Scenario	Breach = 25m	Breach = 50m	Breach = 100m	Breach = 150m
Breach width	25m	50m	100m	150m

Polder width

The width of the polder is a construction parameter, meaning that the width is not a prescribed value, but can be established by the designer himself by placing the perpendicular dikes at a certain distance from each other. Whenever the dimension of the width is changed, the tidal prism will change accordingly. Former test simulations have shown that when the width is increased with the breach width staying constant at $50m$, tidal dampening would occur, meaning that the water level inside the polder changes with a certain phase shift slower than the water level outside the polder. Figure B.11 shows this effect for the different scenarios with equal breach dimensions. Doubling the polder width resulted in tidal damping with nearly $0.5m$ in water level difference between outside and inside the polder. The main reason for this is that the surface area of the breach is too small to accommodate the required discharge following the tidal prism. A damped system results in a significant increase in flow velocity through the breach, leading to extensive erosion pits in between the breach and concentrated flow patterns within the polder. In a normal situation, where the breach would just consist of a cut-out of a normal dike, the high flow speeds would erode the sides of the dikes at the entrance, widening the breach until the equilibrium state of the breach is reached. This process had to be removed from the simulation scenarios in order to acquire a better comparison.

For this reason the decision was made to couple the breach width to the tidal prism, avoiding a damped system. This coupling is possible due to the fact that the breach width is also a design parameter. Figure B.11 shows that there is minimal tidal damping for the base case scenario with a breach width of $50m$. When the polder width is increased by a factor of 1.5 (from $430m$ to $645m$) the tidal prism increases with the same factor. In order to keep flow velocities through the breach constant, the breach surface area needs to increase with the same factor of 1.5. This is done by enlarging the breach with a factor of 1.5. This process is performed on all scenarios for the polder width, as can be seen by the initial bathymetry maps of the separate scenarios displayed by figure 5.10. In order to avoid further secondary effects of change in the breach surface area, the bed at the breach will be assumed to be non-erodible. All the dimensions of the polder width and the breach width are summarized in table4.8.

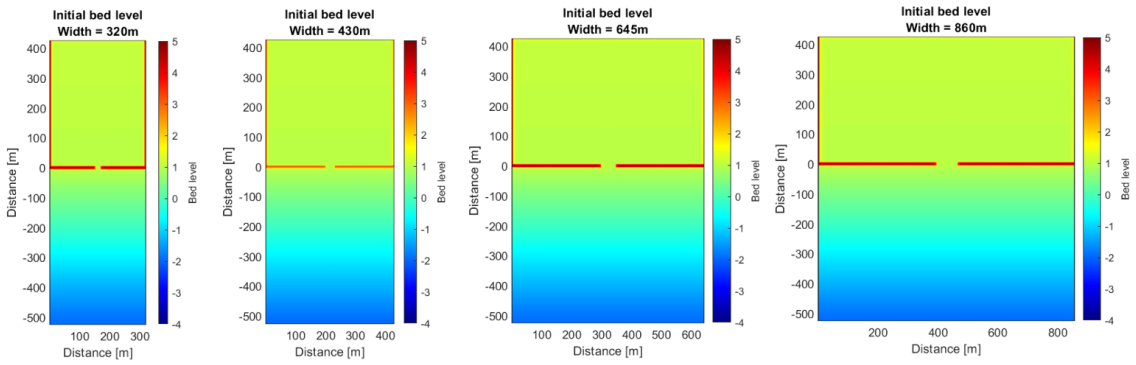

Figure 4.17: Initial bed levels of the polder width scenarios for all individual dimensional polder widths. Bed level is indicated depth relative to the ordnance datum (OD)

Table 4.8: All four scenarios that were used for the determination of the sensitivity of the polder width on sedimentation rates with their assigned dimensions of the polder width and the breach width.

Scenario	Width = 320m	Width = 430m	Width = 645m	Width = 860m
Polder width	320m	430m	645m	860m
Breach width	37m	50m	75m	100m

Polder length

The scenarios for the length of the polder follow the same principle as the scenarios for the width of the polder. A total of 4 scenarios will be compared with a dimensional length ranging from $320m$ to $860m$. All scenarios will have a breach width adjusted to the increase or decrease in tidal prism, similar to the scenarios of the polder width. The separate initial bathymetries for the four scenarios are displayed by figure 5.13. Equal to the scenarios for the determination of the sensitivity of the polder width, the bed surface around the

breach will be assumed to be non-erodible. The dimensions of the polder length and the breach width are summarized in table 4.9.

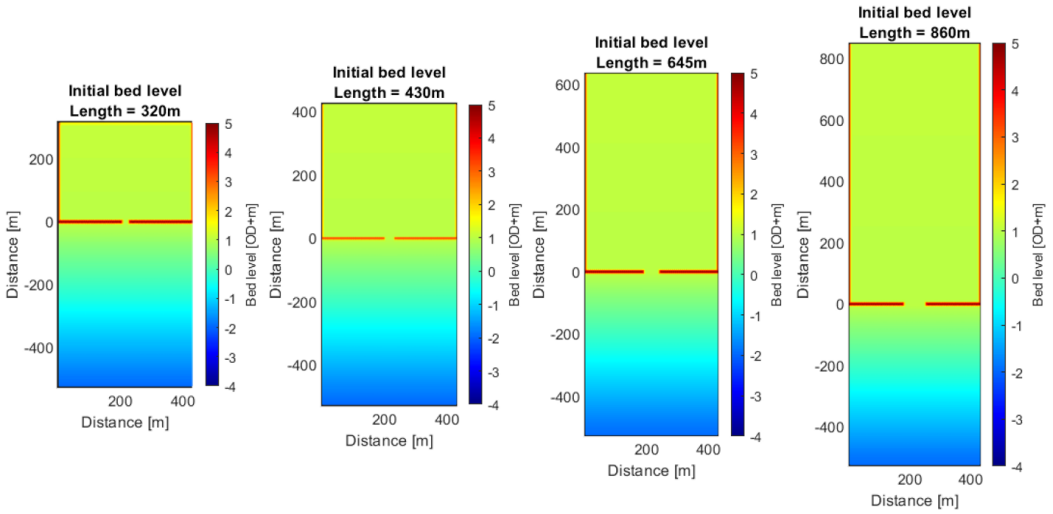

Figure 4.18: Initial bed levels of the polder length scenarios for all individual dimensional polder lengths. Bed level is indicated relative to the ordnance datum (OD)

Table 4.9: All four scenarios that were used for the determination of the sensitivity of the polder length on sedimentation rates with their assigned dimensions of the polder length and the breach width.

Scenario	Length = 320m	Length = 430m	Length = 645m	Length = 860m
Polder length	320m	430m	645m	860m
Breach width	37m	50m	75m	100m

Initial polder bed level

In order to determine the effect of the initial bed level of the polder area on the sedimentation within the polder, a total of five scenarios will be compared. The initial polder bed levels of the scenarios will range from $OD+1m$ to $OD-3m$, all with an equal sloped foreshore. The assumption is made that the bed level of the foreshore at the breach is equal to the bed level of the polder for all polder bed levels so that the transition of the polder bed to the foreshore is equal. Different test models for deeper polder bed levels showed a reduction in sedimentation due to the formation of high-velocity circular flow patterns within the polder, equal to what was observed with the larger polder width and length, and a larger tidal amplitude (due to the increase in the tidal prism, also see section 5.3.1). To overcome this problem, the breach of all the scenarios was widened with a factor 1.4 so that all scenarios would be equally comparable. Figure 4.19 shows the initial bathymetries for all used scenarios. Table 4.10 summarizes the used parameter settings for each scenario.

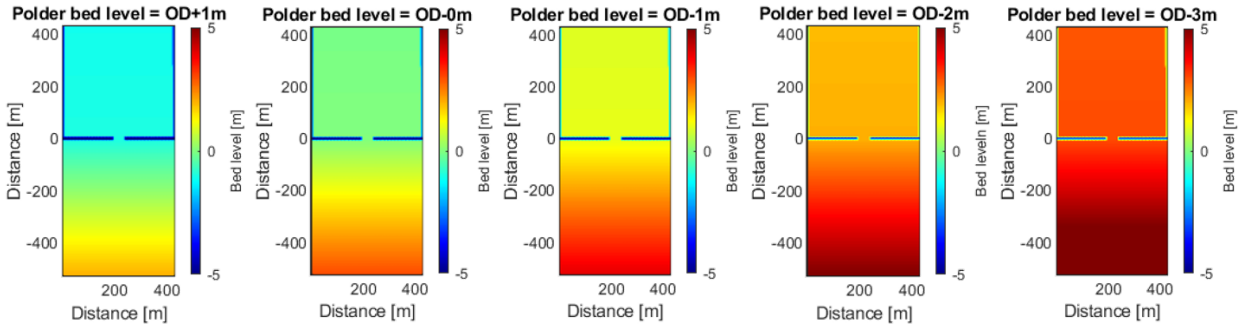

Figure 4.19: Initial bed levels for the 'polder bed level scenarios' for all individual polder bed levels. Bed level is indicated relative to the ordnance datum (OD)

Table 4.10: All five scenarios that were used for the determination of the sensitivity of the initial polder bed level on sedimentation rates with their assigned bed level relative to the Ordnance Datum (OD) and the breach width.

Scenario	Bed level +1m	Bed level -0m	Bed level -1m	Bed level -2m	Bed level -3m
Bed level	OD +1m	OD -0m	OD -1m	OD -2m	OD -3m
Breach width	70m	70m	70m	70m	70m

4.4.3. Hydraulic parameters

Tidal amplitude

The effect of the tidal amplitude on the sedimentation process within the Lease Polder will be determined by comparing three different scenarios with varying tidal amplitudes ranging from a maximum tidal amplitude of $2.0m$ to $3.5m$. The maximum amplitude of the tide is adjusted by means of changing the amplitude of the M2 tidal constituent. The amplitude of the S2 component will be kept constant at a value of $0.435m$. In order to ensure a one-on-one comparison between the scenarios, the polder bed between the breach is assumed to be non-erodible. All the parameter settings for the five scenarios for tidal amplitude are summarized in table 4.11

Table 4.11: All five scenarios that were used for the determination of the sensitivity of the tidal amplitude on sedimentation rates with their values of the M2 and S2 tidal constituent, including the maximum tidal amplitude and maximum tidal range

Scenario	Amp = 2.0m	Amp = 2.35m	Amp = 2.5m	Amp = 3.0m	Amp = 3.5m
M2 amplitude	1.575m	1.925m	2.075m	2.575m	3.075m
S2 amplitude	0.425m	0.425m	0.425m	0.425m	0.425m
Total maximum tidal amplitude	2.0m	2.35m	2.5m	3.0m	3.5m
Maximum tidal range	4.0m	4.7m	5.0m	6.0m	7.0m

Sea level rise - SLR

Sea level rise is an important factor within the usability and the potency of the concept of a Lease Polder. When a Lease Polder is able to accumulate sediment following to some extent the rate of sea level rise, one could consider the Lease Polder to be a self-sustaining form of coastal protection. In order to conclude whether a Lease Polder is able to compromise for sea level rise, or to which extent it can follow the rate of sea level rise a scenario including sea level rise is made based on the base-case. For this scenario, a uniform rate of sea level rise of $4.2mm/year$ is added to the uniform tidal forcing of the base-case by superpositioning a harmonic tidal function with a period of four times the simulation length (24 years) and an amplitude of $0.145m$. This results in a total sea level rise of $0.1m$ in 24 years.

In conclusion to this section, several model setups were described for the separate scenarios that will be used for the parameter sensitivity analysis. Each parameter specific sensitivity analysis will be based on the

comparison of the results for the individual parameter scenarios to the result of the base-case model. All Parameters that do not affect the tidal prism will only have a variation in that parameter for each scenario. Parameters that do influence the tidal prism will have an adjusted breach width to compensate for the increase in discharge. The next chapter will elaborate on the results for all the individual parameter scenarios.

5

Model Results of the parameter scenarios

This chapter will present the model results of all the individual parameter scenarios which were presented in the previous chapter. The results of all scenarios for each parameter will be presented in the form of two-dimensional sedimentation and erosion maps and in the form of the average bed level change presented as a time series. The noticeable differences between the parameter scenarios will be discussed.

5.1. Sediment characteristics

This section will present and discuss the individual parameter results for the sediment related parameters. Subsection 5.1.1 will present the individual scenario results for the sensitivity of the suspended sediment concentration. Subsection 5.1.2 will compare the results for scenarios with varying levels of critical shear stress for erosion for the suspended sediment fraction. Lastly, a comparison is made in Subsection 5.1.3 between the results of the base-case with an erodible bed and the base case without an erodible bed.

5.1.1. Suspended sediment concentration

The separate scenarios for suspended sediment concentration were simulated for a real-time period of 24 years. Figure 5.1 shows the two-dimensional maps of the total sedimentation and erosion over the polder area and the foreshore after 24 years of real-time simulation. The surface area of the polder bed around the breach which shows no accretion shrinks with increasing levels of SSC. This area concerns around 55% of the total polder area for a suspended sediment concentration of $25 mg/l$ and reduces to around 20% of the total polder area for a suspended sediment concentration of $200 mg/l$. The decrease in non-accreeded area is mainly caused by the decrease of the tidal prism over time, due to the slow increase of bed level in the polder. The scenarios with higher levels of SSC show similar sedimentation patterns during earlier operational periods compared to the scenarios with low levels of SSC. The total area of the eroded bed in between the breach after 24 years diminishes with increasing levels of SSC. This level of eroded bed at the breach is nearly equal for all scenarios after the first three months of operation, only decreases faster over time for higher levels of SSC. Due to the faster decline of tidal prism for higher levels of SSC the erosion pit gets 'refilled' with sediment at a faster rate.

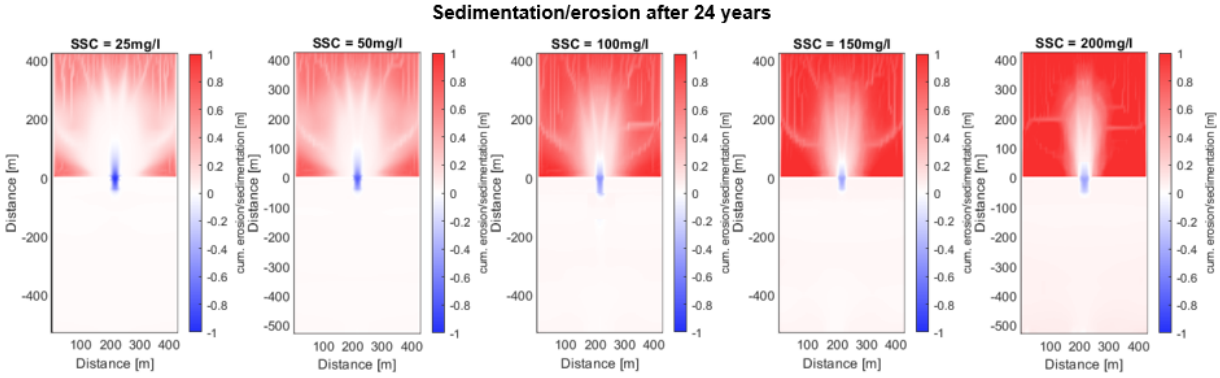

Figure 5.1: The cumulative sedimentation and erosion for different levels of suspended sediment concentration at the boundary after a real-time period of 24 years.

The total average change in bed level during the 24 years for each scenario is displayed in figure 5.2 and is directly proportional to the total volume of imported sediment in the polder area. All scenarios are likely to reach for the same equilibrium bed level at different rates. The initial rate of sedimentation increases, as expected, for increasing levels of SSC. Higher rates of initial sedimentation cause a faster decline of this rate since the equilibrium depth is approached during an earlier stage. For suspended sediment concentration lower than $100 mg/l$ show to follow a more linear trend in average sedimentation, and thus a constant rate of sedimentation, after the first two years of operation, whilst concentrations of $100 mg/l$ or higher indicate a constant decrease in sedimentation rate. However, the linear trend for the lower SSC is likely to transition in an exponential curve for longer simulation periods. The higher-order 'wiggles' that are observed are again due to the effect of neap tide and spring tide in combination with the morphological factor.

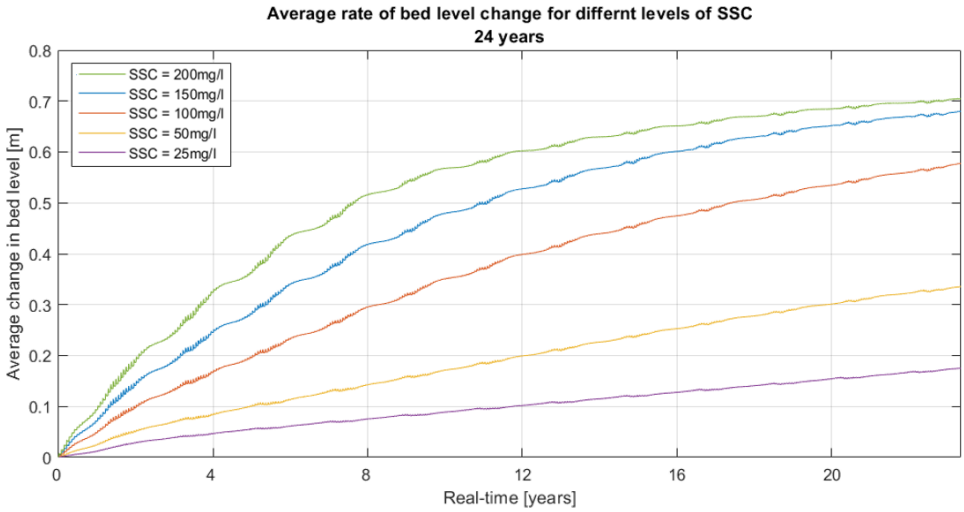

Figure 5.2: The average change in bed level (sedimentation) for different levels of suspended sediment concentration at the boundary during a real-time period of 24 years.

The data that is obtained by the scenario models (shown figure 5.2) can be transformed into a figure showing the relation between SSC in the estuary and the initial rate of sedimentation. This relation is depicted in figure 5.3 where the average initial rate of sedimentation is determined for a 2, 4 and 6 year average for varying levels of SSC. Longer periods of average initial sedimentation result in lower rates of initial sedimentation. A clear linear relationship is observed between levels of SSC and initial sedimentation rates with a statistical accuracy of $R^2 = 0.94$. This accuracy of the linear relation indicates that interpolation for other levels of SSC than simulated with the scenarios is permissible. Extrapolation to parameter values outside the tested parameter range is not advised, since this extrapolation is not yet validated.

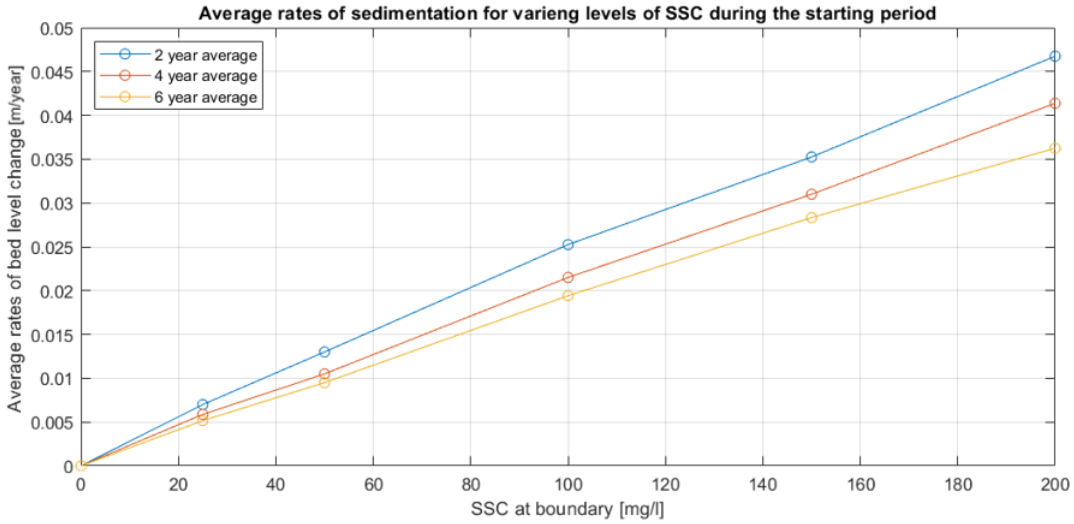

Figure 5.3: The initial average change in bed level (sedimentation) for different levels of suspended sediment concentration at the boundary. Initial averages over the first 2 years, 4 years and 6 years are shown.

Differentiating the numerical fit of the advance in sedimentation shown in figure 5.2 for different operational years allows for the visualization of the relation between SSC, the yearly rate of sedimentation and the operational year shown by figure 5.4. During the advance in the operational period, the relation between SSC and sedimentation rate transforms from a linear increasing relation to a constant horizontal relation. It can be observed that after 24 years of operation the average yearly rate of sedimentation is equal for all levels of SSC. To conclude, the initial rate of sedimentation increases directly proportional to the increase in SSC. However, when the bed level increases relative to the mean sea level, this effect diminishes, leading to an equal rate in bed level change after longer operational periods.

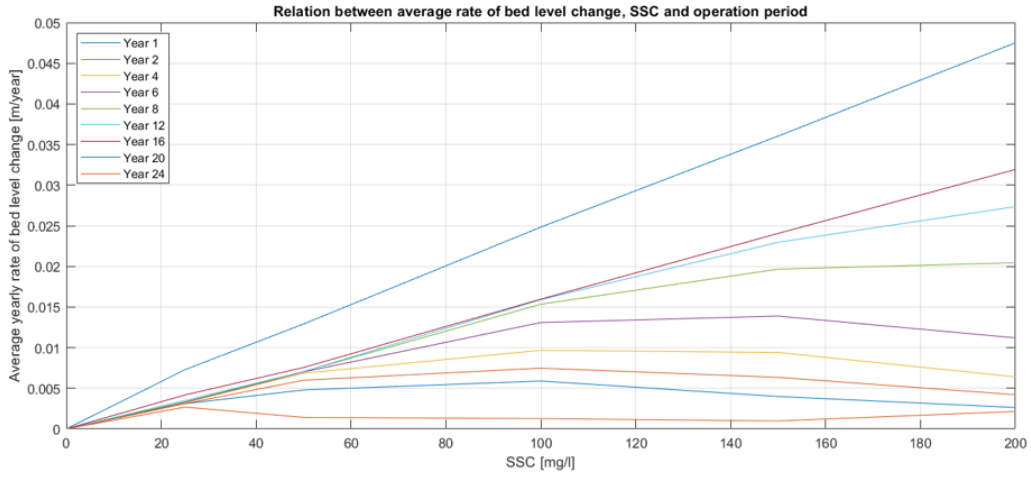

Figure 5.4: Relation between the average rate of bed level change (sedimentation), suspended sediment concentration at the boundary and the operational year. Note that the rate of sedimentation is not the average 'over' the specific period, but represents the sedimentation rate at that year

5.1.2. Critical shear stress for erosion suspended fraction

Figure 5.5 shows the local sedimentation and erosion patterns for all four scenarios with varying values for critical shear stress for erosion after a real-time period of 10 years. All scenarios show similar sedimentation patterns, with slight variations in amplitude. The most significant difference is noticeable on the foreshore of the scenario with a critical shear stress for erosion of $0.20 N/m^2$, where large scale sedimentation takes place. The wave and flow forcing on the foreshore create an average bed shear stress too low for the suspended

sediment fraction to stay in suspension and allows for settlement of suspended sediment on the foreshore. Another noticeable difference is that the non-accreeding area behind the breach is smaller for larger values of critical shear stress for erosion.

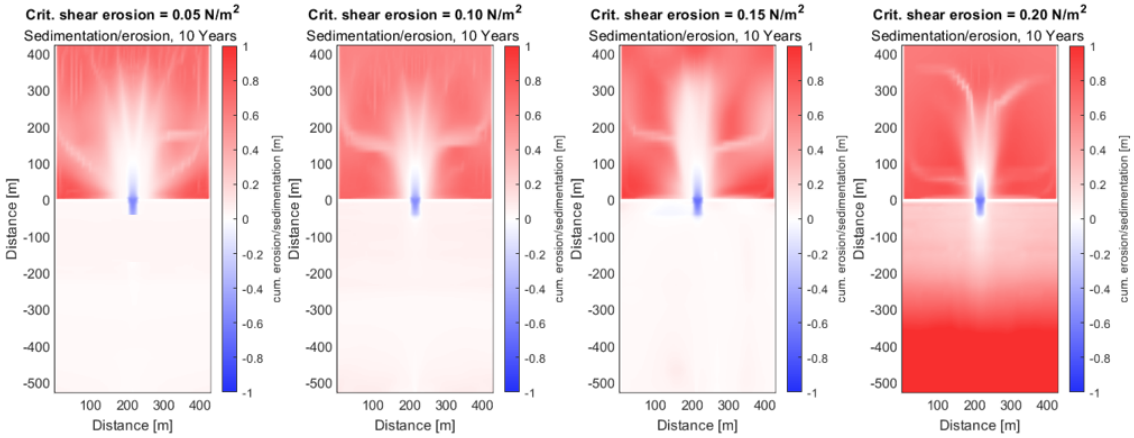

Figure 5.5: The cumulative sedimentation and erosion for different values of critical shear stress for erosion for the suspended sediment fraction after a real-time period of 10 years

The variation in initial sedimentation rates is depicted in figure 5.6, which shows the average change in bed level for the different scenarios during a real-time period of 10 years. The rate of initial sedimentation increases for increasing values of critical shear stress for erosion, but seems to stagnate for a critical shear stress for erosion higher than $0.20 N/m^2$. To conclude, larger and heavier particles with higher levels of critical shear stress for erosion (up to $0.20 N/m^2$) will lead to smaller non-accreeding areas and steeper initial sedimentation rates.

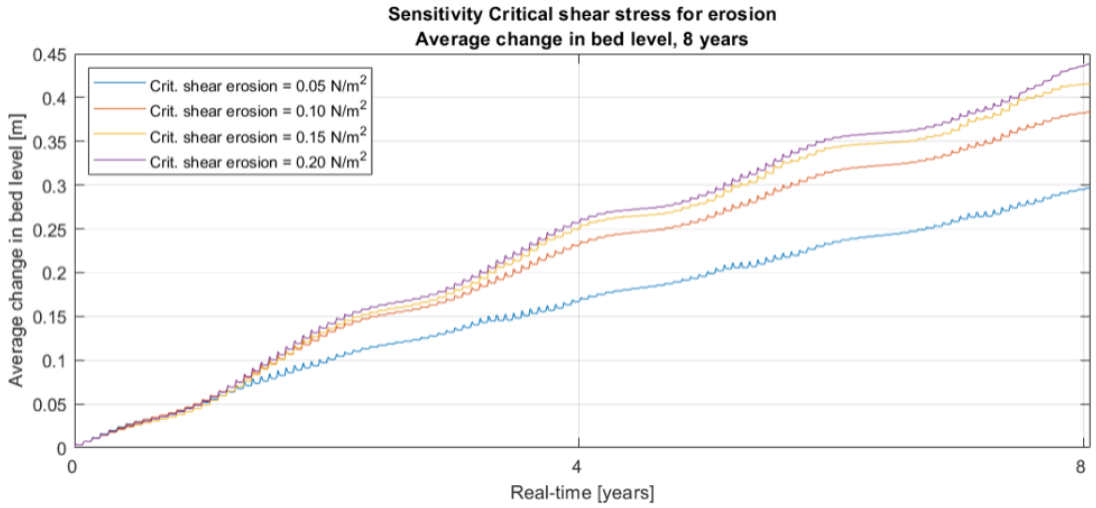

Figure 5.6: The average change in bed level (sedimentation) for different values of critical shear stress for erosion for the suspended sediment fraction during a real-time period of 24years.

5.1.3. Critical shear stress for erosion Bed fraction - non-erodible bed

The results of the two scenarios for an erodible bed and a non-erodible bed are displayed in figure 5.7, which shows both the local sedimentation and erosion patterns after a 24 year real time period and the change in average bed level of the two scenarios during this same period. The two-dimensional sedimentation maps show a small difference in non-accreeding area behind the breach. This difference is mainly caused by the higher flow speeds during incoming tides due to the smaller breach area since the bottom of the breach is not able to erode. This larger area where sedimentation is prevented for the non-erodible bed is reflected in the graph, which shows the average change in bed level over time. The non-erodible bed has a slightly lower

equilibrium of average bed level change. The two models start with equal initial sedimentation rates. The only difference is that after approximately 4 years the non-accreeding area shrinks for the erodible bed. This area stays constant for the non-erodible bed, causing a small decrease in average bed level change after 4 years. To conclude, the assumption of a non-erodible bed produces similar results to the base case, with the only difference being the larger non-accreeding area and the slight decrease in average bed level change after 4 years.

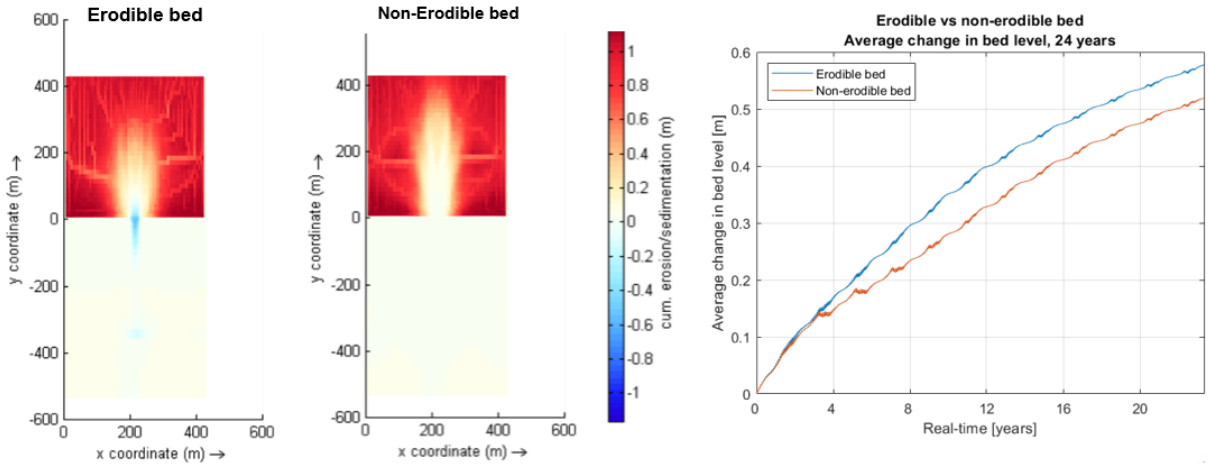

Figure 5.7: The average change in bed level (sedimentation) for both the base-case with an erodible bed (left figure) and without an erodible bed (middle figure) a real-time period of 24years. The right figure shows the average change in bed level during the same period of 24 years

5.2. Dimensional characteristics

This section will present and discuss all the scenario results for dimensional parameters. First, the results for the scenarios with varying breach widths will be presented in Subsection 5.2.2. After that, Subsection 5.2.2 and 5.2.3 will elaborate on the scenario results for the horizontal dimensions, namely the polder width and the polder length. Lastly, the scenario results for the initial polder bed level will be discussed in Subsection 5.2.4.

5.2.1. Breach width

All the scenarios for the determination of the sensitivity of the breach width were simulated for a real-time period of 24 years. Figure 5.8 shows the two-dimensional map results of the cumulative sedimentation and erosion after 24 years of operation. With increasing breach width, the horizontal flow area increases, allowing for lower flow speeds for an equal total discharge through the breach. The reduction in flow speed through the breach of $100m$ causes the area in the breach to show less erosion. This reduction is even larger for the breach of $150m$ which shows no erosion at all in the breach. Another noticeable effect is the increasing non-accreedable area for increasing breach width. Larger breach openings allow for more wave penetration into the polder area causing the non-accreedable area to reach all the way to the backside of the polder. Figure C.1 shows the observed significant wave height at the back of the polder in line with the breach. A significant increase in observed wave height is noticeable for increasing breach widths.

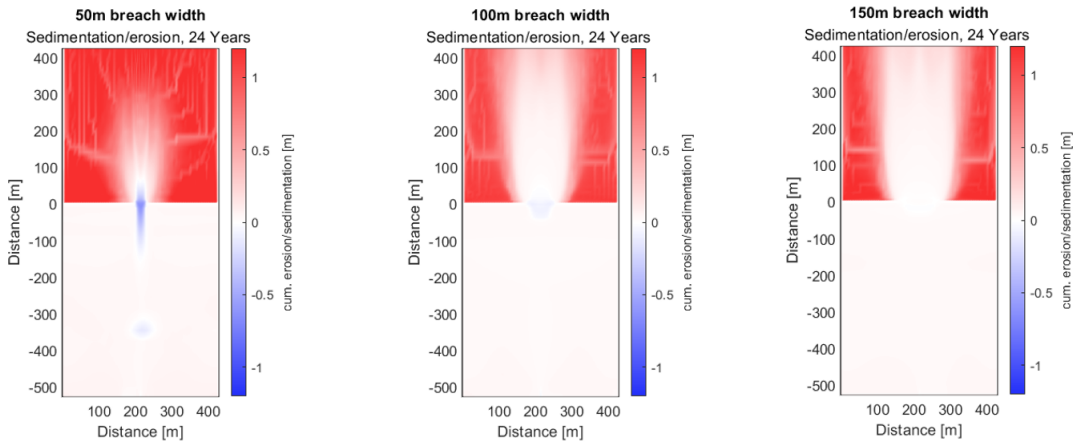

Figure 5.8: The cumulative sedimentation and erosion for different dimensions of the breach width after a real-time period of 24 years.

Figure 5.9 shows the average change in bed level for all three scenarios over a real-time period of 24 years. The facts noted in the previous figure are also resembled in this figure. The increase in non-accreeding area for larger breach widths results in a decrease in equilibrium depth that is being reached by the average bed level change. All the initial rates of sedimentation are nearly equal for all scenarios, since the sizes of the non-accreeded areas are nearly equal for all scenarios after four years. The non-accreeding areas do however shrink more for the smaller breach widths, causing the difference in equilibrium bed level.

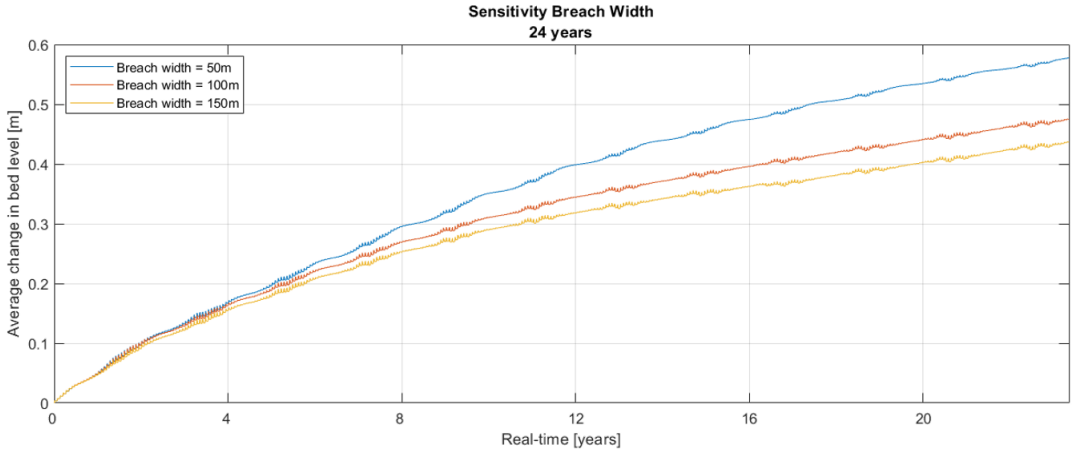

Figure 5.9: The average change in bed level (sedimentation) for different dimensions of the breach width during a real-time period of 24 years.

5.2.2. Polder width

The two-dimensional map results visualizing the cumulative sedimentation and erosion after a real-time period of 24 years of the polder width scenarios are displayed by figure 5.10. The scenarios were assumed to have non-erodable beds and the width of the breach was directly proportional to the increase in surface area. The results show that the sides of the polder for each scenario reach similar levels of sedimentation. The main difference in sedimentation pattern occurs at the breach area of the polder right behind the breach stretching through the middle of the polder, where sedimentation is prohibited. With increasing polder width, this area increases in both width and length, reaching all the way to the secondary dike for the larger breach widths. The predominant reason for this is the increase in wave energy that passes through the breach for increasing breach width. This is caused by the same process as was explained for the breach width scenarios.

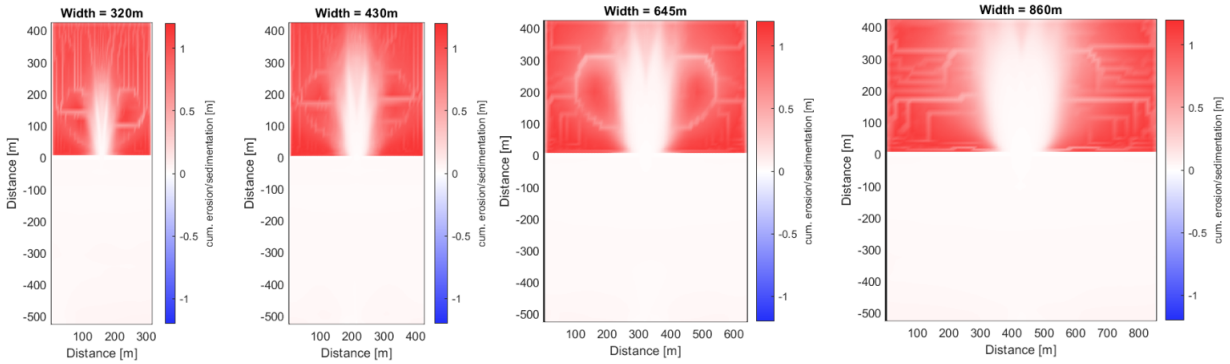

Figure 5.10: The cumulative sedimentation and erosion for values of dimensional width of the polder after a real-time period of 24 years.

The cumulative volume imported through the breach is plotted over time by figure 5.11 during a period of 24 years. For these parameter scenarios, the amount of imported sediment volume is not directly proportional to the average rate in bed level change, since the surface area of the polder bed is also altered. Therefore it is important to evaluate these results separately. The sediment volume displayed by this plot is adjusted to its dry bed density, meaning that the imported volume measures the same volume as the volume of settled sediment, including pores. All four scenarios show similarly shaped patterns of sediment import in their time series, only with different initial rates of sediment import and different levels of equilibrium imported sediment which they reach for.

Figure 5.11: The cumulative volume of imported sediment through the breach for values of dimensional width of the polder after a real-time period of 24 years.

The imported sediment volume data mentioned above can now be transformed into a time series presenting the average rate of bed level change by using the assigned polder surface area. This time series is shown by figure 5.12 on the overall effect of the variation in the polder width. The figure shows that the initial rate of sedimentation is very similar for all variations of polder width. The wider polders (with a width of 645m and 860m) have a lower equilibrium level that they are reaching for, mainly caused by the different ratio of non-accreeding area behind the breach over the total polder surface area. The exact differences in equilibrium bed level will be further substantiated in Chapter D.

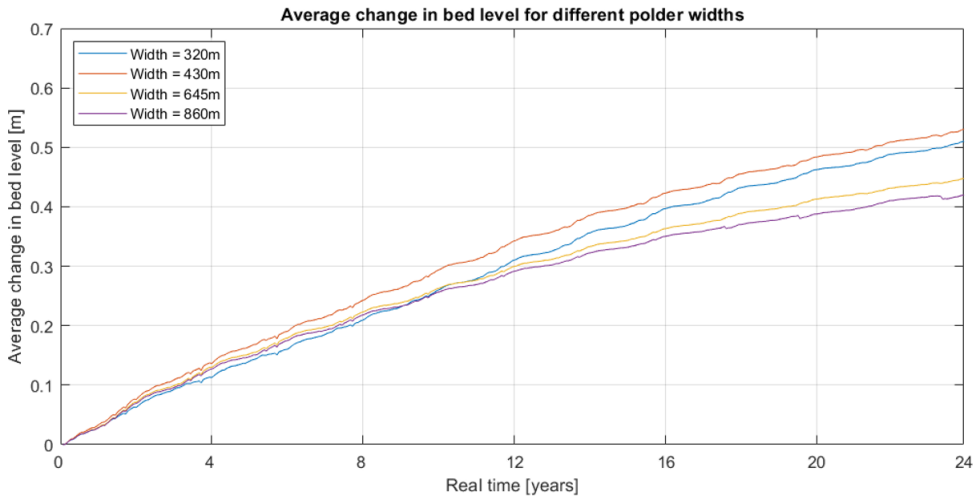

Figure 5.12: The average change in bed level (sedimentation) for values of dimensional width of the polder after a real-time period of 24 years.

5.2.3. Polder length

The results of the scenarios for the determination of the sensitivity of the dimensional polder length are processed equally to the results for the polder width. Similar to the scenarios for the polder width, the scenarios were assumed to have non-erodable beds and the width of the breach was directly proportional to the increase in surface area. Figure 5.13 shows the two-dimensional map of cumulative sedimentation and erosion over the polder area. Similar patterns are observed compared to the scenarios for polder width. The main difference is that the non-accreeding area behind the breach for the two scenarios with a greater dimensional polder length of $645m$ and $860m$ can now be fully stretched out without reaching the secondary dike. On the one hand, this increases the ratio of non-accreeding area over the total polder surface area, lowering the equilibrium of average bed level change. On the other hand, now that the non-accreeding area is not reaching to the back of the polder, the coastal safety is preserved to a higher extent now that the complete backside of the polder elevates its bed level over time.

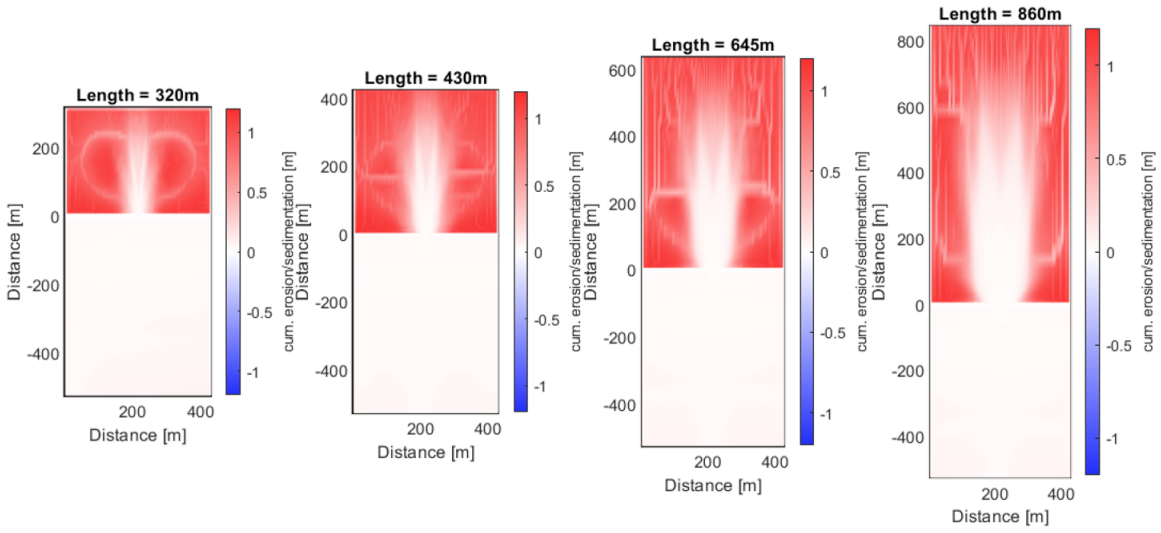

Figure 5.13: The cumulative sedimentation and erosion for different values of dimensional length of the polder after a real-time period of 24 years.

Figure 5.14 presents the cumulative imported sediment over a time period of 24 years. A larger volume of sediment gets imported for an increasing length of the polder. The sediment volume represents the same wet volume with a dry bed density of $660 kg/m^3$ as was used with the scenarios for polder width.

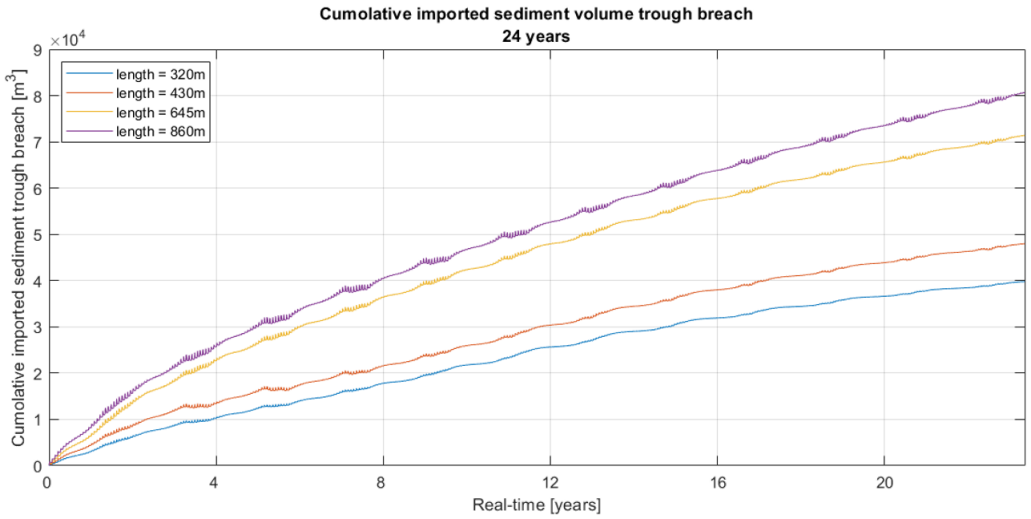

Figure 5.14: The cumulative volume of imported sediment through the breach for values of dimensional length of the polder after a real-time period of 24 years. (The small scale wiggles that have a more significant presence for the scenarios with larger polder lengths are due to the increase in polder surface area. One wiggle represents the short-time settlement during tidal slack, which gets washed away again during tidal outflow.)

When the data is transformed to the time series presenting the average rate of bed level change, the same initial rate of sedimentation is observed in comparison to the scenarios for polder width, which can be seen in figure 5.15. The equilibrium that is reached for differs relative to the breach width scenarios, since the ratio of non-accreeding area over total polder area increases for longer polders.

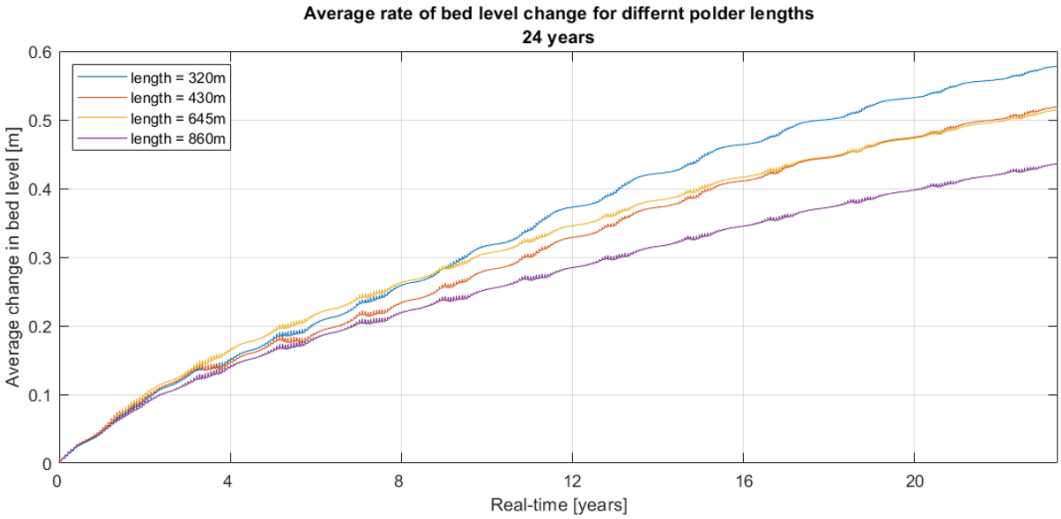

Figure 5.15: The average change in bed level (sedimentation) for different values of dimensional length of the polder after a real-time period of 24 years.

5.2.4. Initial polder bed level

Figure 5.16 shows the two-dimensional map results of the total sedimentation of all five scenarios after a real-time period of 4 years. This relatively short operational period shows an increasing trend in sedimentation volumes for decreasing initial polder bed levels during this period of 4 years. This trend gets cut off when the two-dimensional map results after 8 years are evaluated (see figure C.5). An initial polder bed level of $OD-2m$ shows little difference in sedimentation patterns between 4 and 8 years, suggesting a stop in sedimentation. The overall non-accreding area behind the polder is for each scenario larger than was the case with the base-case, due to the wider breach opening. Lastly, when the initial polder bed depth surpasses a depth of $OD-2m$, sedimentation starts to occur at the foreshore. The deeper lying foreshores are too deep for the assigned

waves to create sufficient bed shear stress for keeping sediment in suspension, causing sedimentation.

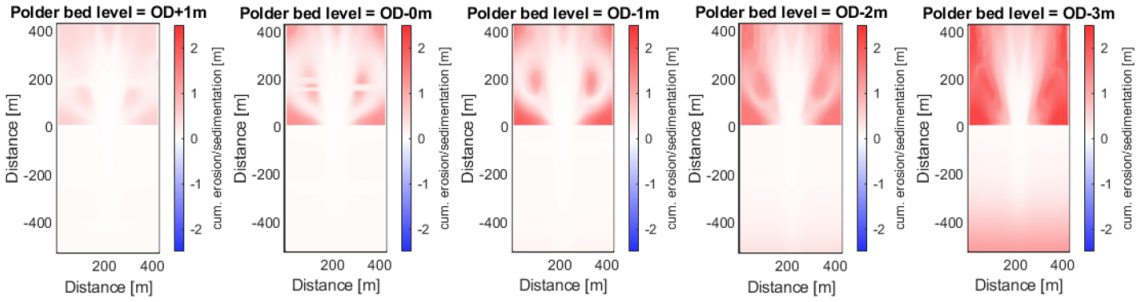

Figure 5.16: The cumulative sedimentation and erosion for different values of initial polder bed levels after a real-time period of 4 years.

The stop in the trend of increasing sedimentation for deeper initial polder bed levels is better reflected in figure 5.17, which shows the average bed level change over a real-time period of 8 years for all scenarios. Here it is clearly depicted that for an initial polder bed level of $OD-2m$ the rate of average bed level change starts to slow down after 4 years before oscillating around an equilibrium. This same process is occurring for an initial polder bed level of $OD-3m$ after around 6 years. An explanation for this process will be given later on in this section. All the scenarios show increasing rates of initial sedimentation for deeper lying polder beds.

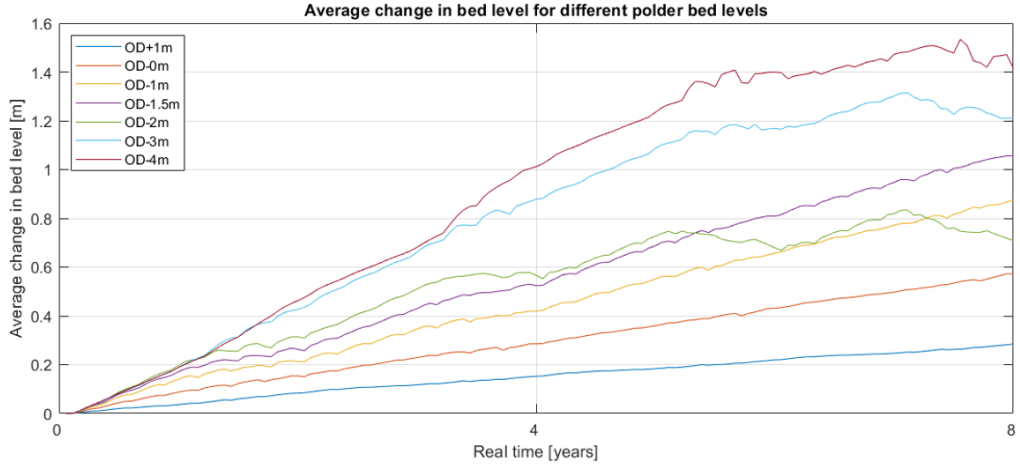

Figure 5.17: The average change in bed level (sedimentation) for different values of initial polder bed level during a real-time period of 8 years. (The scenario models for a tidal amplitude of $3.0m$ and $3.5m$ were simulated for a shorter period due to the occurrence of a numerical error. This error did not seem to affect the results.)

Figure 5.18 presents the evolution of the bed level of the side of the polder over a period of 8 years. The scenarios with an initial polder bed ranging from $OD+1m$ to $OD-1m$ show the reach for the same equilibrium bed level at the side of the polder of around $2m$. The scenarios for an initial bed level of $OD-2m$ and $OD-3m$ show this same reach during the first four years, only suddenly reaching an equilibrium bed level around $OD-0.3m$. The probable cause of this stagnation of sedimentation is hypothesized to be the increased wave energy dissipating on the side areas of the polder. To substantiate this hypothesis, a comparison is made between a scenario that does not show the stagnation is sedimentation (initial bed level of $OD-0m$) and a scenario that does show this stagnation (initial bed level of $OD-2m$). Figure C.6 shows the maximum shear stress during high tide after an operational period of 6 years for both the scenario with an initial polder bed level of $OD-0m$ and with $OD-2m$, with the latter scenario already being in its oscillating equilibrium form.

The scenario with a bed level of $OD-0m$ shows very low levels of bed shear stress at the side flanks of the polder, while the shear stresses are high at the breach (due to flow) and at the foreshore (due to depth induced wave energy dissipation). The scenario with an initial bed level of $OD-2m$ indicates that the increased bed shear stress at the foreshore due to depth induced wave dissipation is located far more landward and even

extends into the polder. This is due to the fact that the complete foreshore is $2m$ deeper causing the incoming waves to maintain most of their energy while entering the polder. The figure also shows the bed shear stress on the side flanks of the polder to be significantly higher than with the shallower polder scenario. Maximum bed shear stresses of around $0.1N/m^2$ are measured on the flanks, while the critical shear stress for erosion of the settled sediment is around $0.05N/m^2$, indicating the start of erosion of the flanks.

Figure C.7 substantiates this hypothesis by showing the significant wave height measured on the side flanks of the polder for both scenarios, where the significant wave height measured at the deeper scenario is significantly higher than the wave height measured at the same location at the shallower scenario. Figure C.8 explains why the halt in sedimentation only starts after a certain change in bed level, by showing the relation between the change in bed level and the peak orbital velocity measured at the side flanks of the polder for the scenario with the initial polder bed level of $OD-2m$. With increasing bed level, the peak orbital velocity will increase accordingly, with the peaks being measured during spring tide. The present waves at the flanks start to 'feel' the bottom when the bed level passes a certain level, causing an increase in orbital velocity, which results in a shear stress higher than the critical shear stress for erosion, making the settled sediment to erode again.

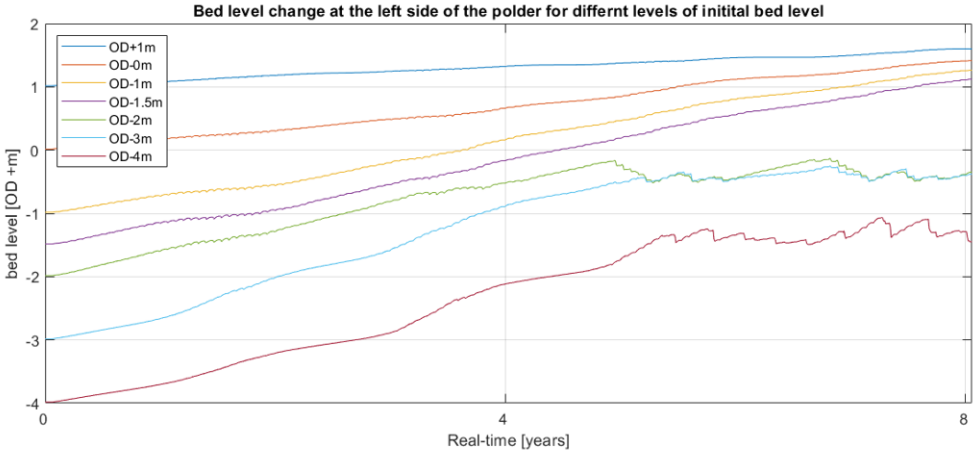

Figure 5.18: The average bed level at the side of the polder for different values of initial polder bed level during a real-time period of 8 years.

5.3. Hydraulic parameters

This section will present and discuss the individual parameter results for the hydraulic related parameters. Subsection 5.3.1 will present the scenario results for the sensitivity of the maximum tidal amplitude. Subsection 5.3.2 will compare the results for base-case with sea level rise with the results for the base-case without sea level rise.

5.3.1. Tidal amplitude

The two-dimensional map results presenting the local sedimentation and erosion for all five scenarios for varying tidal amplitudes after a real-time period of 24 years are displayed by figure 5.19. The scenarios with tidal amplitudes ranging from $2.0m$ to $2.5m$ show increasing levels of cumulative sedimentation all around the sides of the polder for increasing levels of tidal amplitude. The scenarios with tidal amplitudes of $3.0m$ and higher break this trend of increasing levels of sedimentation. With increasing levels of tidal amplitude, the tidal prism increases such that the flow patterns within the polder change and form a strong circular current. These circular currents have higher flow velocities, preventing the settlement of the fine sediment. The increase in flow velocity for increasing tidal amplitudes is visualized in figure C.9. The origin of these circular flows are visualised by plotting the velocity vector fields during rising tide over the two-dimensional sedimentation and erosion maps, displayed by figures C.2, C.3 and C.4.

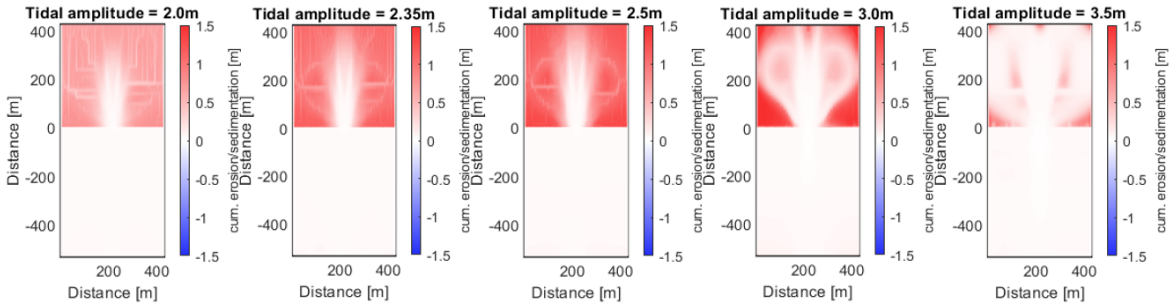

Figure 5.19: The cumulative sedimentation and erosion for different maximum tidal amplitudes after a real-time period of 24 years.

Figure 5.20 presents the average change in bed level over a real-time period of 24 years. The figure shows the increase of initial sedimentation rate and the increase of equilibrium level for increasing tidal amplitudes ranging from $2.0m$ to $2.5m$. When the tidal amplitude surpasses a value of $2.5m$, a stagnation in the increase of the initial sedimentation rate is noticeable. Amplitudes of $3.5m$ and higher show a complete stagnation in sedimentation rate after around three years of operation and form a sinusoidal signal around an equilibrium average change in bed level of around $0.1m$, due to the formerly stated arising circular flow patterns.

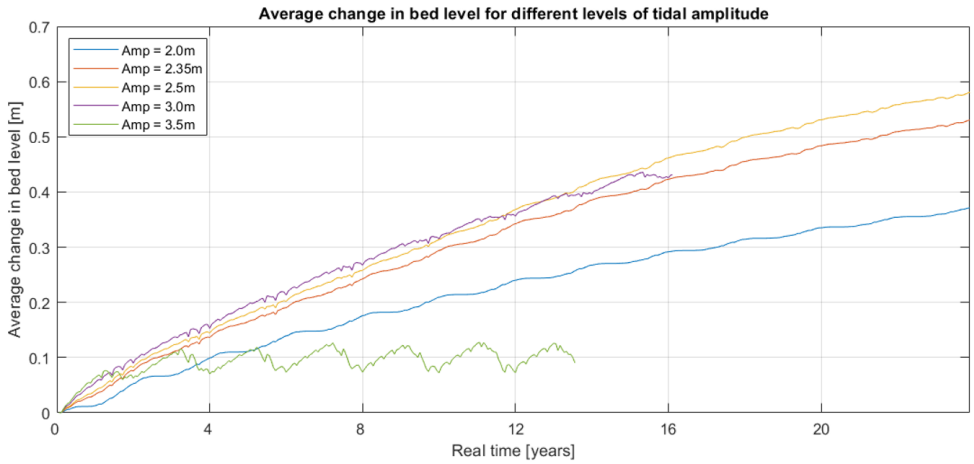

Figure 5.20: The average change in bed level (sedimentation) for different maximum tidal amplitudes during a real-time period of 24 years.

5.3.2. Sea level rise

The two-dimensional results of sedimentation and erosion for both the base-case scenario without sea level rise and the scenario with a constant sea level rise of $4.2mm/year$ after a real-time simulation period of 24 years are shown by the left two figures in figure 5.21. The polder areas show similar patterns of sedimentation, but with slight variations in amplitude. The right plot in figure 5.21 shows the difference in sedimentation and erosion between the scenario with and without sea level rise. From this image, it can be observed that for the scenario with sea level rise the areas at the sides of the polder show stronger levels of sedimentation (indicated in red). The area around the breach to the model of the polder shows less sedimentation in comparison to the base-case model without sea level rise.

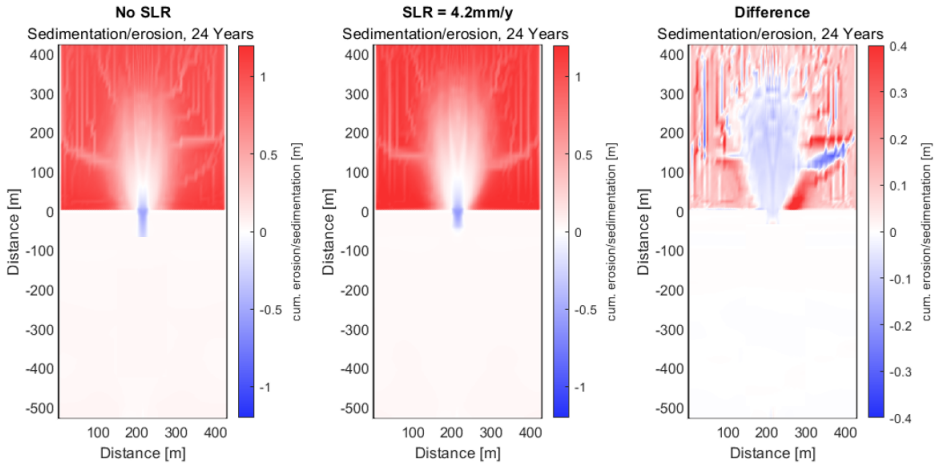

Figure 5.21: Comparison between the cumulative sedimentation and erosion of the base-case model without sea level rise and with a model with a constant sea level rise of $4.2mm$. Both with the same real-time period of 24 years. Left: base-case model without sea level rise. Middle: Base-case with a constant sea level rise of $4.2mm/year$. Right figure: Difference in sedimentation and erosion between the two models (scenario without sea level rise subtracted from the scenario with sea level rise)

When the comparison is made between the average bed level change, which is directly proportional to the total volume of imported sediment, one can see that the scenario with sea level rise has a net import of sediment higher than the scenario without sea level rise. Figure 5.22 shows this comparison by plotting the average change in bed level over a real-time period of 24 years for both scenarios. The difference in average bed level change of the two scenarios is plotted by the yellow line. When comparing this difference to the sea level rise (purple dotted line) one can deduct that the bed level on average only follows the sea level rise by a factor of $1/2$.

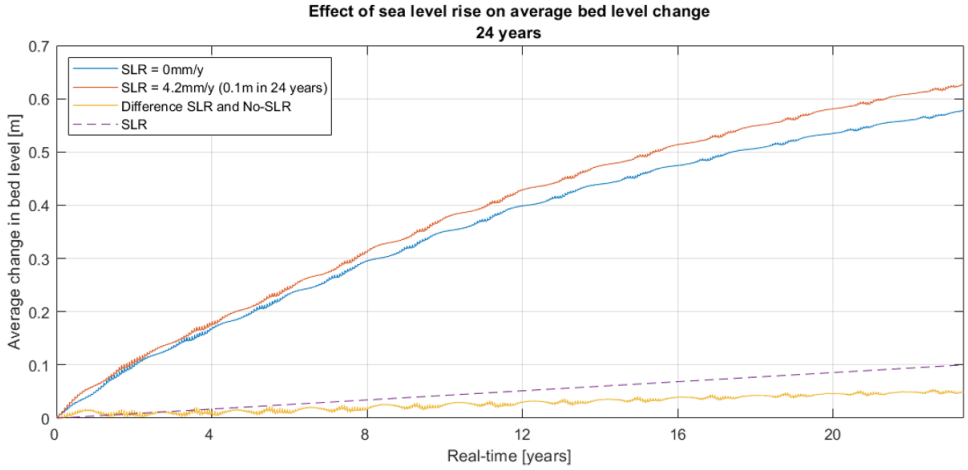

Figure 5.22: The average change in bed level for both the base-case without sea level rise (SLR = $0mm/year$)and the scenario of the base-case with a constant rate of sea level rise of $4.2mm/year$. The yellow line shows the difference in average bed level change for both scenarios. The purple line displays the rate of sea level rise.

However, when the focus is placed on coastal safety, the Lease Polder is able to fully counteract the rate of sea level rise, despite the relatively low rate of increase in average bed level, which can be deducted from figure 5.23. This figure shows the change in bed level over the back side of the polder area near the secondary polder. The difference between the scenario with and without sea level rise is again plotted in yellow. The rise of the back side of the polder turns out to rise at nearly exactly the same rate as the rate of sea level rise. As was explained in chapter 2, the importance of remaining coastal safety lays for a significant part at the development of bed level at the back side of the polder, where waves can dissipate before reaching the secondary dike. With the back area of the polder rising at a similar rate as the rate of sea level rise, the Lease Polder becomes a partly self-sustaining system of coastal defence.

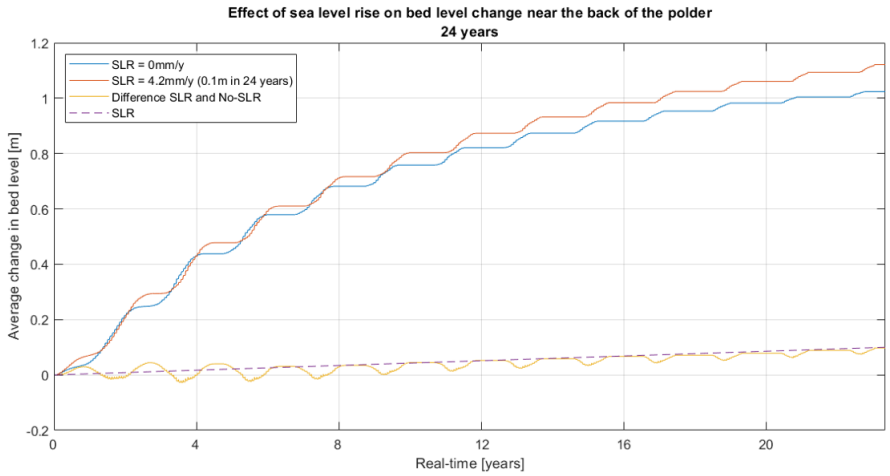

Figure 5.23: The change in bed level of the back side of the polder for both the base-case without sea level rise (SLR = $0 mm/year$)and the scenario of the base-case with a constant rate of sea level rise of $4.2 mm/year$. The yellow line shows the difference in average bed level change for both scenarios. The purple line displays the rate of sea level rise. (note that the wiggles in the line of the difference between two scenarios are caused by the fact that the two tidal motions of the separate scenarios are slightly out of phase)

The scenario results presented in this chapter help with giving a better understanding of the individual influence of the tested parameters on the morphological results within the Lease Polder. Valuable insights are obtained regarding the effect of sea level rise on the catchment rate. Important findings were that the dimensional width and length of the polder did not significantly affect the sedimentation rate and that there is a transitions between two morphological regimes for varying tidal amplitude and initial polder bed level. The non-accreeding area behind the breach turned out to be a normative factor in the equilibrium average bed level and its physical extend could potentially influence the level of coastal protection. The sensitivity of the SSC showed similar results to the expectations that were described in other studies.

The next chapter will convert the scenario results that were found in this chapter into quantitative formulations expressing the dependency of the sedimentation curve on the parameter value. The formulations for the sensitivity of the SSC, tidal amplitude, breach width, initial bed level, polder length and polder width will be used in the final assessment tool in the next chapter.

6

Feasibility Study Lease Polder assessment tool

The final evaluation around the implementation of the concept of Lease Polder consists of a feasibility study for case-specific Lease Polder opportunities. This chapter will go over the complete process of how the results from the parameter sensitivity numerical model study are transformed and implemented in a life cycle tool that can determine the expected sedimentation curve for a specific Lease Polder case, given the case-specific parameters. This life cycle tool is created in Excel and is called the WisLi-tool. Once the tool has obtained this curve, it will utilize this curve to simulate the complete life cycle during a specific period. For example, a period of 150 years, including multiple openings and closings of the Lease Polder. By means of the implementation of certain input variables - like the cost of the closing and opening, expected revenue during the closed period and certain levels of sea level rise and land subsidence - the tool will be able to calculate the expected overall costs and benefits for the given input parameters. Lastly, the tool will perform an optimization evaluation for the main influential design parameter, being the period for which the Lease Polder will be kept open for sedimentation. In the end, the WisLi-tool will act as a guideline for the optimal implementation design of a Lease Polder.

6.1. Model result transformation

Before the WisLi-tool can be implemented, the results from the parameter sensitivity model study need to be transformed into usable data first. The product that will be used by the tool will consist of separate equations which can calculate a dimensionless factor for each individual parameter, based on a certain input value for that parameter. For each individual parameter, the dimensionless factors will describe the ratio of the equilibrium bed level change that will be reached for and the initial sedimentation rate during the first 4 years relative to the base case results. This section will describe the complete process for the transformation of the model results to the dimensionless factor formulas in a total of six steps. The implementation of these formulas in the actual WisLi-tool will be elaborated in section 6.2. A total of six parameters will be transformed and used in the WisLi-tool, consisting of the suspended sediment concentration (SSC), tidal amplitude, breach width, initial polder bed level, dimensional polder length and the dimensional polder width (figure 6.1).

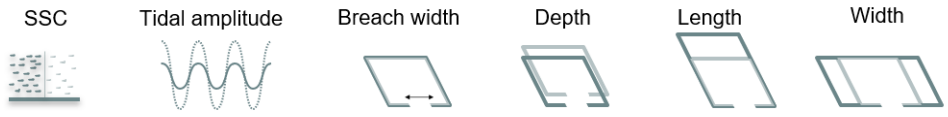

Figure 6.1: All parameters that will be transformed into dimensionless parameter factors and will be used by the WisLi-tool

As was explained above, the results of the previous chapter will be transformed into dimensionless factor formulas in a total of six steps. These steps will be explained below in a schematic manner containing fictional values and are displayed by figures 6.2 (step 1 to 4) and 6.3 (step 5 to 7). With this schematization, the results

for the suspended sediment concentration will be presented in different figures and tables. The results for the other five parameters that were included in this study will be presented in Appendix D.

Step 1 The first step of the transformation of the model results to the dimensionless factor formulas consists of the import from the data which represents the average bed level change for each individual parameter that was obtained in the parameter sensitivity model study. Each parameter has its own number of scenarios with varying parameter values.
Step 2 Once the data set for the specific parameter is loaded in, each individual scenario will be fitted by a MATLAB script following an adjusted exponential function in the form of: $y(t) = a \cdot (1 - e^{-b \cdot t})$ and is displayed by step 2 in figure 6.2, where $y(t)$ represents the average change in bed level at time t. The script will give the a- and b-factors as an output which are listed in table 6.1 in the first two columns for the parameter results for the SSC. The fitted lines are displayed in figure 6.4.
Step 3 Now that the fitted exponential functions are obtained, the equilibrium level for the average bed level change and the initial sedimentation rate can be determined for each individual scenario. The a-factor of the fitted exponential function represents the equilibrium level that is reached for and can thus be directly deducted. the b-factor represents the rate at which the equilibrium will be reached. However, the b-factor is dependent on the a-factor (fitting parameters), which makes it erroneous to assume that the b-factor represents the initial rate of sedimentation. Therefore, the initial rate of sedimentation will be obtained by retrieving the average rate of sedimentation during 4 years from the fitted function. The separate initial rates of sedimentation are shown in table 6.1 in the third column.
Step 4 The equilibrium bed level change (factor a) and the initial rate of sedimentation can now be plotted over the parameter values on the x-axis, as is schematized by step 4 in figure 6.2.

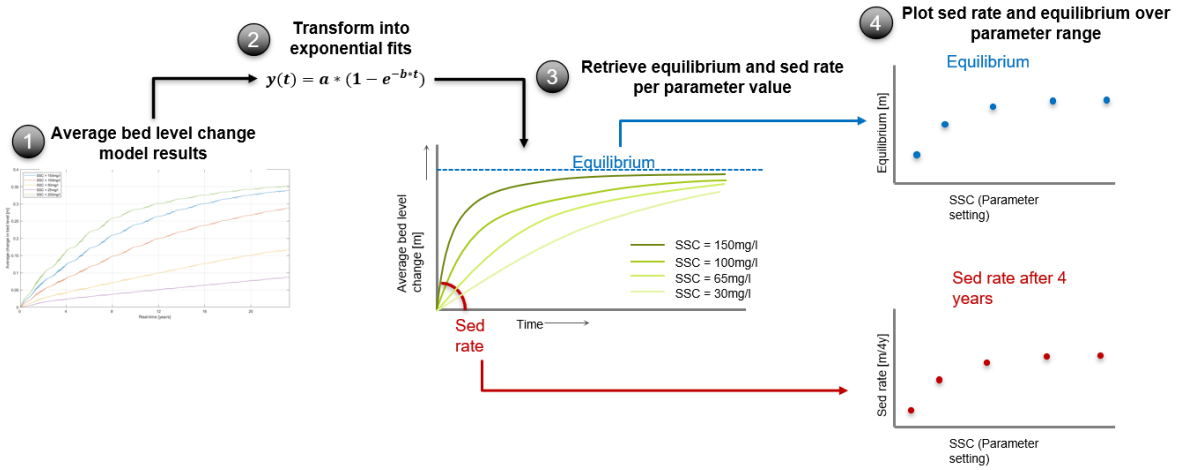

Figure 6.2: Schematizing of the transformation of the model results to parameter-specific equilibrium bed levels and initial sedimentation rates (steps 1 to 4)

Step 5 In order to be able to properly compare and combine the results for the equilibrium change in bed level and the initial rate of sedimentation, the data obtained at step four needs to be transformed into dimensionless factors relative to the base-case (see figure 6.3). The dimensionless data points for the equilibrium factor (factor a) and the initial sedimentation rate are shown in columns four and six of table 6.1.
Step 6 Once this data is obtained, a function can again be fitted through the newly obtained dimensionless data points. These functions will now describe the relation between every parameter value within a certain range and the ratio difference between the equilibrium depth and the initial sedimentation rate relative to the base-case. Depending on the relation, several fit types can be used and can for example range from exponential fits to polynomial fits or normalized fits. The fitted formulas for the SSC parameter are shown by equation 6.1 and 6.2 with their associated constants. The fitted graphs through the dimensionless data points are shown in figure 6.5.

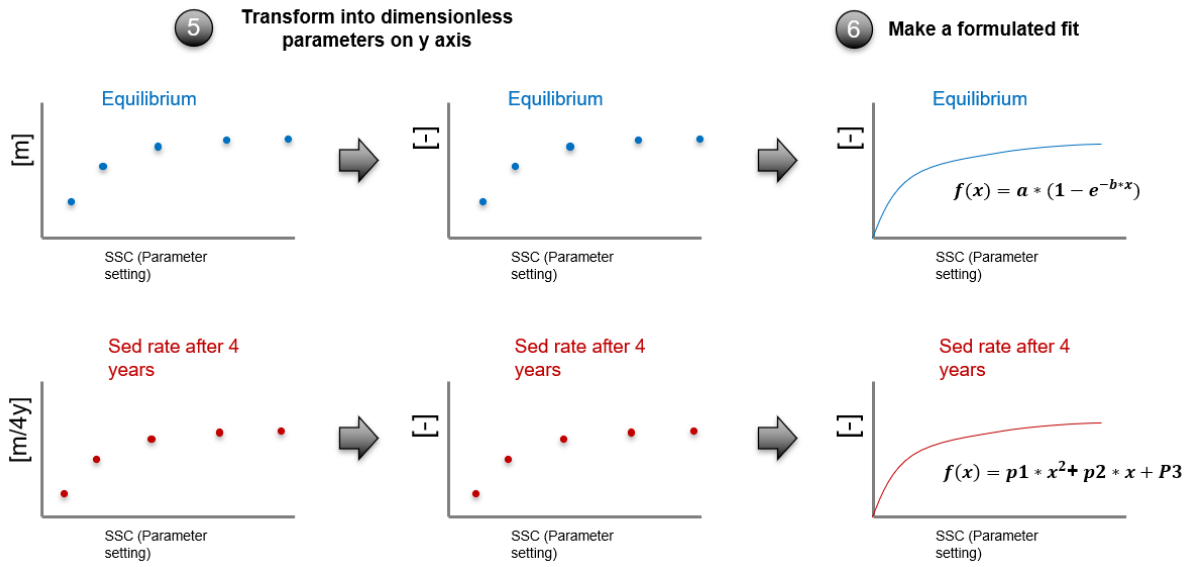

Figure 6.3: Schematizing of the transformation of the parameter-specific equilibrium bed levels and initial sedimentation rates to dimensionless functions (steps 5 and 6)

6.1.1. Parameter transformation results for the SSC

This subsection will present the process and results for the transformation of the scenario results for the SSC into the dimensionless parameter sensitivity functions, following steps 1 to 6 from section 6.1. The results for all other parameters are presented similarly in Appendix D.

The transformation of the sedimentation curve obtained from the model results to the fitted exponential curves are displayed in figure 6.4 and resemble step 2 from figure 6.2. The exponential factors a and b for each fit are presented in the first two columns of table 6.1. The retrieval of the equilibrium bed level and the initial sedimentation rate after 4 years that is depicted by step 3 and 4 result in the values that are presented by the first and third column in table A.2, where the a-factor is equal to the equilibrium bed level. The last three columns in table 6.1 represent the transformation of the results from the previous steps to the dimensionless factors relative to the base-case (step 5).

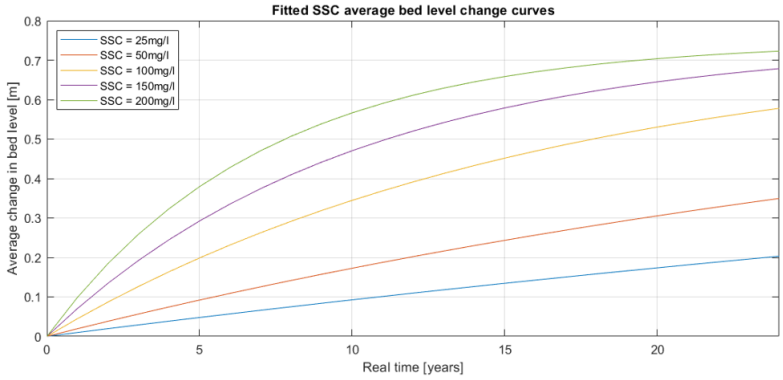

Figure 6.4: Fitted curves for the bed level change curves of the SSC parameter results by an adjusted exponential function

Table 6.1: Results for the a- and b-factor for each scenario which represent the exponential fit and the deducted initial sedimentation rate (during 4 years) for the parameter SSC. Both in absolute values and dimensionless values relative to the base-case scenario.

	Absolute			**Dimensionless**		
SSC	a-factor [-]	b-factor [-]	Initial sed rate during 4 years [m/4y]	a-factor [-]	b-factor [-]	Initial sed rate during 4 years [-]
25mg/l	0.747707	0.013206	0.038471	1	0.213873	0.235106
50mg/l	0.747707	0.026242	0.074506	1	0.424995	0.455322
100mg/l	0.747707	0.061746	0.163634	1	1	1
150mg/l	0.747707	0.099167	0.24483	1	1.606028	1.496203
200mg/l	0.747707	0.141623	0.323374	1	2.293619	1.976195

The final step 6 consisted of deriving a formulation that fits through the dimensionless data for the equilibrium depth (a-factor) and the initial sedimentation rate during 4 years. These formulations for the SSC dimensionless data are presented by formulas 6.1 and 6.2. These two fits are plotted with their data points in figure 6.5.

Dimensionless a-factor

$$f(x) = a \cdot e^{-b \cdot x} + c$$

With:

$$a = -1$$
$$b = 0.5176$$
$$c = 1 \quad (6.1)$$

Dimensionless initial sed rate after 4 years

$$f(x) = p_1 \cdot x + p_2$$

With:

$$p_1 = 0.0099$$
$$p_2 = -0.01362 \quad (6.2)$$

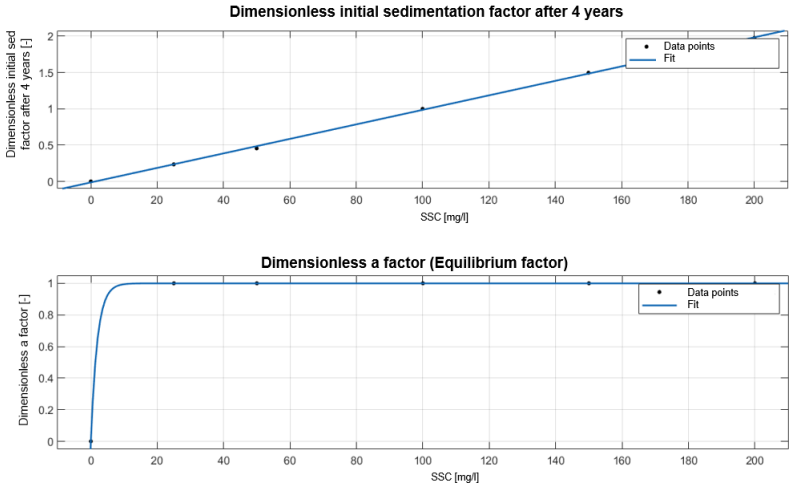

Figure 6.5: Top figure: fitted formula for determining the dimensionless initial sedimentation factor for arbitrary levels of SSC. Bottom figure: fitted formula for determining the dimensionless a-factor (dimensionless equilibrium factor) for arbitrary levels of SSC.

6.2. Lease Polder life cycle tool - WisLi-Tool

This section will go over the process that is used by the WisLi-tool to predict the expected sedimentation curve for an arbitrary case and how it will use this curve to assess the cost and benefits of a complete life cycle of a newly constructed Lease Polder. Subsection 6.2.1 will discuss how the tool will use the dimensionless parameter factor functions that were obtained in the previous section to predict a case-specific sedimentation curve, based on the case-specific parameters. Subsection 6.2.3 will describe the procedure that will be performed by the WisLi-tool, where the expected sedimentation curve resulting from the case-specific parameter factors will be coupled to certain input costs and benefits to predict the feasibility of a Lease Polder by evaluating its complete life cycle.

6.2.1. Case-specific sedimentation curve

Following the six steps that were used to obtain the dimensionless parameter factor functions, as was explained in the previous section, an additional six steps (steps 7 to 12) will be used to transform the parameters of an arbitrary Lease Polder case to an expected sedimentation curve (where step 7 to 9 are displayed by figure 6.6 and steps 10 to 12 by figure 6.7).

Step 7 & 8 The partial input for the WisLi-tool consists of the parameter values for an arbitrary Lease Polder case. All the separate dimensionless parameter factor functions that were obtained at step 6 are embedded in the tool. These functions will automatically transform the input parameters into dimensionless parameter factors for the equilibrium bed level change and the initial rate of sedimentation.
Step 9 Now that each parameter value has been transformed into its individual dimensionless factors, these factors can be combined by multiplication to form the expected dimensionless factor the equilibrium bed level change and the initial rate of sedimentation for the assigned combination of parameter values. The factors describe the ratio difference between the absolute values for the base-case scenario, for both the initial sedimentation rate and equilibrium bed level change.

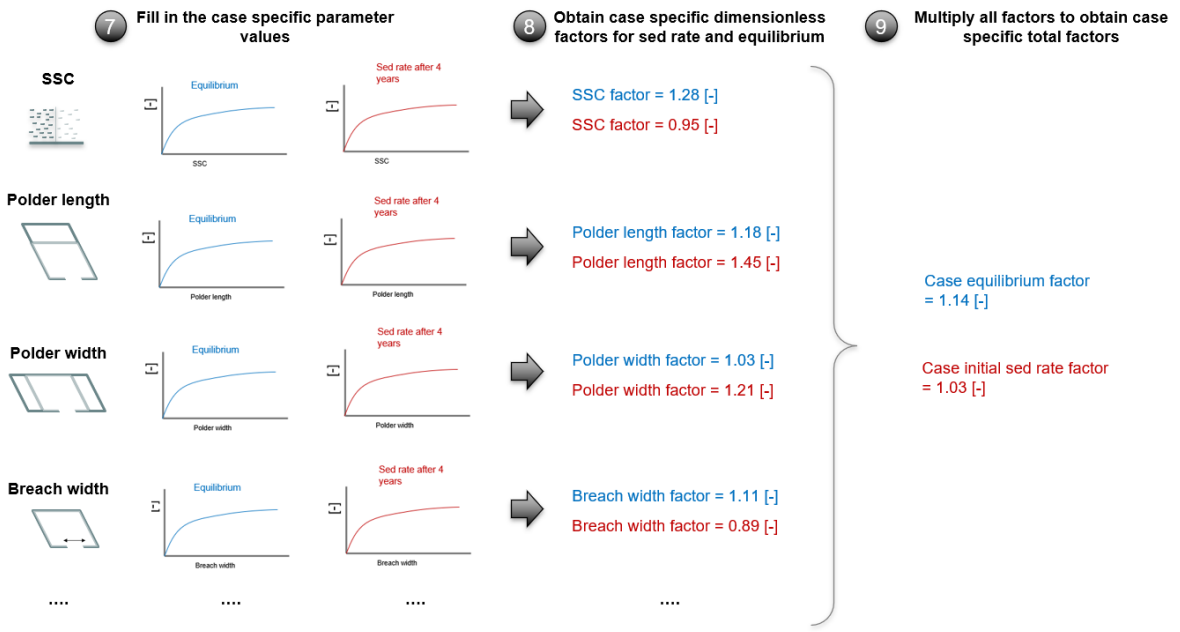

Figure 6.6: Schematizing of the transitions of arbitrary Lease Polder case parameters into a case-specific equilibrium factor and a case-specific initial sedimentation rate factor (Steps 7 to 9)

Step 10 In order to transform the resulting dimensionless factors for both the initial rate of sedimentation and the equilibrium bed level to absolute values, the tool needs to multiply the two factors with the absolute values that resulted from the base-case scenario.
Step 11 The tool can now create an exponential function that describes the expected sedimentation curve now that the absolute values for initial sedimentation rate and equilibrium bed level are known for the arbitrary Lease Polder case. This can be done by rewriting the exponential function to factor b and solve with the

t, y and a factor originating from step 10. Here, y is representing the average bed level change after 4 years, t represents the 4 year period and the a factor is equal to the equilibrium bed level.
Step 12 The script has now created an exponential function that describes the expected sedimentation curve which will be used to generate the life cycle cost-benefit analyses.

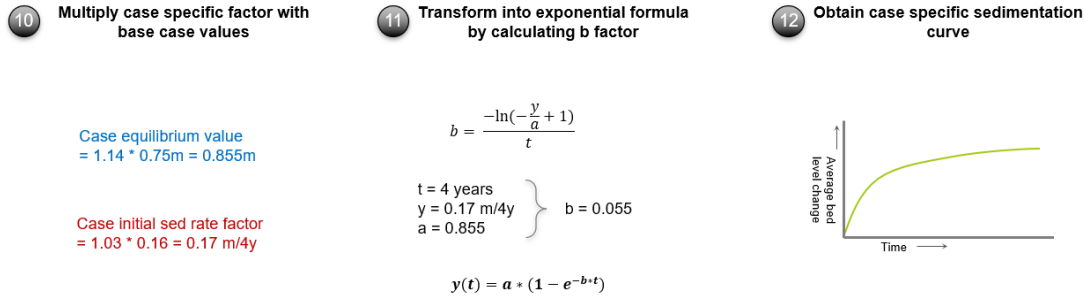

Figure 6.7: Schematizing of the transition of the case-specific equilibrium factor and the case-specific initial sedimentation rate factor to the case-specific sedimentation curve (steps 10 to 12)

6.2.2. Case-specific Delft3D model vs. WisLi-tool sedimentation curve

In order to evaluate the accuracy to which the WisLi-tool is capable of predicting the sedimentation curve for arbitrary Lease Polder cases, a comparison is made between the resulting sedimentation curve predicted by the WisLi-tool and the sedimentation curve resulting from a Delft3D model. The parameter values were arbitrarily chosen and are presented in table 6.2.

Table 6.2: Parameter settings for the test case that is used for the comparison between the results of the WisLi-tool and the Delft3D model

Parameter settings	SSC	Polder width	Polder length	initial bed level	tidal amp	Breach width
Test case	45 mg/l	610m	500m	0.5m	2.1m	82m

The results for both the WisLi-tool prediction and the Delft3D model are presented by figure 6.8. The comparison shows that the WisLi-tool is able to predict similar results to the Delft3D model within a 90% accuracy range.

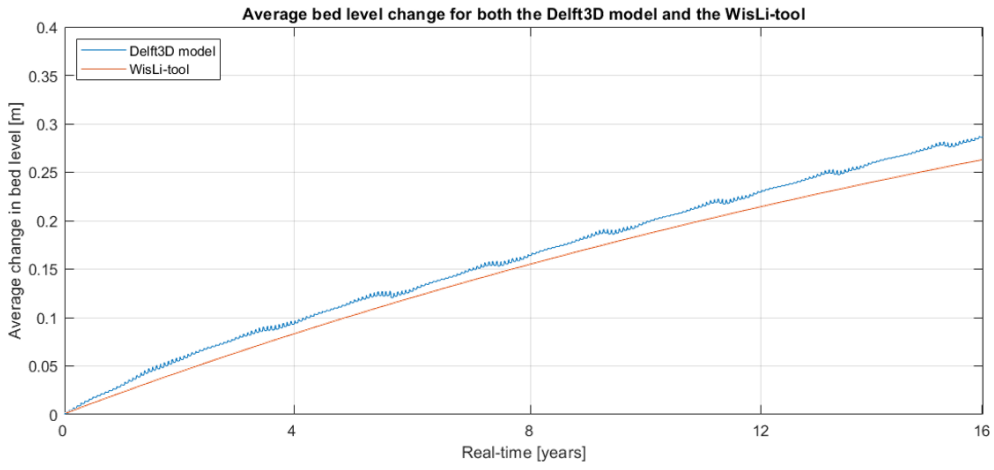

Figure 6.8: The comparison between the average bed level change for an arbitrary case computed by a Delft3D numerical model and estimated by the WisLi-tool

6.2.3. Lease Polder life cycle cost analysis

Now that the tool has obtained the expected sedimentation curve for the arbitrary case that was used as input, the tool can create a complete life cycle during a given time span. The life cycle consists of a primary opening of the Lease Polder, followed by subsequent closings and re-openings of the Lease Polder. The tool

will start with computing the evolution of the average bed level originating from the initial bed level that was assigned as an input parameter. A certain upper threshold value for the maximum average bed level relative to mean sea level can be assigned which instructs the tool to compute the bed level change until that maximum threshold is reached. From that point, the tool will close the polder, after which the bed level will follow a pre-assigned function describing the land subsidence. This function can either be linear or exponential, depending on the user's input preferences.

The evolution of land subsidence will be computed until the average bed level reaches the lower safety threshold. This lower safety threshold can be set by the user to an arbitrary level of bed elevation relative to the mean sea level. The value of this lower threshold can be based on a specific level of coastal safety that is required for the assurance of coastal protection for the hinterland, given the case-specific secondary dike and hydraulic conditions like waves and storm surges. Once the minimum threshold is reached after a period of land subsidence, the tool will open the polder again computing the change in bed level from the point of opening. The evolution of the bed level will be calculated based on the average bed level relative to the mean sea level during the point of opening. The period for which the polder will be kept open and will thus undergo siltation and a rise in bed level is what will be referred to as the Lease Polder period. This period, therefore, represents the time between the reopening of the Lease Polder and the subsequent closure of the Lease Polder.

The length of this Lease Polder period is a design parameter that will influence the number of openings and closings and will thus affect the resulting costs and benefits of the Lease Polder. Figure 6.9 shows a schematization of the computed life cycle of a Lease Polder for both a long Lease Polder period and a short Lease Polder period. The schematization does not include sea level rise. However, the WisLi-tool does include an option for setting a certain rate of sea level rise which will be taken into account during the life cycle computations.

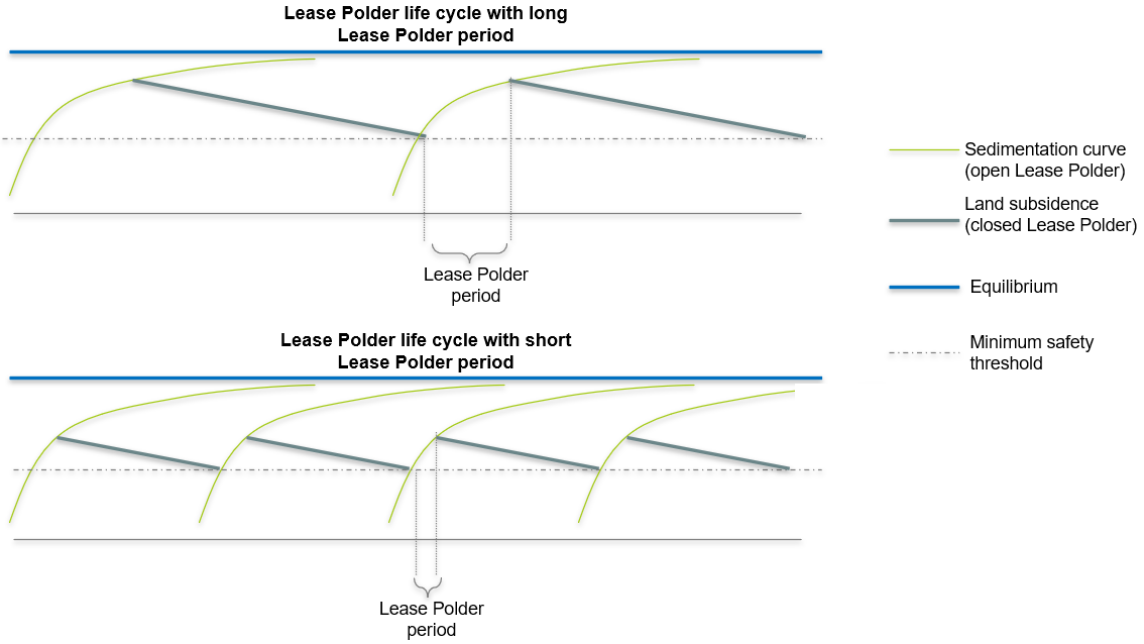

Figure 6.9: Schematizing the life cycle of a Lease Polder with a relatively long Lease Polder period (top figure) and a relatively short Lease Polder period (bottom figure)

Now that the script within the tool has computed the whole life cycle for a given set of input parameters, a certain set of financial input variables can be assigned in order to perform a complete cost-benefit analysis for the given life cycle period. The financial input variables consist of:

- **Cost for the initial installation and opening:** When the decision is made to start the construction for a Lease Polder, certain initial expenditures need to be made before and during the construction of the Lease Polder to ensure a safe initiation.
- **Cost for closing the polder:** The closing of a Lease Polder need to be performed by for example excavators or manual labour. A fixed cost can be labelled to this procedure.

- **Cost for opening the polder:** Similar to the closing of the Lease Polder, a fixed price can be labelled to the opening of the Lease Polder.
- **Revenue during closed period:** The polder land can be used for agricultural purposes during the period that the Lease Polder is closed off. Depending on the type of agriculture, a certain rate of revenue per year can be produced.
- **Revenue during open period:** As explained in the previous chapters, there is a possibility for the Lease Polder to be utilized for saline agriculture or for oyster farms during the open state of the Lease Polder. Depending on the type of utilization, a certain yearly revenue can be realized.
- **Cost for re-levelling of the polder bed:** Whenever the polder is closed of, the decision can be made to re-level the bed surface to an equal depth over the complete polder. This can be either done in order to improve the area for agriculture purposes or for the improvement of coastal safety.

Now that the individual costs and benefits are prescribed for the specific case and country, a complete cost-benefit analysis can be performed by the WisLi-tool. The timeline of the life cycle of the specific Lease Polder case will be underlined with costs and benefits, after which a total net income or total costs for the complete life cycle can be calculated as is schematically depicted by the top figure in figure 6.10. The WisLi-tool will now loop through this procedure for all possible lengths of Lease Polder periods, obtaining different outcomes for the total net income or cost. The tool can now determine the optimal point where a specific length for the Lease Polder period will maximize the total revenue, as is shown by the bottom figure in figure 6.10.

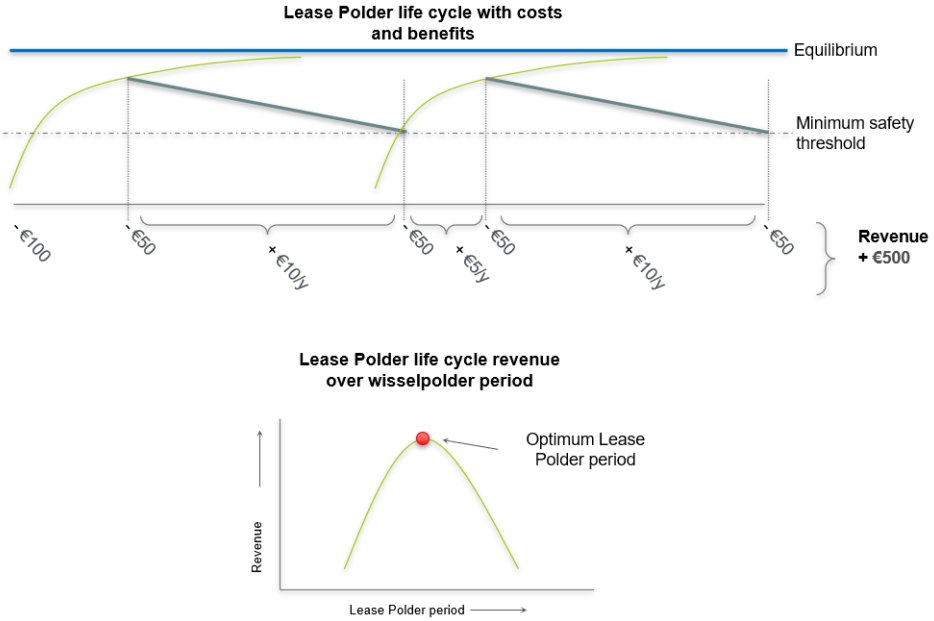

Figure 6.10: Schematized representation of the cost-benefit analysis on the life cycle of a Lease Polder, including the optimization of the final Lease Polder period

The revenue of a Lease Polder during its lifetime is depending on multiple factors which causes the optimum Lease Polder period to be a non-uniform value. Each arbitrary Lease Polder case has a different optimal Lease Polder period based on the combination of financial input parameters and physical case parameters.
In conclusion, the WisLi tool has been shown to be effective to some extent in predicting the sedimentation curve for arbitrary Lease Polder cases, similar to the results that are retrieved from a Delft3D model. The ability to assess the expected sedimentation curve by only filling in the input parameter values drastically reduces the computational time from 3 days to merely a couple of seconds, without the need for knowledge on numerical modelling. The tool is designed in such a way that it is usable for a layperson. The fact that there is such a short computation time brings the benefit of letting the user be able to 'play' with the parameter settings in order to show the effect of a parameter change on the sedimentation curve. It is however important to state that the WisLi-tool is advised to only be used in the first stages of the design process in order to quickly

assess the situation. Due to the fact that the tool only incorporates a limited set of parameters with their own limited range and that these parameters are independently evaluated without correlations results in the advice that a proper Delft3D study is always performed for the final assessment.

7

Discussion

7.1. Base-case model

In the essence of obtaining a simplified base-case model for the sensitivity analysis of the influential parameters on the siltation rate of the Lease Polder, a series of parameter simplifications had to be maintained. Some of these parameter simplifications could however have a significant impact on the final results, but were mandatory to remain simplicity and comparability. For example, the boundary conditions were drastically simplified. The assumption of a tidal forcing consisting of only an S2 and M2 constituent transformed the intricate tidal signal with surges and slacks into a consistent sinusoidal signal containing spring and neap tides. This causes the morphological results to show the same constant signal in average siltation rates. The addition of an M4 overtide could introduce the effect of tidal slacks, which would lead to a net import or export of fines depending on the $M2-M4$ phase shift. For example, a phase shift of $\phi_{M4-2} = 3\pi/2$ would lead to vertical asymmetry in the tidal signal with longer high water slack duration's, leading to a net import of fine sediment in the system (Bosboom and Stive 2012). Such a flood-dominant system would be induced by the presence of shallow channels and limited storage on the tidal flats. An ebb-dominant system with longer low water slack duration on the other hand would lead to a net export of fine sediment. These effects of tidal slacks are however not taken into account by the simplification of the tidal signal, but would be interesting for further research.

The simplification of the sediment characteristics implied that the model only consisted of two sediment fractions, where one resembled the consolidated bed sediment fraction and the other the suspended sediment fraction. By making this assumption, a part of the consolidation process of fine sediments is taken into account by artificially making the bed layer more resistant to erosion (higher critical shear stress for erosion). If the bed layer would consist of the same sediment fraction as the suspended sediments, extensive erosion would cause physically inaccurate results. However, by making the initial bed more erosion-resistant, only a part of the consolidation process is incorporated. All the sediment that settles originating from the suspended sediment fraction will remain its high erodible characteristics and can very easily be re-suspended by relatively small levels of bead shear stress. In reality, the sedimentation process of cohesive fines would include the process of coagulation and flocculation, where the latter causes the suspended particles to clump together forming heavier particles with higher resistance to erosion. This process of flocculation is currently not incorporated in the Delft3D modules. The absence of flocculation affects the results in such a way that the non-siltating area behind the breach is larger than in reality would be the case. This can be deducted from the results of section 5.1.2, where higher levels of critical shear stress for erosion for the suspended sediment fraction led to smaller non-siltating areas behind the breach, resulting in higher equilibrium average bed level profiles. In addition to that, the results showed higher initial sedimentation rates for higher levels of critical shear stress for erosion. This concludes that the results of the base case can be slightly underestimated in comparison to a real-life scenario, based on this effect.

Another important aspect of the base-case model is that wind forces are not directly included in the simulations, but were indirectly accounted for by a transformation of the average wind speeds to wind-generated waves. This resulted in a constant wave forcing originating from the southern boundary including directional

spreading of around 20 degrees. Literature has shown that extreme wave forcing can cause significant levels of resuspension of fine sediment in and around the polder, causing a redistribution of the settled sediment (Oevelen et al. 2000). Waves will cause higher rates of resuspension of the settled sediment in the polder compared to outside the polder due to the shallower depth inside the polder. The result is a net export of sediment from the polder. Besides that, the indirect implementation of wind energy results in the exclusion of the fetch length effect. Longer or wider polders will allow for larger stretches of open water bodies that are more susceptible to the transformation of wind energy into wind-generated waves, further enhancing the process of re-suspension inside the polder. From this, the conclusion can be drawn that the results of the base-case can undergo a slight overestimation in comparison to a real-life scenario, based on this simplification.

Despite the significant model simplifications, the base-case model was able to recreate similar morphological results to the observed data from the Tollesbury case study. With some simplifications causing an underestimation and others causing an overestimation, the overall results were able to cancel the individual effects out, recreating an accurate representation of the Tollesbury case.

7.2. parameter scenario models

The parameter sensitivity of the suspended sediment concentration on the change in bed level within a Lease Polder was estimated based on the literature by Williams et al. (2004) and is shown in figure A.1. The shape of the scenario results that were obtained by the model in this study shows a direct resemblance with the predicted sedimentation curves, backing the estimation by Williams et al. (2004). The relation between the SSC and the initial sedimentation rate which were found during this study shows a nearly linear relationship, suggesting a direct connection between the SSC and the initial sedimentation rate.

Oevelen et al. (2000) showed in their study that there was a negative relation present between the breach width and the sedimentation rate for compared cases. He could however not explain this negative relation since he expected the decrease in flow velocity through the breach to cause a rise in sedimentation rate. Fortunately, the model results for the sensitivity analysis of the breach width show this same negative relationship and further analysis of these results were able to clarify this negative relationship. Figure C.1 showed that the decrease in sedimentation is a result of the increase in significant wave height that penetrates into the polder, for increasing breach widths. The non-accreeding area behind the breach is therefore predominantly dependent on the wave regime and the breach width.

The sensitivity analysis for the tidal amplitude however did not show a similar linear relationship and appeared to transfer to a different regime for tidal amplitudes surpassing $3m$. This regime for high tidal amplitudes showed the occurrence of higher velocity circular flows, as were visualized by figure C.2. The regime for lower tidal amplitudes showed the absence of these circular flows, with ebb-flows following a more linear line to the breach. Oevelen et al. (2000) showed through different case studies that cases with larger tidal amplitudes showed higher erosive forces within the polder. However, higher tidal amplitudes lead to larger tidal prisms, which offer a larger net sediment budget. There seems to be a trade-off between these two principles, which is also noticeable in the models. Similar scenario runs for tidal amplitude with a smaller breach width resulted in a shift of the transition between the two regimens, where circular flows were already observed for tidal amplitudes of $2.5m$. This suggests that the transition is dependent on the flow speed through the breach. It remains unclear whether the transition to the other regime is only dependent on this flow speed until more parameter combinations are compared. The models do however show a decreasing rise in initial sedimentation rates for increasing tidal amplitudes during the regime with lower tidal amplitudes. Another noticeable effect of the increase in tidal amplitude is the extension of the non-accreeding area behind the breach due to the increase in water depth.

The scenarios with variations in the initial polder bed level showed an increasing relationship between the decrease in initial bed level and the initial rate of sedimentation. However, this trend only applied for initial polder bed levels ranging from $OD+1m$ to $OD-1.5m$. A different morphological regime is entered during the transition of an initial bed level of $OD-1.5m$ and $OD-2m$. This 'deep polder regime' results in a stop in sedimentation after around 5 years of operation. Section 5.2.4 assessed that the stop in sedimentation occurs on the side flanks of the polder due to the high orbital velocity created by waves, which is caused by the fact that the waves can enter the polder at greater depths. The reason that this process does not diminish over

time is because of the permanent absence of sedimentation at the non-accreeding area behind the breach, letting the incoming waves continuously enter the polder without significant dissipation. The question now arises whether the permanent presence of the non-accreeding area for deeper polders will be as significant for real scenarios. As earlier explained, the numerical model assumes a constant wave field, leading to the permanent absence of sedimentation in the area behind the breach. In reality, the wave forcing will be not constant and will sometimes even be absent. With the temporary absence of waves, sediment is able to settle closer behind the breach, where flow velocities have sufficiently decreased. Depending on the level of flocculation and short time consolidation, the possibility exists that the settled sediment has increased its critical shear stress for erosion to a level that can withstand the possible following wave fields. However, this is only a hypothesis and needs to be verified during follow-up studies.

A possibility for the mitigation of the permanent absence of sedimentation on the area behind the breach could be the alternation of the breach location after each Lease Polder cycle. Whenever the new breach is opened at a significant distance next to the old breach, the soil behind the new breach will already be higher and fully consolidated.

Multiple previous studies of different Lease Polders and salt marshes in the literature indicated that some of the cases were able to outgrow the rate of sea level rise. A direct link between the rate of sea level rise and the difference in bed level change was however hard to quantify due to the high variability in different parameters (Oevelen et al. 2000, J. V. Belzen, T. J. Bouma, and Ysebaert 2020, Price 2016). This study was able to compare the base-case scenario without sea level rise to the base case with sea level rise with a rate of $4.2 mm/year$, which ruled out the influence of all other parameters. The results showed that the difference between the sedimentation rates at the back of the polder for the two scenarios was exactly equal to the rate of sea level rise that was set at the boundary. This can lead to the conclusion that, for SSC rates of $100 mg/l$ or higher and comparable environment to the base case, a rate of sea level rise of $4.2 mm/year$ can be completely counteracted. Future studies could use the same method to map the complete potency of counteracting different rates of sea level rise for varying parameter settings.

At last, the sensitivity analysis on the dimensional length and width showed to have no significant effect on the initial rate of sedimentation. With the polder width being one of the design parameters, this would suggest that it would be economically advantageous to make the polders as wide as possible to lower the construction cost of orthogonal dikes. Nevertheless, with the increasing width of the polder, the breach had to be widened accordingly to accommodate the larger tidal prism. The widening of the breach for the wider and longer scenarios showed the same increase in non-accreeding area behind the breach similar to the breach width scenarios. This will lead to the absence of sedimentation near the end of the polder for wider polders. A possible mitigation for this can be the construction of two smaller breaches side by side, which would possibly decrease the lengths of the individual non-accreeding areas.

7.3. Quick assessment tool - WisLi-tool

The principle behind the quick assessment WisLi-tool is based on the assumption that the sensitivity of six Lease Polder parameters can be individually assessed and combined in order to predict the sedimentation curve for arbitrary Lease Polder cases. This assumption however brings a set of uncertainties. The assessment of the individual parameter sensitivity analysis stands on the exponential fit of the Delft3D scenario results. However, not all scenario results follow an exponential progression. For example, the scenario for $SSC = 25 mg/l$ shows a more linear relation during the first 20 years of operation. Other examples are the scenarios for initial polder bed level during the 'deep polder bed regime', which show an immediate cessation of sedimentation after 5 years of operation. Despite the fact that not all scenarios follow a perfect exponential regression, the exponential fits are able to isolate the two important characteristics that are utilized by the tool, namely the initial sedimentation rate and the equilibrium profile.

The other uncertainty comes with the transformation of the initial sedimentation rate and the equilibrium profile to a dimensionless factor. This transformation implies that all factors are dependent on the base-case sedimentation profile. The question to which extend these dimensionless factors can be individually combined without the inclusion of correlation remains unanswered. For example, further research has to be done on the correlation between initial bed level and tidal amplitude. There can be a significant effect of

resulting from the balance between tidal amplitude and initial bed level, where a certain balance can lead to the transition to a permanently inundated polder. The effects of these balances, for now, remain in a grey area and need further research before statements can be made.

The parameter specific factor fits that were made in step 6 in Chapter 6 are based on the scenario results for each parameter. These fits can with a certain level of confidence predict the effect on the initial rate of sedimentation and equilibrium profile for arbitrary parameter values within the upper and lower bound of the parameter scenarios. The possibility exists for the fits to predict factors for parameter settings outside the upper and lower boundary. This is however not advisable since more scenarios need to be simulated in order to verify these extrapolations. It is especially dissuaded to extrapolate the factor fits which are based on polynomial functions.

The tool has a built-in option where one can assign the re-levelling of the bed. This can either be done in order to improve the area for agriculture purposes or for the improvement of coastal safety. This can specifically be of interest for cases where the non-accreeding area extends all the way to the back end of the polder. When the bed is re-levelled, the initial polder bed level differs from the original polder bed level. This new initial polder bed level will be looped through the tool in order to calculate a new sedimentation curve that will be used for the second opening of the polder. The tool will perform this loop for each cycle of the Lease Polder.

The strength of the WisLi-tool is found in its adaptability for future changes and improvements of the parameter sensitivity. When new scenarios will be simulated for the expansion of the predictability range, the results can easily be transformed to new factor fits for the initial sedimentation rate and the equilibrium depth. These newly fitted formulas now only have to be changed in a designated area after which they will be fully incorporated into the tool. This also applies to the input parameters for the costs and the benefits, which can all be adjusted on the input dashboard of the tool.

7.4. Physical derivation of the sedimentation process

During this study, the majority of the results were based on numerical computations resulting from the Delft3D model. These results were thereafter empirically fitted to exponential functions. With the goal of proving the nature of these exponential fits and divining the origin of the found relations, one could take a step back and transform the system into a simplified system describes by a mass balance. The complete summarized derivation in this section can be found in Appendix E. Within this mass balance, the net variation in the cumulative sediment mass within a Lease Polder M can be defined by the difference in gross sediment mass input S_{in} and output S_{out}:

$$\frac{dM}{dt} = +S_{in} - S_{out} \tag{7.1}$$

Since the sediment mass which settles is several orders higher than in the water column, the assumption can be made that net variation in cumulative sediment mass is predominantly caused by the change in bed level z. The net variation in the cumulative sediment mass within a Lease Polder can now be rewritten to a variation in bed level multiplied by the dimensional length L and width W of the polder, and the dry bulk density of the soil ρ_d. The right-hand side can be simplified and defined as an incoming discharge Q times the incoming concentration c_{in} and an efficiency factor α. The factor α describes the trapping efficiency and would in reality be depended on multiple factors such as the depth of the polder, sediment characteristics and the internal wave energy.

$$\rho_d LW \frac{dz}{dt} = \alpha c_{in} Q \tag{7.2}$$

The assumption is made that the polder bed is moving from its initial level z_0 where the discharge is Q_0 to its equilibrium state z_{eq} where the discharge is zero. The relation between the bed level and the discharge is assumed to be linear. The discharge can now be rewritten to a dependency of the initial discharge Q_0 on the normalized ratio of the bed level relative to the equilibrium. The variation in bed level on the left-hand side can be expressed as the variation in bed level relative to the equilibrium bed level z_{eq}.

$$\rho_d LW \frac{d\left(z - z_{eq}\right)}{dt} = \alpha c_{in} Q_0 \left(\frac{z - z_{eq}}{z_0 - z_{eq}} \right) \tag{7.3}$$

With $\tilde{z}$ being the normalized bed level factor written as:

$$\tilde{z} = \frac{z - z_{eq}}{z_0 - z_{eq}} \tag{7.4}$$

Equation 7.3 can now be rewritten to a set of integrals and can be solved for the bed level z with $\tilde{z}$ in its original form (see Appendix E for the complete derivation):

$$z = z_{eq} + \left(z_0 - z_{eq}\right) \exp(-t/T) \tag{7.5}$$

Where T represents a timescale in the form of:

$$T = \frac{1}{\alpha\beta} \frac{\left(z_{eq} - z_0\right)}{\Delta\eta} \frac{\rho_d}{c_{in}} T_t \tag{7.6}$$

Here, the timescale T is depended on the bed level difference, tidal rang $\Delta\eta$, tidal period T_t and the ratio between the dry bed density ρ_d and the SSC c_{in} at the boundary. The α and β are the factors that are partly depended on these parameters and depended on external factors.

Equation 7.5 now describes a function for the development of the bed level over time. Comparing this formula to the formula that was used for the exponential fits in Chapter 6, namely $y(t) = a(1-exp(-b \cdot t))$, results in a similar relation. The a represents the total equilibrium bed level change (starts at zero), equation 7.5 represents the equilibrium bed level relative to the initial bed level. Both principles form an equivalent net result.

The b can be denoted by $1/T$, with T being equal to equation 7.6. By following the basic theoretical principle, one can now see the direct origin of the found relations during this study. For example, the model scenarios showed that the dimensional width and length of the polder did not have a direct significant effect on the initial sedimentation rate. Equation E.13 from the full theoretical derivation reveals that the dimensional polder length and width is cancelled out of the timescale T.

The expression for the timescale T indicates the presence of a linear dependency on the remaining parameters. This is, however, a sham dependency since the α and β factors also depend on the indicated parameters. For example, when the tidal period T_t doubles for a diurnal tide relative to a semi-diurnal tide, the time scale would also double. However, the α factor is likely to also rise for an increasing tidal period, since the sediment catchment efficiency will improve for lower flow speeds through the breach and longer settling periods. One could conclude that the α and β factors include the correlation between processes and parameters, but are difficult to derive. Moreover, the model results showed the transition between different process regimes for certain bed levels, which indicates that these factors are expected to be not linear, but depended on the actual bed level state.

The above-stated facts prove the added value of the relations found during the model study. The values of the α and β factors from the derived relationships are difficult, if not impossible to uniformly derive for arbitrary Lease Polder parameters following the current theoretical physics. The model study succeeded in empirically deriving these relations in the form of a parameter specific a and b factor.

8

Conclusion and Recommendation

8.1. Conclusion

This section will assess the answers to the individual research sub-questions based on the results which were obtained during this study, followed by the assessment of the main research question.

What type of numerical modelling can simulate siltation processes observed in former Lease Polder cases?
During the first phase of this study it was found that a numerical model based on 2DH Delft3D was able to simulate the siltation process and rates within the Lease Polder for a simplified model, based on the Tollesbury Lease Polder case study. By coupling the Delft3D FLOW module with the Delft3D Wave module, a workable morphodynamic model can be constructed simulating fine sediment dynamics within a Lease Polder system. The aim of the study was to create a simplified model of a Lease Polder with the intention of obtaining a benchmark model on which different parameter scenarios could be compared in a one-on-one manner. By simplifying the model, the individual effects of the different parameters could be more isolated which resulted in better observations. The simplifications that were carried out consisted of dimensional simplifications, as well as hydrodynamic, sediment and forcing simplifications. The bathymetry of the Tollesbury case was projected by a rectangularization of the grid, the assumption of an alongshore symmetrical foreshore consisting of a single tidal channel and tidal flats and a uniformly sloped polder bed. The forcing conditions were reduced to a constant wave forcing, a symmetrical M2S2 tide coupling and a constant suspended sediment concentration at the boundary, all of which were based on the Tollesbury case. The morphological results of the simplified model were compared to the Tollesbury historical date in figure 4.9, and were able to show significant resemblance in both absolute bed level change and local sedimentation patterns.

How can a numerical model help with the determination of the sensitivity of different parameters on the rate of siltation within the polder?
The sensitivity of the individual parameters on the siltation process can be assessed by comparing the siltation results of a specific scenario where one parameter(set) is adjusted to a validated base-case model. In order to consequently change and compare a specific parameter, without undermining the essence of a one-on-one benchmark, two more dimensional simplifications were mandatory to obtain a sound base-case. These simplifications consisted of replacing the tidal channel and tidal flats with an equally sloped alongshore uniform foreshore and by replacing the sloped polder bed with a near-horizontal polder bed. The processes and results were validated for both simplifications. Following this method, the sensitivity of the suspended sediment concentration, breach width, polder width, polder length, polder bed level and maximum tidal amplitude were assessed. The result will be summarized below.

Suspended sediment concentration The sensitivity of the suspended sediment concentration in the estuary was assessed by comparing five scenarios with SSC rates ranging from $25 mg/l$ to $200 mg/l$. The results showed a linear relationship between the increase in SSC and the increase in initial sedimentation rate, ranging from $9,6 mm/year$ for an SSC of $25 mg/l$ to $80,9 mm/year$ for an SSC of $200 mg/l$ during the first four years. The local sedimentation patterns do not differ for changes in the SSC and each scenario reaches for an equal equilibrium profile depth, only at different rates.

Breach width The model results for varying breach widths showed that the width of the breach has a significant influence on the amount of wave penetration into the polder. Increasing breach widths resulted in an increase of wave energy transferred into the polder, resulting in larger areas where sediment is not able to settle. Breach widths of $100m$ and larger resulted in non-accreedable areas reaching all the way to the secondary polder, decreasing the effectiveness of creating coastal protection. Narrower breaches with a width of $50m$ show direct erosion at the surface within the breach. Both the initial rate of sedimentation and the average equilibrium depth showed to have a negative relationship for larger breach widths.

Polder width and length The sensitivity of horizontal dimensions for the polder was analysed by simulating polders with varying widths and lengths, ranging from $320m$ to $860m$ for both width and length individually. The change in horizontal dimensions was directly coupled to the change in the width of the breach, given that the tidal prism is directly proportional to the horizontal dimensions. This way, the flow speeds through the breach stays relatively constant. Moreover, Escoffier (1977) showed that the breach of a tidal basin will always reach for an equilibrium surface area in order to reach the equilibrium flow velocity. The morphological results showed that the variations in horizontal dimensions have an insignificant effect on the initial sedimentation rate within the polder. The average equilibrium bed level does show to be decreasing for increasing horizontal dimensions, indicating that smaller polders are more favorable for their net sediment import. This decrease in average equilibrium depth for increasing dimensions is mostly caused by the increase in non-acreedable area due to the wider breaches for larger polder dimensions. For wider polders, these non-accreedable areas reached all the way to the end of the polder, making it less desirable for securing coastal protection.

Initial polder bed level The scenarios with variations in initial polder bed levels ranging from $OD+1m$ to $OD-4m$ showed an increasing S-shaped relationship between the decrease in initial bed level and the initial rate of sedimentation, where the initial rate of sedimentation reaches a maximum at $OD-4m$. The set of scenarios showed a separation into two different regimes for the average equilibrium bed levels. For initial polder bed levels ranging from $OD+1m$ to $OD-1.5m$, a near-linear increase in equilibrium polder bed level was observed for decreasing initial polder bed levels, which was called the 'Shallow polder bed regime'. Initial polder bed levels ranging from $OD-2m$ to $OD-4m$ showed an abrupt stop in sedimentation rate after around 5 years of operation after which the average bed level oscillated around an equilibrium. This range was called the 'deep polder bed regime'. The stop in sedimentation occurs on the side flanks of the polder due to the high orbital velocity created by waves, which is caused by the fact that the waves can enter the polder at greater depths. The reason that this process does not diminish over time is because of the permanent absence of sedimentation at the non-accreeding area behind the breach, letting the incoming waves continuously enter the polder without significant dissipation.

Tidal amplitude The sensitivity analysis for the tidal amplitude showed that the scenarios with tidal amplitudes ranging from $2.0m$ to $2.5m$ displayed increasing levels of cumulative sedimentation for increasing levels of tidal amplitude. The scenarios with tidal amplitudes of $3.0m$ and higher break this trend of increasing levels of sedimentation. With increasing levels of tidal amplitude, the tidal prism increases such that the flow velocities through the breach increase. This causes flow patterns within the polder to change and form a strong circular current. These circular currents have higher flow velocities, preventing the settlement of the fine sediment and lower the average equilibrium bed level profile.

All the results for the sensitivity analysis for the above-mentioned parameters are summarized in Chapter D in the Appendix. These include the deducted parameter sensitivity functions which formulate the parameter dependency of the initial sedimentation rate and the average equilibrium bed level.

To which extend can the siltation in a Lease Polder counteract the impact of a certain rate of sea level rise on coastal protection?

The results of the base-case model simulation with the implementation of sea level rise with a rate of $4.2mm/year$ presented in section 5.3.2 suggested in the first instance that the average rate in bed level change is able to follow the sea level rise with a factor $1/2$ compared to the base-case model without sea level rise. However, when the main objective of the Lease Polder is to retain a certain level of coastal protection, one should not focus on the average change in bed level only, but should also consider the local change in bed level. As was explained in section 2.1.3, the importance of remaining coastal safety lays for a significant part at the development of

bed level at the back side of the polder, where the protruding waves can partly dissipate before reaching the secondary dike. The analysis of the average bed level change over the area that is located directly in front of the secondary landward dike showed that the polder bed level can directly follow the rate of sea level rise, even during the initiation phase of the Lease Polder. With the back area of the polder rising at a similar rate as the rate of sea level rise, the Lease Polder can be seen as a partly self-sustaining system of coastal defence.

To what degree can the parameter sensitivity be utilized to predict siltation rates for arbitrary Lease Polder cases with the help of a quick assessment tool?
The WisLi-tool is an Excel tool created with the purpose of quick assessing the initial sedimentation rate for arbitrary Lease Polder cases. It utilizes the results from the sensitivity analysis to make a vast estimation for the initial sedimentation rate and the average equilibrium bed level. The results from the sensitivity analysis have to be transformed into usable functions first, in order for the WisLi-tool to properly use the results. The transformation consists of converting the individual scenario results to functions describing the dimensionless sensitivity of each parameter on the initial sedimentation rate and the average equilibrium bed level. These functions are embedded in the WisLi-tool and can now produce dimensionless sensitivity factors for arbitrary parameters within the researched boundaries. Section 6.2 elaborates on how the tool subsequently combines these dimensionless factors into a single exponential function that describes the expected sedimentation curve for the arbitrary case-specific parameters.

The sedimentation curve that is computed by the WisLi-tool for an arbitrary case is compared to the model results simulated by Delft3D in Section 6.2.2. The Wisli-tool is able to predict the sedimentation curve within a 90% accuracy range relative to the Delft3D computation for an equal arbitrary Lease Polder case. The Wisli-tool can therefore serve as a time-saving replacement for a Delft3D model for quickly estimating the expected sedimentation for arbitrary Lease Polder cases.

What are the main design parameters and how can these design parameters be improved to optimize the efficiency of a Lease Polder?

Breach width The breach width can be seen as an indirect design parameter. Although the breach can be made arbitrarily wide, a certain set of guidelines has to be followed in order to optimize the sediment catchment. This study showed that the non-accreeding area behind the breach increases for increasing breach width. Therefore the breach needs to be kept as narrow as possible. On the other hand, when the breach gets too narrow, flow velocities through the breach increase to such a level that high-velocity circular flows arise within the polder which prevent the settling of sediment. A rule of thumb can be followed where the width of the breach needs to be 0.02% of the maximum tidal prism. The models in this study showed that by following this rule no circular flows arise.

Horizontal polder dimensions In the case of the absence of the landward secondary dikes and the dividing dikes in between the polders, the engineer himself can design the horizontal dimensions of the dike. The results of the sensitivity analysis for the polder width and length show that smaller dimensions are more favorable in terms of the average equilibrium bed level that is reached. These effects are however evaluated individually. Further research on the combined effect of changes in the horizontal dimensions still has to be performed.

When the focus is placed on the economic aspect, the construction of wider polders would lead to a reduction in the cost for the placement of the perpendicular dividing dikes. However, the models showed that widening of the dike led to non-accreeding areas reaching all the way to the landward secondary dike. This causes the polders to have a limit to the maximum width of the polder in order to prevent the need for re-levelling around the landward secondary dike, which would bring extra costs. The extent of the non-accreeding area is dependent on several case-dependent factors, which makes the limit of the breach width equally dependent on these factors. Further research is needed to set up universal rules for the determination of the maximum width of the polder. This study does however show that the construction of two evenly spaced smaller breaches could significantly shorten the reach of the non-accreedable area.

Lease Polder period The remaining design parameter, once the dimensional design of the Lease Polder is established, is the Lease Polder period. The Lease Polder period is the duration for which the Lease Polder is

in its open state so that the polder is hydraulically connected to the estuary. During this period, sediment-rich water can enter the polder during each tide causing siltation within the polder. The duration of this period can be chosen by the engineer himself. Longer duration's lead to higher eventual changes in bed level. However, due to the exponential shape of the sedimentation curve, lower rates of sedimentation will be utilized during the later stages of operation, making the siltation less efficient. The opposite is valid for shorter duration's but will lead to more openings and closings.

The impact of the Lease Polder period on the total cost-benefit analysis is led by a trade-off between opening and closing costs, revenues during open and closed stages and the shape of the expected sedimentation curve. These parameters are all location-specific, making it impossible to determine a universal optimal Lease Polder period. The WisLi-tool however can compute the optimal Lease Polder period for an arbitrary case, based on the case-specific input parameters. The optimal Lease Polder period results in the maximum profit or minimum loss during the complete life cycle of a Lease Polder.

8.2. Recommendations

This study accomplished to offer a proper foundation on the simplified modelling of a Lease Polder and the transformation of the resulting parameter sensitivities into a usable quick assessment tool on the feasibility of a Lease Polder. The following section will advise on the improvements that can be made to the foundation and will provide interesting research suggestions that can be built upon this foundation.

8.2.1. Model improvements

The most significant improvement of the numerical model would consist of the implementation of the consolidation process after the sediment has settled. This can be done by adding a time-dependent function to the critical shear stress for erosion for the newly settled sediment. The longer the sediment would be in place, the higher the critical shear stress for erosion will be. This way the model will perform more conform reality and will remove a significant part of the uncertainties.

Other aspects that can be added to the model are the addition of vegetation in the polder in order to increase the flow resistance in the polder. Several additional aspects that can be added to the model were already discussed in section 7.1 in the previous chapter.

8.2.2. WisLi-tool improvements

The first and foremost improvement of the WisLi-tool would be the addition of correlation effects between certain parameters. The addition of correlations would strongly improve the accuracy with which the tool can predict the case-specific sedimentation curves. The addition of a broader set of parameters would improve application purposes. To give an example, only the sediment concentration is now accounted for. By coupling the settling velocity to the critical shear stress for erosion in a separate sensitivity analysis, different ranges of cohesive sediment types and sizes can be incorporated. Not only the number of parameter sensitivity analyses can be improved, but also the range within each parameter can be increased.

Another significant improvement of the WisLi-tool would be the coupling of country-specific costs and benefits to the tool. The user then only has to select the country of which the tool would have a database with the corresponding input values. The cost and benefit analysis could also be expended to not only assess the feasibility of a single dike, but to assess a complete stretch of coastline.

8.2.3. Future research suggestions

The concept of a Lease Polder is still in its infancy and a lot of innovation is still possible within the concept. An interesting feature could be the implementation of oyster farm fields within the polder area during its open state. The sheltered polder area serves as a favorable habitat for the growth of oysters and mussels. These shellfish will not only increase the yearly benefit of the polder, but will also secrete significant amounts of organic sediments, which would further increase the sedimentation efficiency of the Lease Polder. Besides shellfish, the Lease Polder could also offer the perfect habitat for mangroves, which are known for not only their sediment retainment, but also for their coastal protection.

Next to the utilization for the growth of shellfish and mangroves, other methods can be hypothesised for

the improvement of sediment catchment. One way to improve this catchment can be replacing the open breach with an operable gate or set of aquifers can exempt the possibility of tidal retention, where the water in the polder can be held in place during a complete tidal cycle, which could optimize the possible catchment rate for light cohesive particles. The use of aquifers could also eliminate the erosive wave effect. Another method for enhancing the sedimentation could be the injection of sediment into the estuary in front of the polder. Coastal systems with relatively low levels of suspended sediment could thereby artificially helped with the improvement of sediment catchment. The viability of these innovations can be further simulated and analysed in future studies.

Another concern which followed from the Lease Polder models was the non-accreedable area. Different methods for reducing the size of this area can be thought of. A way of reducing the entering wave forces could be the placement of thin dams right behind the breach opening. These thin dams can be constructed by simply piling tree logs in the ground. This can offer a relatively cheap solution for mitigating the non-accreeding area behind the breach. An alternative method could be the variation in the location of the breach after each re-opening of the Lease Polder. The raised bed behind the new breach resulting from the previous Lease Polder cycle has now been completely consolidated and can offer significant resistance for erosion. The non-raised area from the previous cycle can now be filled up without the effect of erosion forces.

A

Theoretical background

A.1. Influential parameters

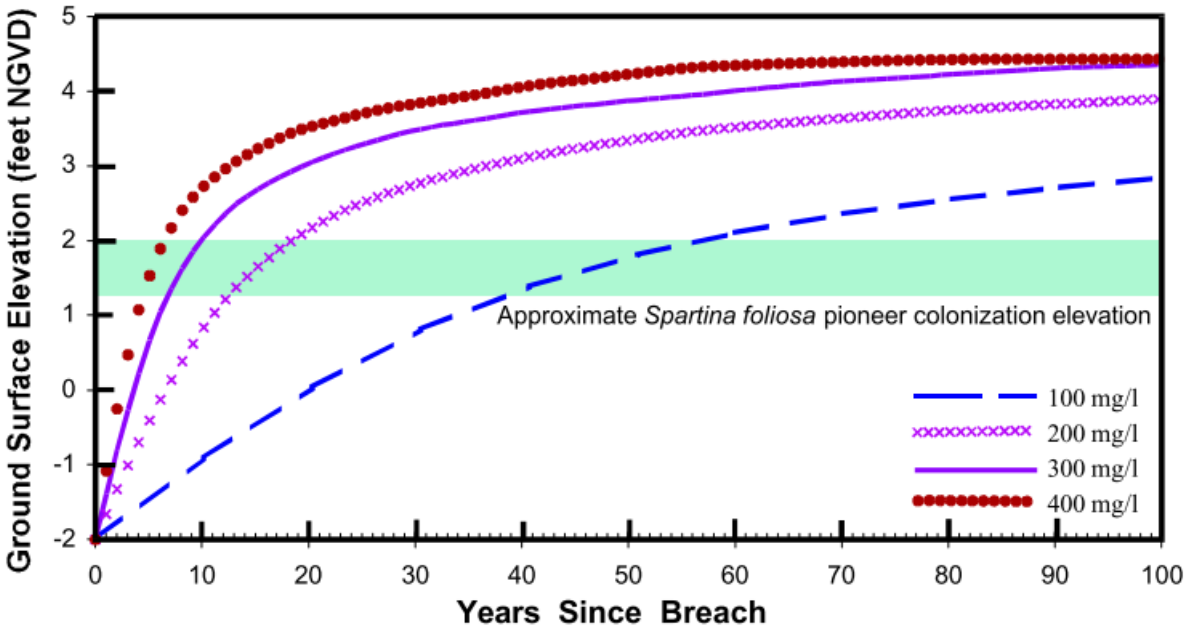

Figure A.1: A prediction of the influence of the suspended sediment concentration on the ground surface elevation within a salt march (Williams, Associates, and Faber 2004)

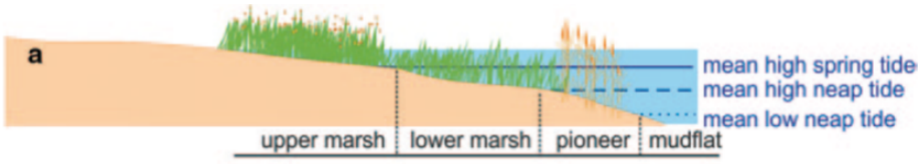

Figure A.2: Ecological habitat for different tidal levels Esteves 2019

A.2. Tollesbury tidal and wind data

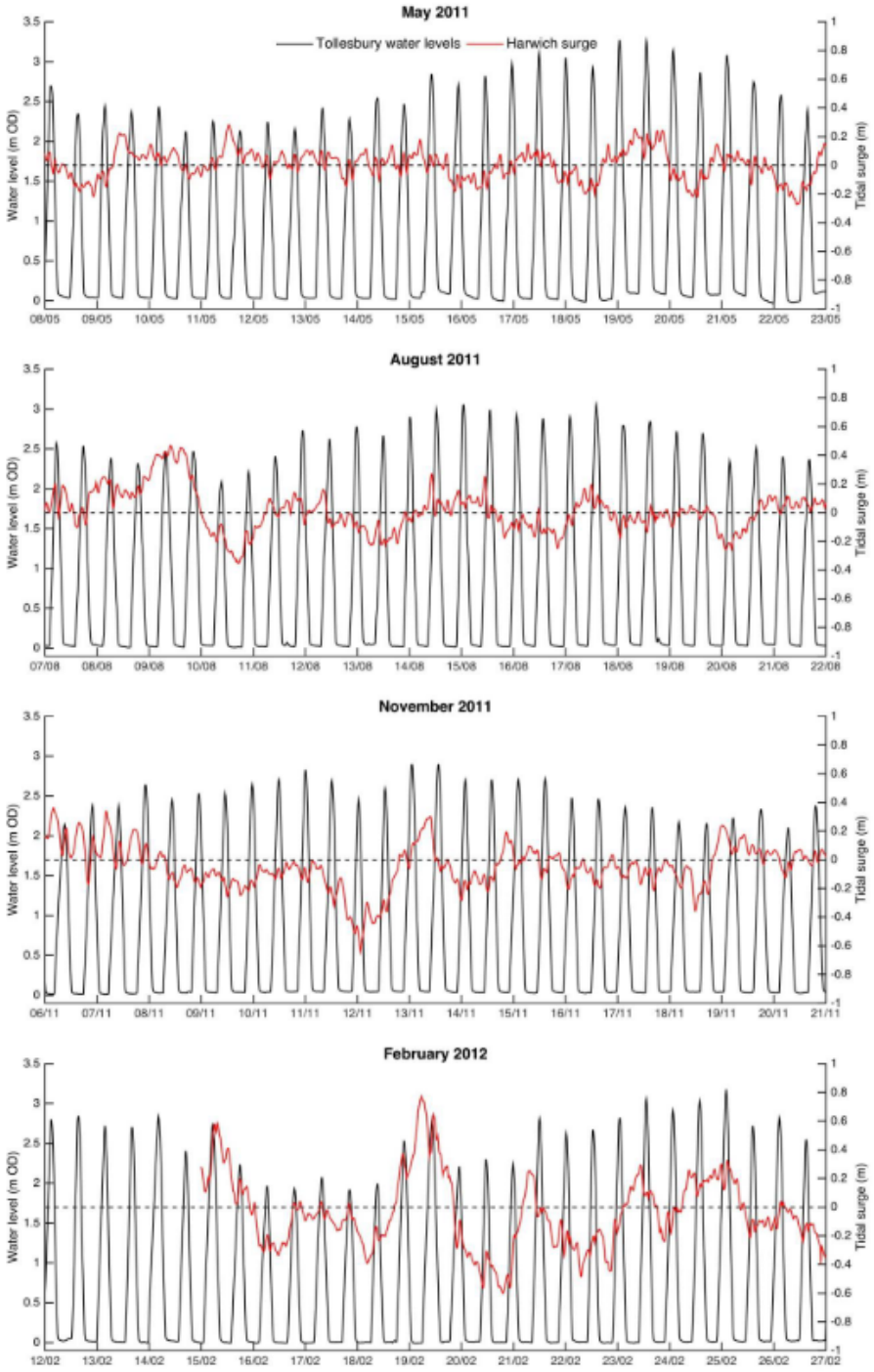

Figure A.3: Water level measured in Tollesbury (Black line) and tidal surge measured in Harwich (Red line) during the months May, August November 2011 and February 2012 Price 2016

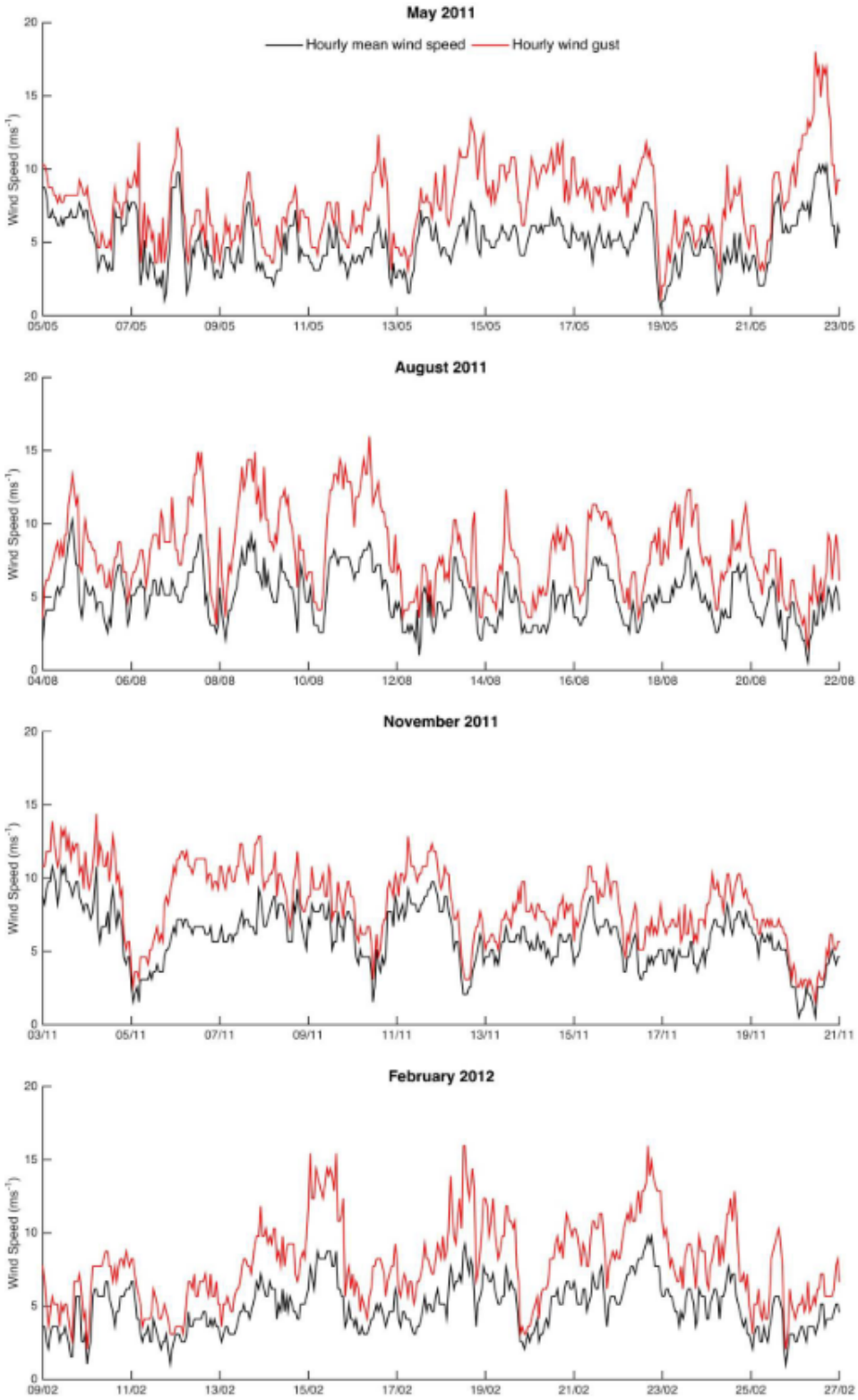

Figure A.4: Hourly mean wind speed (Black line) and hourly wind gust (Red line) measured in Tollesbury during the months May, August November 2011 and February 2012 Price 2016

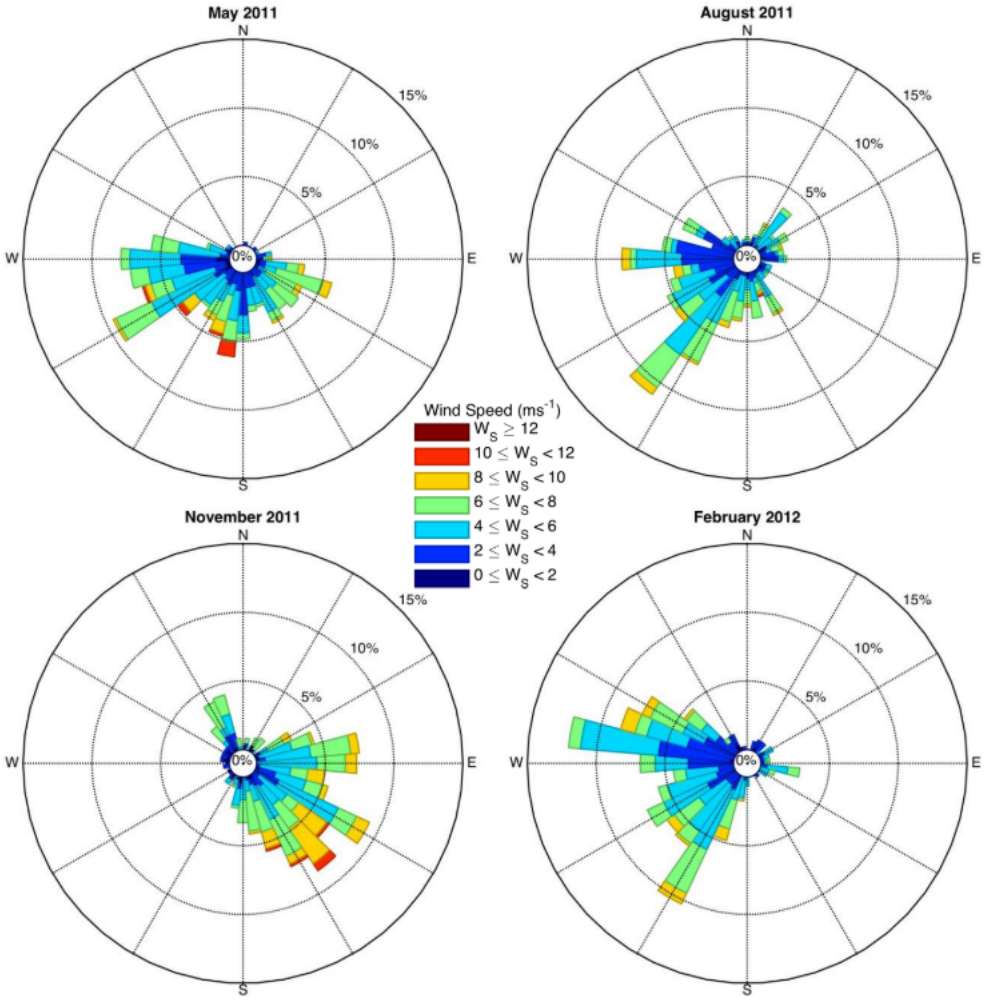

Figure A.5: Wind roses for mean wind velocities measured in Tollesbury during the months May, August November 2011 and February 2012 Price 2016

A.3. Tollesbury sediment characteristics

According to the study of Price 2016, the local suspended sediment concentration at the Tollesbury marsh was measured via a siphon sampler. A total of 34 siphon samplers were placed in and around the research area. Figure A.6 shows the exact locations of the sampling points. The results of the averages values SSC per week are depicted in figure A.7. The average SSC turns out to be around $150 mg/l$. A different study used remotely-sensed CASI data to determine the SSC at Tollesbury of which the results are shown in figure A.10 (Elsner 2009). This study showed an average SSC of around $70 mg/l$, about half of the Price study. Allison et al. 2020 measured the SSC at deeper points in the Blackwater estuary which resulted in SSC levels of $30 mg/l$.

A study regarding sediment characteristics in the River Crouch estuary near Tollesbury measured the particle diameter of suspended sediments in the water column (Sheldon 1968). The study showed a particle diameter range between 4 and 32 microns with the highest concentration around 8-10 microns. The full-size frequency spectrum is shown in figure A.11. This particle diameter corresponds to clayey and silty soil found by Hazelden and Boorman.

Soil samples were taken from the Tollesbury research site and analyzed by Watts et al. 2003 in order to analyse the soil sediment characteristics. These characteristics consisted of mass ratios between different sediment types, dry and wet bulk density and measures for surface shear strength. The soil samples were taken from different zones within the Tollesbury realignment site. Figure A.12 shows a top view of the site with five different sample areas. The area 'SM' represents the soil of the Tollesbury salt marsh in front of the research site, which have been growing naturally over the past centuries. The bed level of the area where these samples were taken was relatively high, around $OD + 2.4m$ and had an inundation ratio of 15%. The zone 'FL' represents the 'Field Soil'. This soil appears to neither have been eroded nor accumulated and represents the original surface soil of the site. The Field Soil bed level is around $OD + 1.1m$ and has an inundation ratio of 45%. Area's 3, 4 and 5 are located as a strip right in the middle of the research site, ranging all the way to the back of the site. The bed level at area 3 started at $OD + 1.3m$ and increased gradually to $OD + 2.3m$ at the end of area 5. Samples from area 3g ware taken right next to one of the gullies and differed significantly from the other areas. The results of these samples are shown in table A.1.

Table A.1: Sediment characteristics of the Tollesbury research site. Mass ratio of the soil types clay, silt and sand $[g/g]$. Dry and wet bulk density $[kgm^{-3}]$. Water content in $[g/g]$. (Watts et al. 2003)

	Particle type			**Bulk density**		**Water content**
Area	Clay (g/g)	Silt (g/g)	Sand (g/g)	Wet (kgm^{-3})	Dry $(kgm^{-3}$	(g/g)
5	0.44	0.49	0.07	1350	580	1.35
4	0.51	0.42	0.07	1320	520	1.53
3	0.52	0.42	0.06	1280	460	1.78
3g	0.49	0.45	0.06	1390	630	1.21
FL	0.55	0.39	0.06	1400	660	1.14
SM	0.49	0.47	0.04	1390	640	1.09

Following the soil study of Watts et al. 2003, the agricultural sub soil 'FL' that has been inundated each tide for six years (at time of the measurements) appeared to be a very strong and erosion resistant soil with an average surface shear strength of $\tau_f = 228 kPa$ and a critical shear stress of $\tau_{0crt} = 6.23 Nm^{-2}$. The area sites 3, 4 and 5 show an increasing critical shear stress ranging from $\tau_{0crt} = 1.53 Nm^{-2}$ at area 3 to $\tau_{0crt} = 3.03 Nm^{-2}$ at area 5. All the results for the other areas are shown in table A.2.

Table A.2: Measured critical shear stresses at the different areas within the Tollesbury research site. Obtained using a cohesive strength meter. s.e. stands for the 'standard error' (Watts et al. 2003)

Area	5	4	3	3g	SM	FL
Mean τ_{0crt}	3.03	1.93	1.53	4.28	2.45	6.23
s.e.	0.31	0.19	0.26	0.68	0.67	0.59

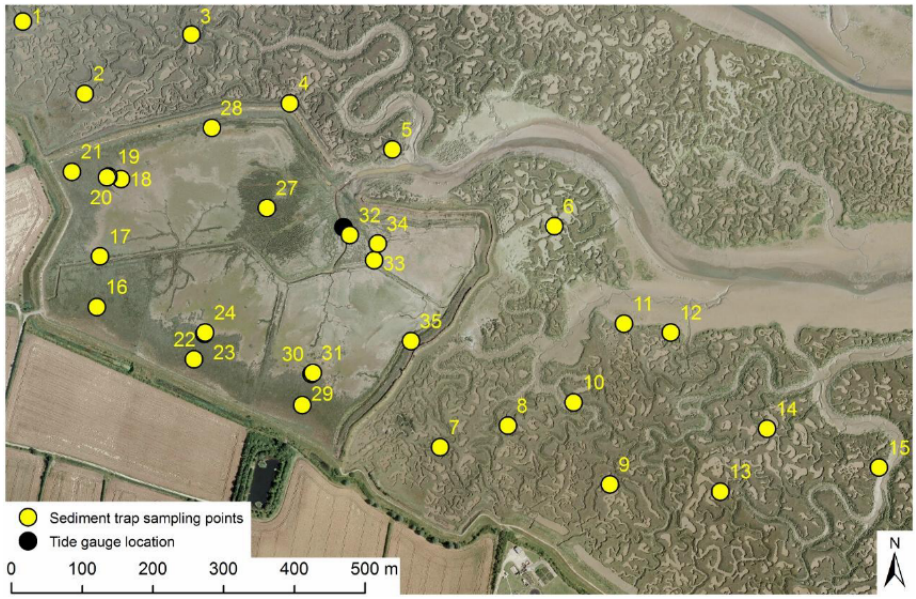

Figure A.6: Map of the sediment trap sampling points in the Tollesbury Estuary, Essex, UK. All yellow dots indicate a single sediment trap. Price 2016

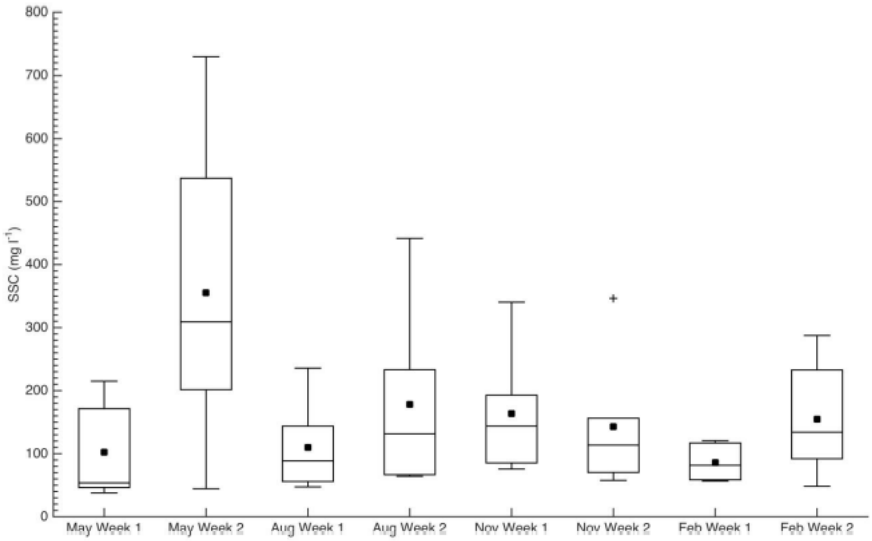

Figure A.7: Measured rates of SSC, measured 10cm above bed level at Tollesbury during the months May, August November 2011 and February 2012 Price 2016

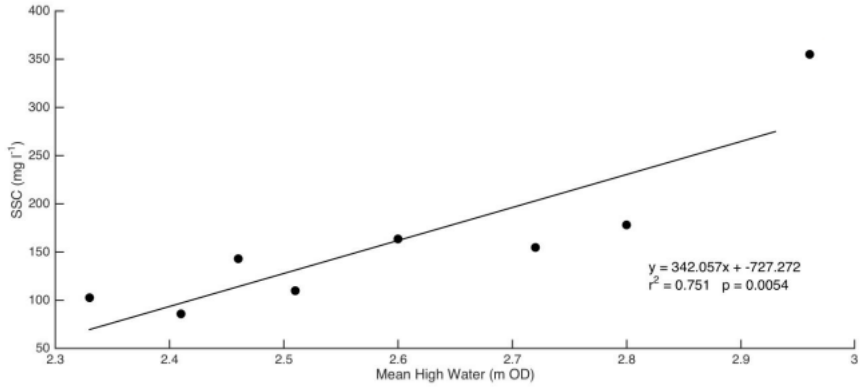

Figure A.8: Correlation between Mean High Water [m OD] and SSC [mg/l] at Tollesbury during the months May, August November 2011 and February 2012 Price 2016

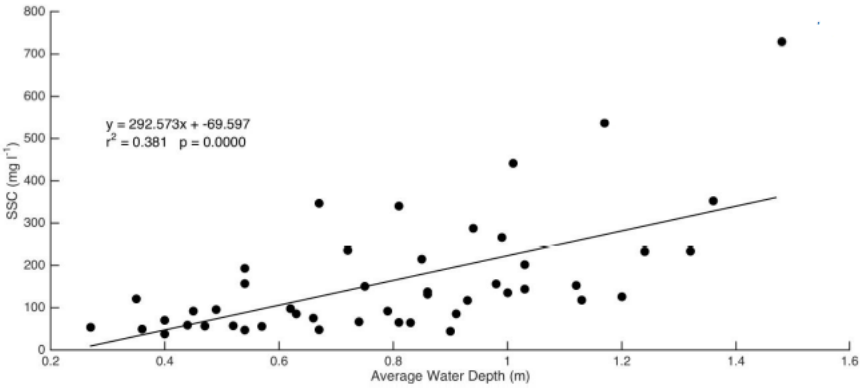

Figure A.9: Correlation between Average water depth [m] and SSC [mg/l] at Tollesbury during the months May, August November 2011 and February 2012 Price 2016

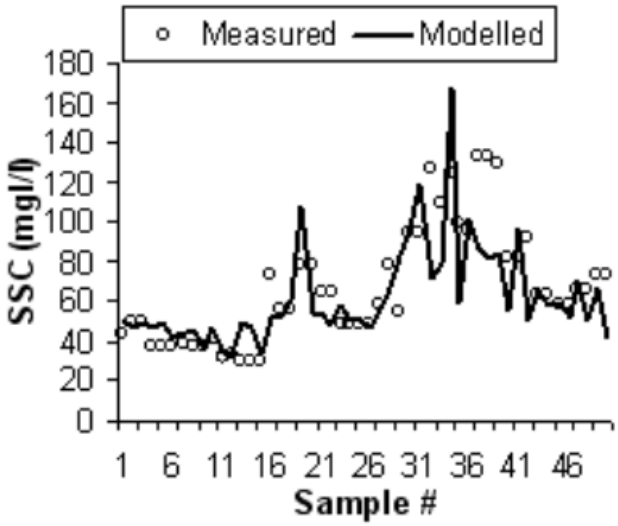

Figure A.10: Sampling study of SSC at Tollesbury based on a Hydro-optical remotely-sensed CASI dataset Elsner 2009

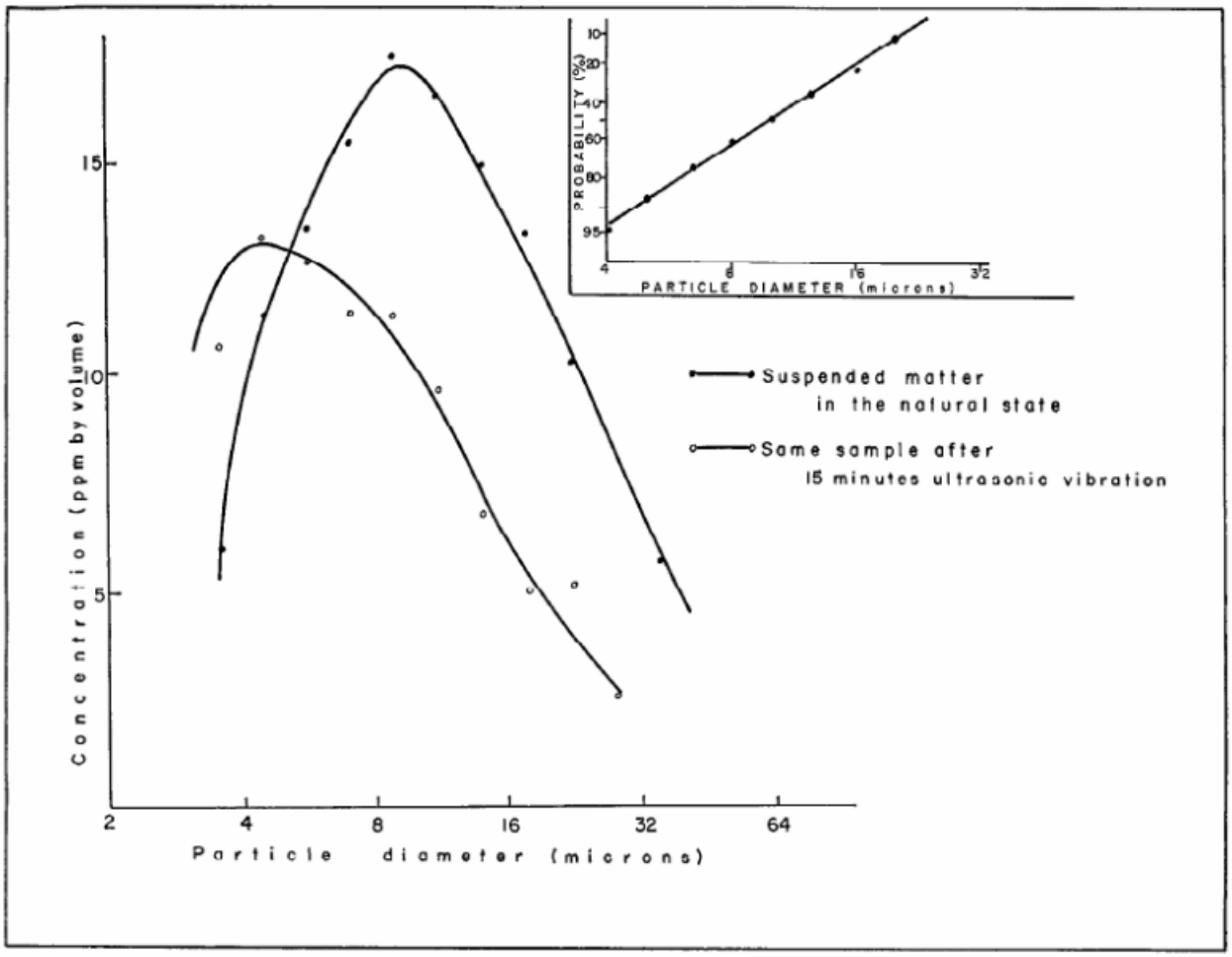

Figure A.11: Particle size frequency distribution of suspended matter in the River Crouch Estuary Sheldon 1968

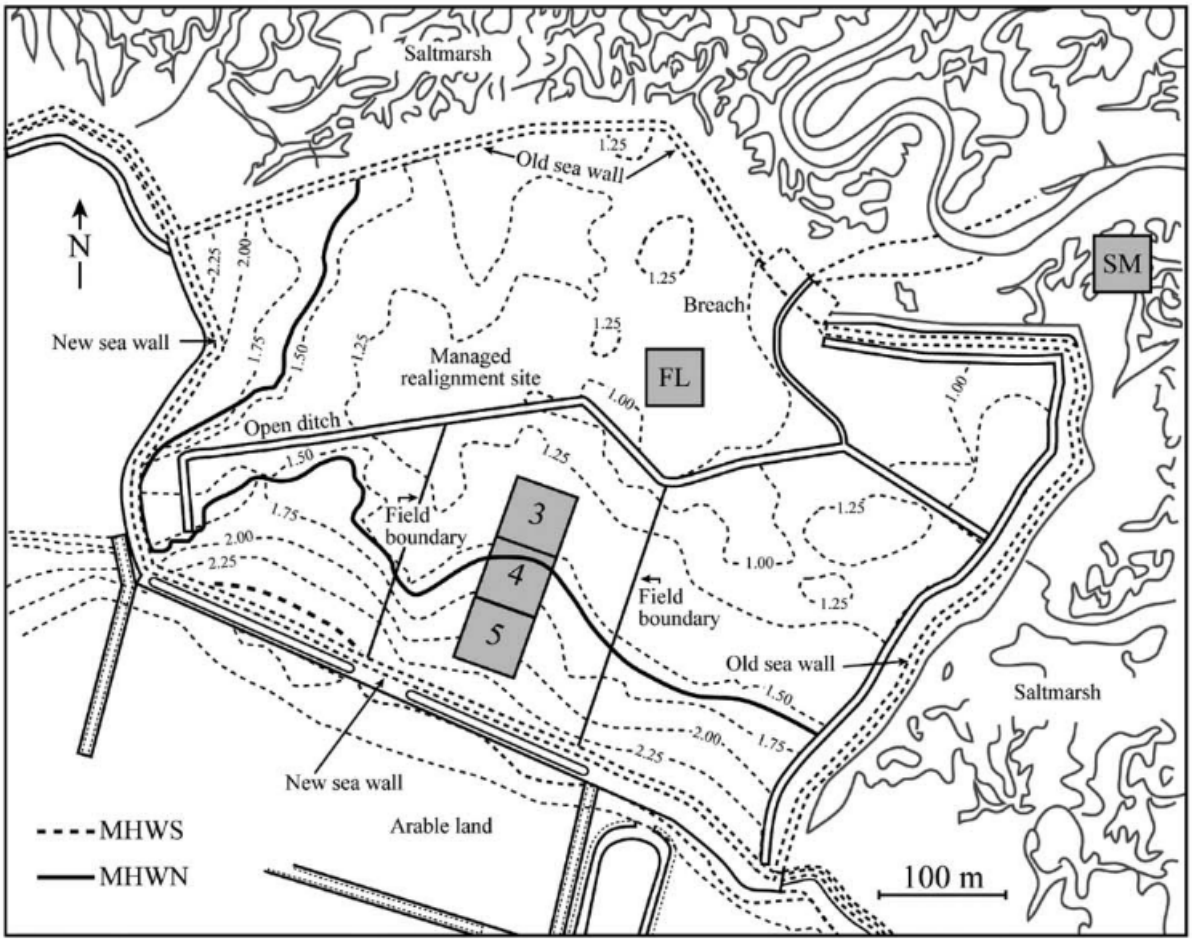

Figure A.12: Map of the research site at Tollesbury showing the different sample areas that were used for analyzing the soil sediment characteristics Watts et al. 2003

A.4. Tollesbury bathymetry

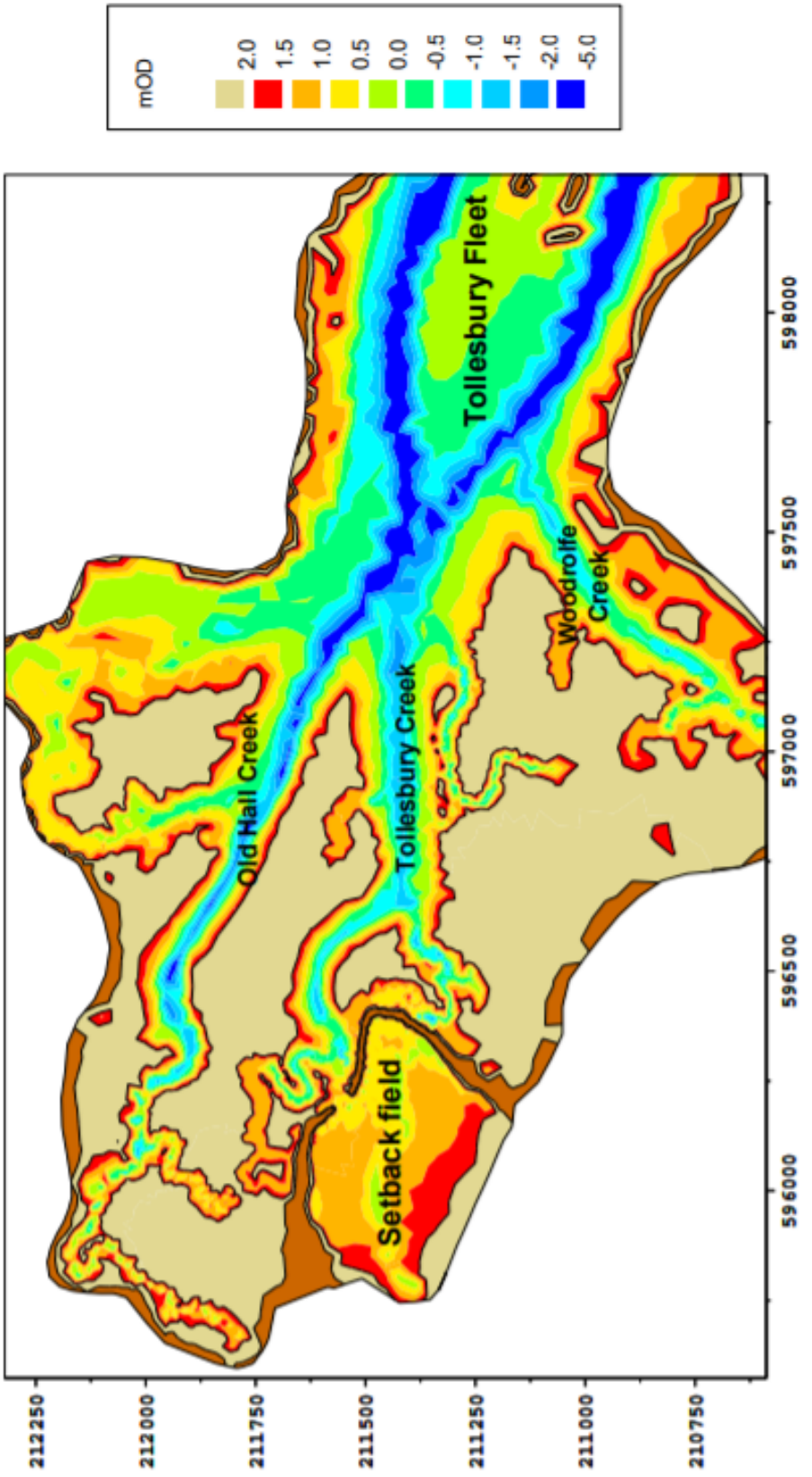

Figure A.13: bathymetry map of the research site at Tollesbury including the bathymetry of the Tollesbury marsh in front of the research site (the foreshore) Hall 2001

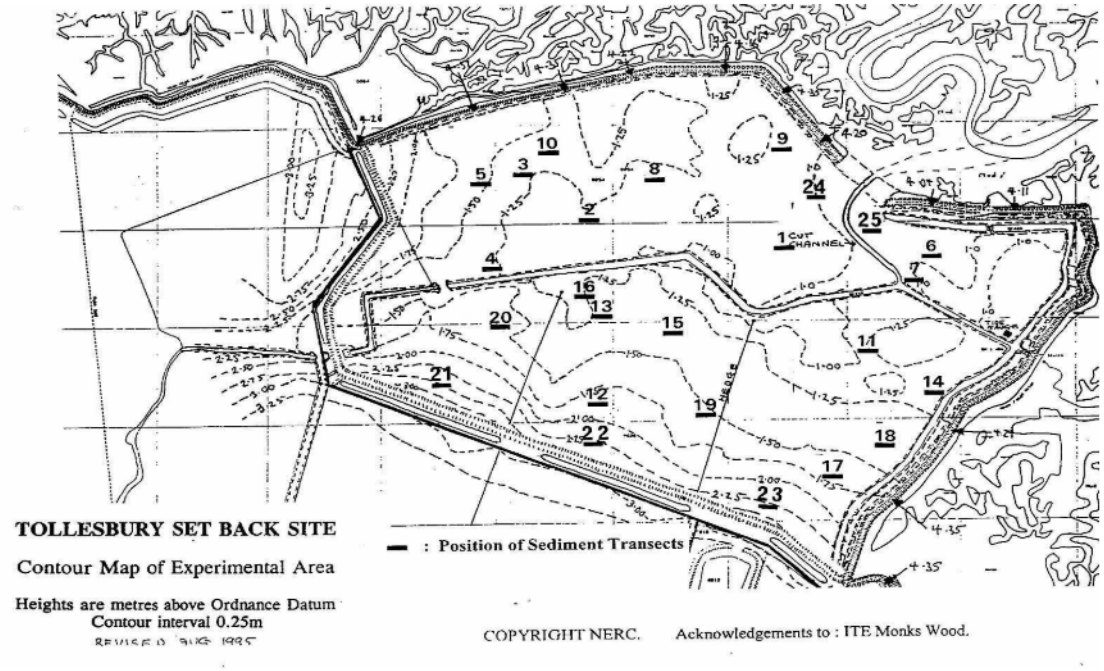

Figure A.14: bathymetry map of the research site at Tollesbury including the bathymetry Showing the locations of the sediment transacts Goudie 2008

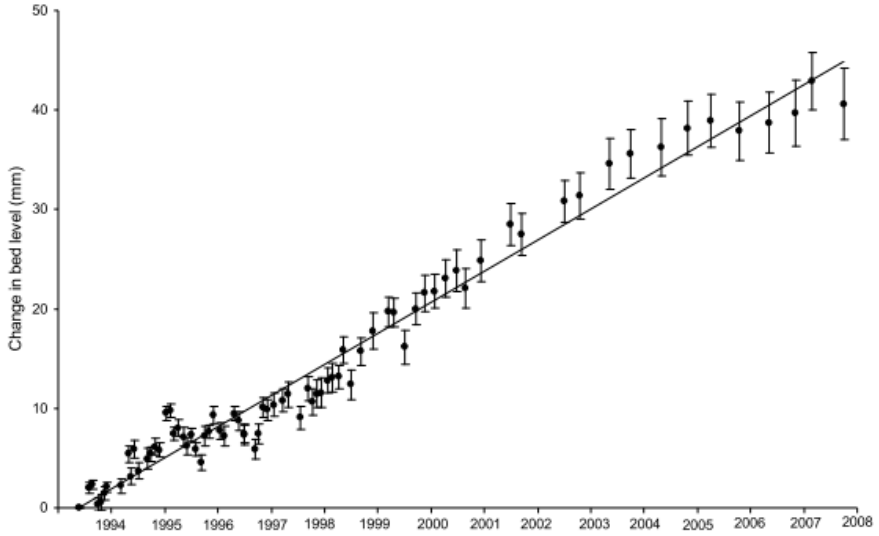

Figure A.15: Average annual bed level change at the Tollesbury Hall estuary outside of the research site during the years 1995 until 2006. Goudie 2008

Figure A.16: Aerial photograph of the Tollesbury research site in 1997. Price 2016

Figure A.17: Aerial photograph of the Tollesbury research site in 2011. Price 2016

A.5. Tollesbury vegetation

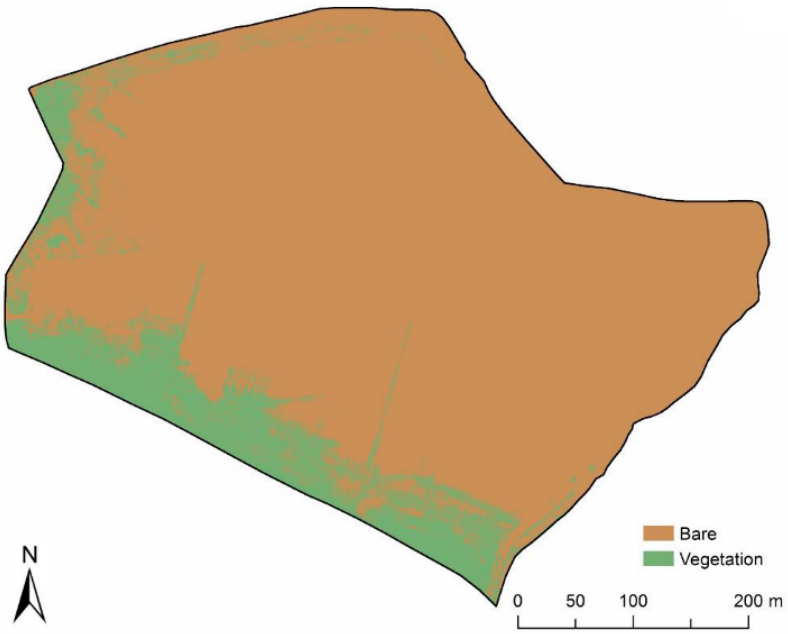

Figure A.18: Aerial map of the Tollesbury research site in 1997 distinguishing between vegetated area and unvegetated area (bare). Price 2016

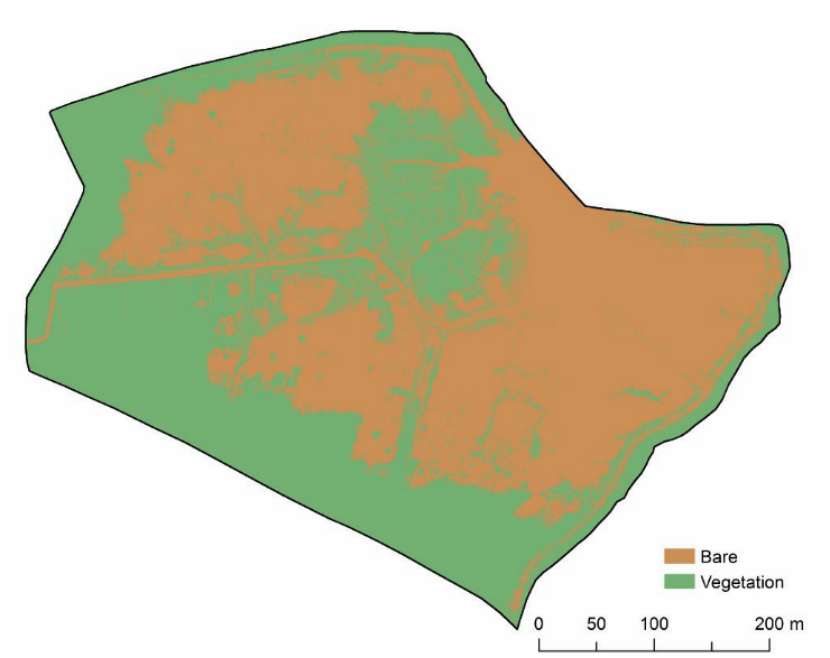

Figure A.19: Aerial map of the Tollesbury research site in 2011 distinguishing between vegetated area and unvegetated area (bare). Price 2016

B

Model Setup and Validation

B.1. Model setup

Monitoring

Proper and consistent monitoring of hydrological and morphological processes within a numerical model is of great importance in order to draw sound conclusions. Within the Delft3D model, there are two important types of monitoring used: observation points and cross-sections. Observation points are certain preselected grid cells of which all hydrological and morphological data is stored in a history file. For that specific grid cell processes like flow speed, water level, bed shear stress and bed level elevation are monitored and stored during the complete simulation with a specific storage interval. This History interval can be preset by the user for each individual run. This study used a history interval time of 9 minutes for checking short term processes like flow speeds and shear stresses in the breach. An interval of 90 minutes is used for determining bed level changes in order to reduce file size. A total of 35 observation points are assigned throughout the model. A cross-section measures averages and total processes through a certain section across the grid lines. With this model, a cross-section is assigned measuring the total transport of sediment and hydraulic discharge through the breach. Figure B.1 shows the locations of both the observation points and the cross-section for the Tollesbury base-case model.

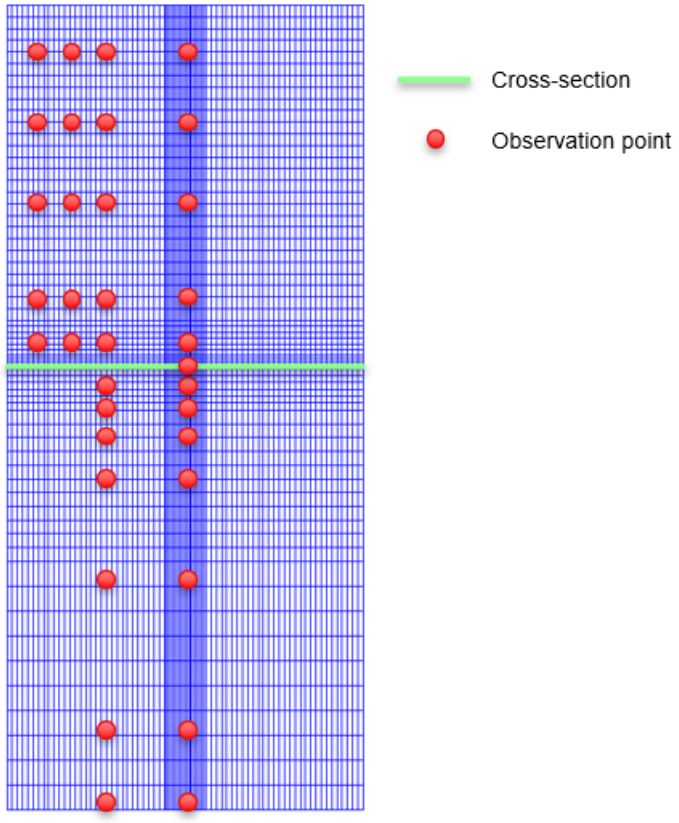

Figure B.1: Locations of observation points and cross-section appointed at the base case Delft3D model. Red dots: observations points. Green line: cross-section

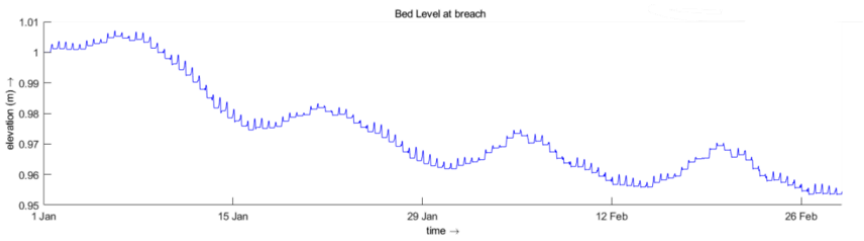

Figure B.2: Bed level change at breach during two months for the base-case validation model

B.2. Tollesbury calibration model

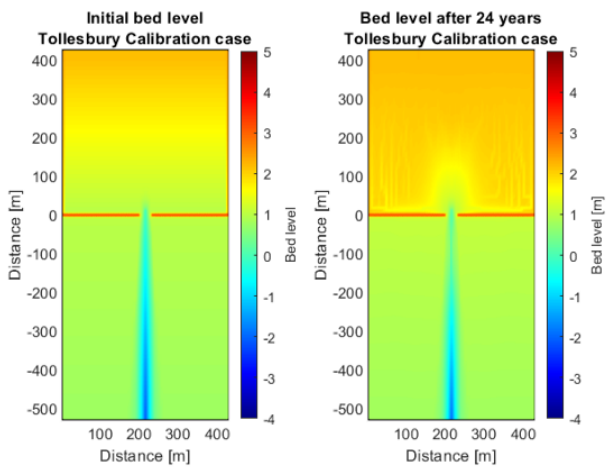

(a) Both the initial bed level on the left and the bed level after 24 real-time years.

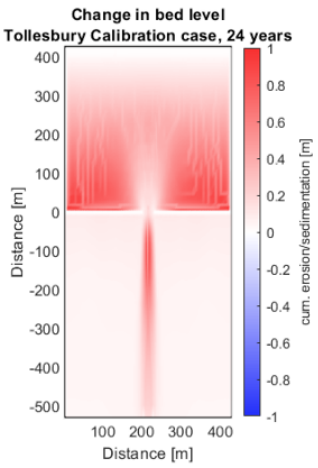

(b) Change in bed level plotted by cumulative sedimentation/erosion.

Figure B.3: Bed level change of the Tollesbury calibration model after a real time period of 24 years.

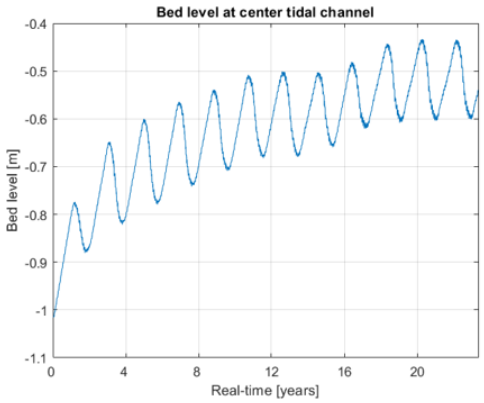

Figure B.4: Bed level change at the center of the tidal channel of the Tollesbury calibration model during a real time period of 24 years.

B.3. Uniform Foreshore validation model

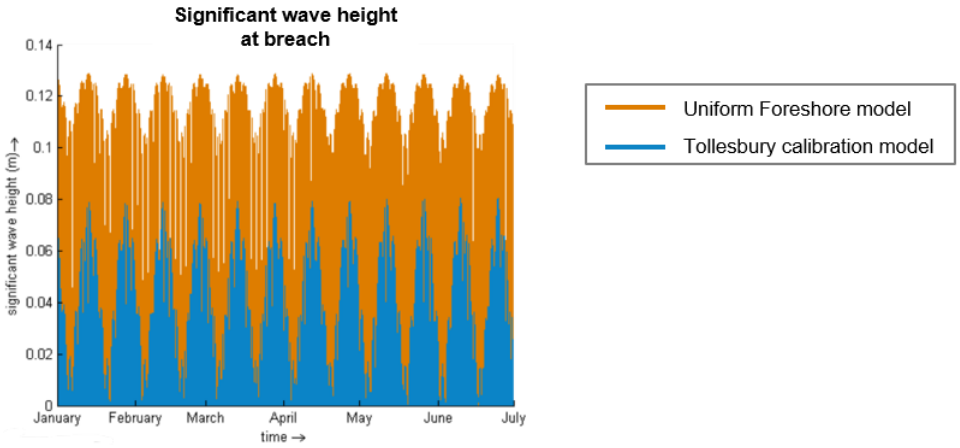

Figure B.5: Significant wave height right in front of the breach for both the Tollesbury calibration model and the Uniform Foreshore validation model during a modeling period of 4 months.

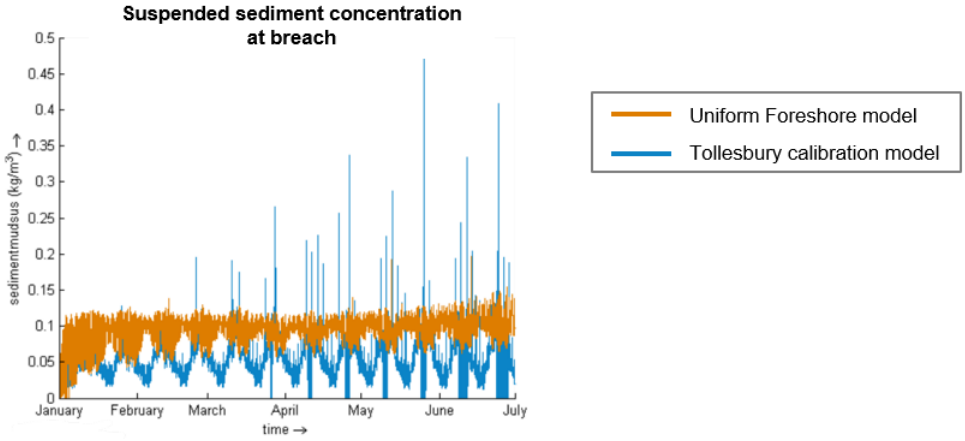

Figure B.6: Suspended sediment concentration right in front of the breach for both the Tollesbury calibration model and the Uniform Foreshore validation model during a modeling period of 4 months.

B.4. Near-horizontal polder bed model - Base case

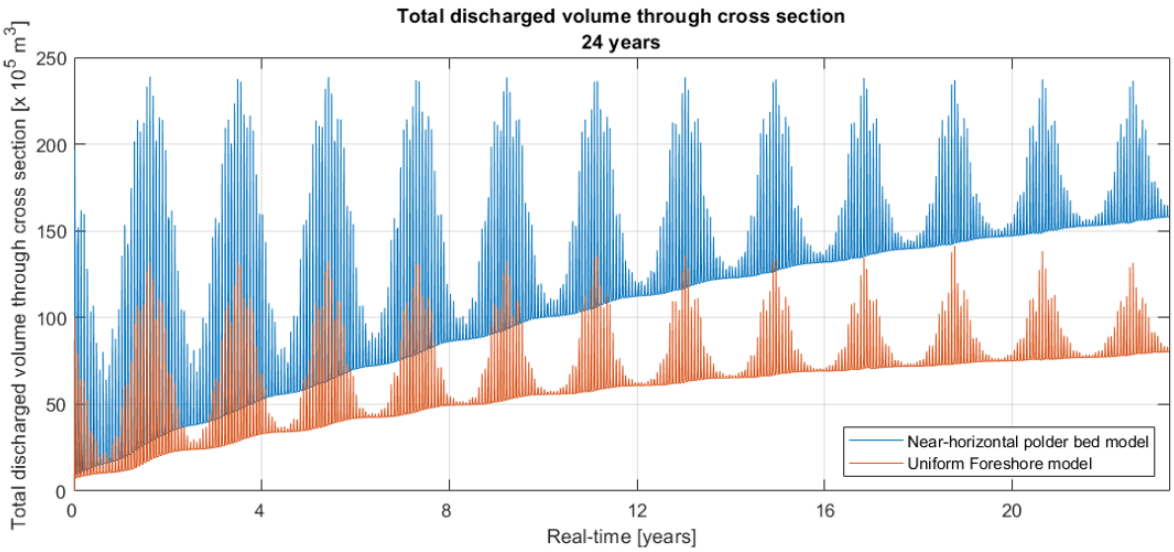

Figure B.7: Tidal prism entering the Lease Polder for both the Uniform Foreshore validation model and the Near horizontal polder bed model (Base-case) during a real time period of 24 years.

B.5. Numerical validation

B.5.1. Time step validation

In order to validate whether the allocated time step is small enough not to cause inaccuracies in the computations, a certain check must be performed. A first estimation to see if the time step is sufficiently small is to check the Courant-Friedrichs-Lewy number (CFL) computed by equation B.1.

$$CFL = \frac{\Delta t \sqrt{gH}}{\{\Delta x, \Delta y\}} \tag{B.1}$$

Where Δx and Δy are the dimensions of the grid cell, Δt is the time step and H is the depth, assuming that the flow magnitude is smaller than the velocity of wave propagation (Deltares 2014). Values of the Courant number must not exceed a value of 10 to avoid inaccuracies. Several test runs showed that a time step of 0.15 minutes complies with this criterion.

In order to properly check the validity of the time step, a run with half of the computed time step needs to be compared to the original time step. This check is performed for the base-case model (Horizontal Polder model). When no differences are noted in processes between the two runs one can assume the original time step to be valid. Figure B.5.1 shows three individual plots for the flow velocity in the y-direction, water level and suspended sediment concentration at the centre of the breach for both the time step of 9 seconds and a time step around half of that, namely 4 seconds. All plots show clear overlapping of the observed values of the different time steps and no differences where present in the morphological results. It can now be concluded that the time step of $\Delta t = 9s$ will suffice.

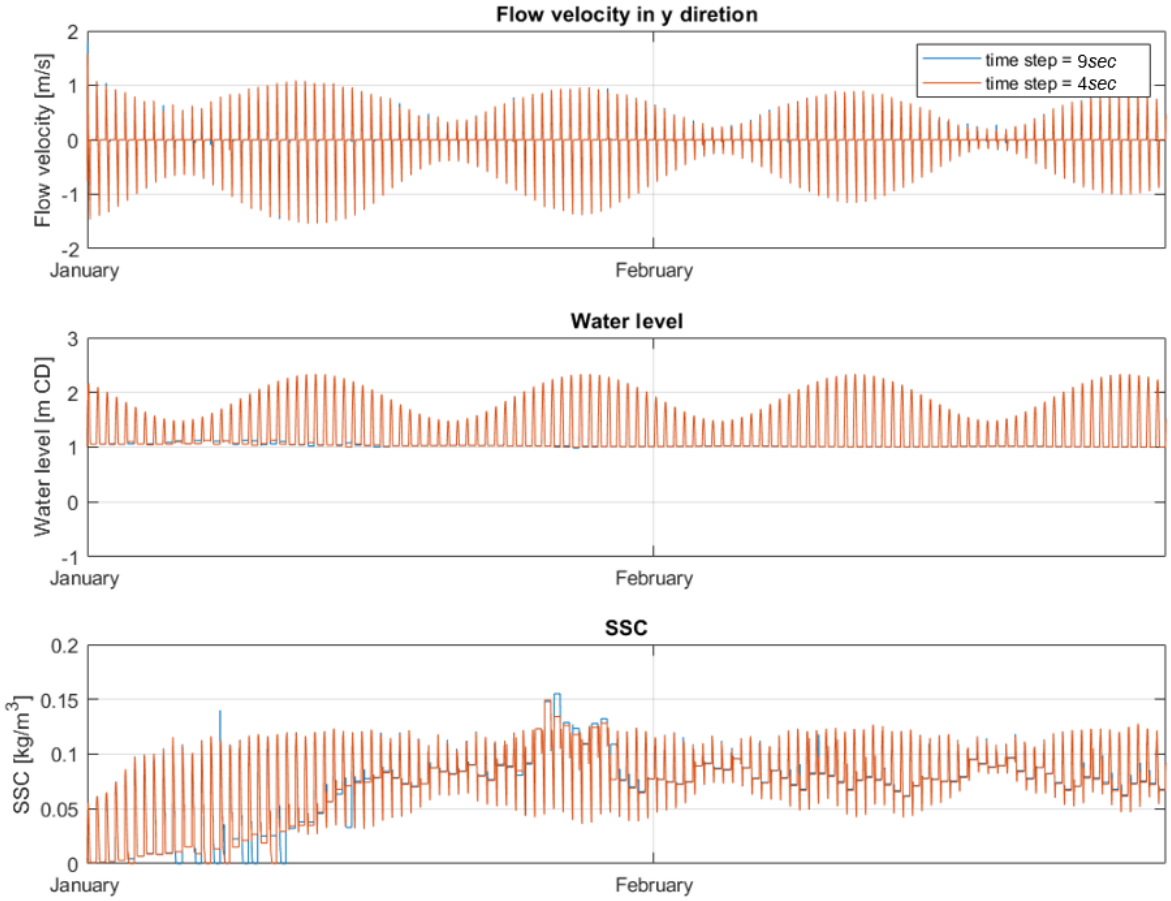

Figure B.8: Validation of the time step: Flow velocity in y-direction, Water level and SSC at the center of the breach for a period of two months for a time step of 0.15 min and 0.8 min

B.5.2. Morphological factor validation

The Morphological factor can be verified to be appropriate by varying it with a factor of 2 and checking that it would not change the overall morphological results of the simulation. When the final sedimentation patterns in the 2D map results and total net sediment transport through the breach are reasonably similar for the different morphological factors, for the same real-time periods. The term real-time period is used to denote the morphological results in real-time, where:

$$\text{Real-time period} = MorFac \cdot \text{simulation period.} \tag{B.2}$$

Figure B.9 presents the two-dimensional results for sedimentation and erosion for both the MorFac's, including a map of the differences between both results showing the difference between the two MorFacs. The first plot has a MorFac of 24 whilst the second has a MorFac of 48. Both simulations are run for the same real-time period.

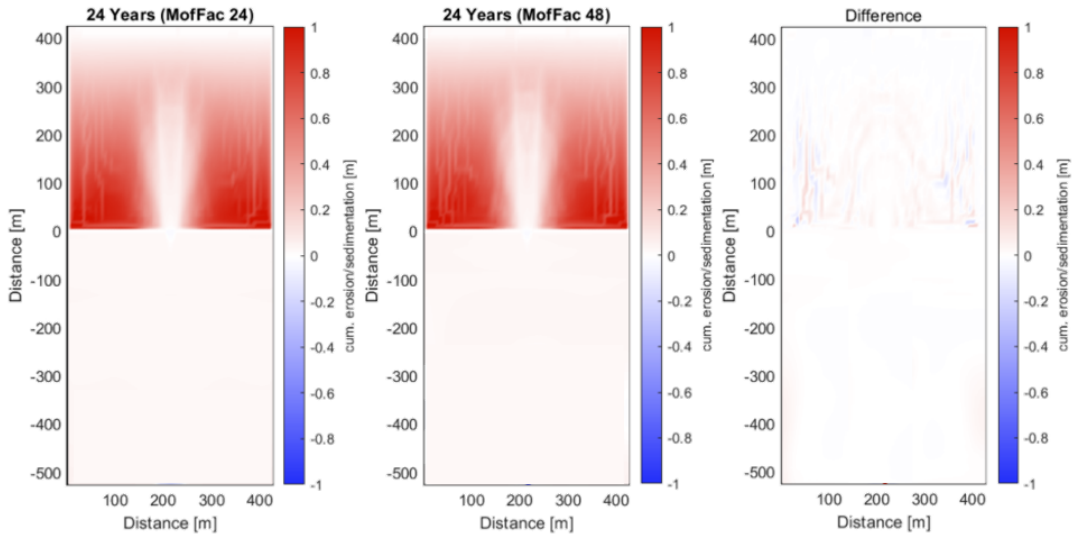

Figure B.9: Validation of the Morphological factor: Cumulative sedimentation and erosion for two runs with different MorFac's and the same real-time period of 24 years. Left: MorFac of 24. Middle: MorFac of 48. Right figure: Difference in sedimentation and erosion between the two MorFac's

The magnitude of the differences between the two plots are insignificant in comparison to the reduction in computational time. In addition, the fact that it is a fictional case used for a sensitivity analysis makes the difference permissible. This can also be deducted from figure B.10, which shows the cumulative sediment import through the breach for both MorFac's over time. There is no difference in trend visible between the two MorFac's. To conclude, a MorFac of 48 does not influence the morphological results and will be used in the future of this study. Tests showed that higher MorFac's led to differences that were not acceptable due to instabilities near the boundary.

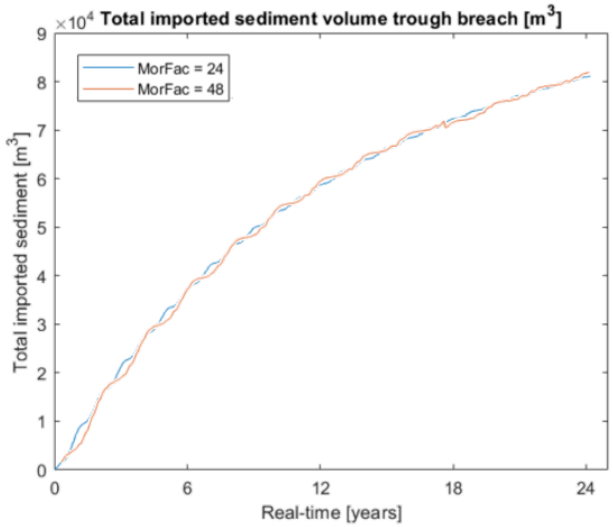

Figure B.10: Validation of the Morphological factor: Total sediment import trough breach for two runs with different MorFac's and the same real-time period of 24 years.

B.6. Parameter scenarios

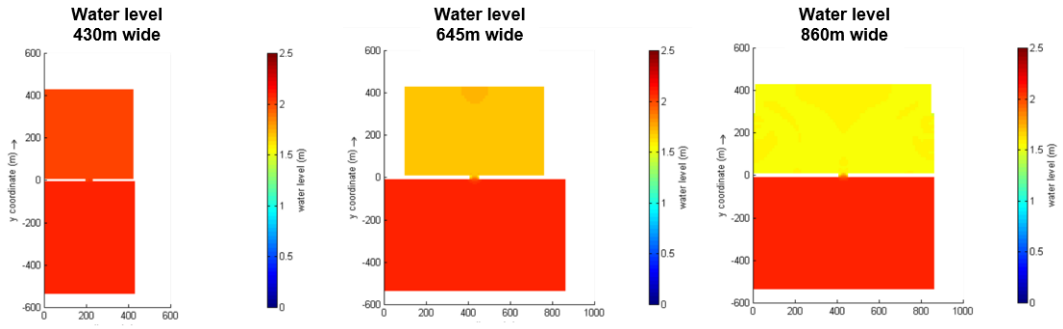

Figure B.11: visualization of the effect of tidal damping by comparing the water level of three separate polder width scenarios with equal breach dimensions ant at the same time of tidal filling.

C

Result Plots

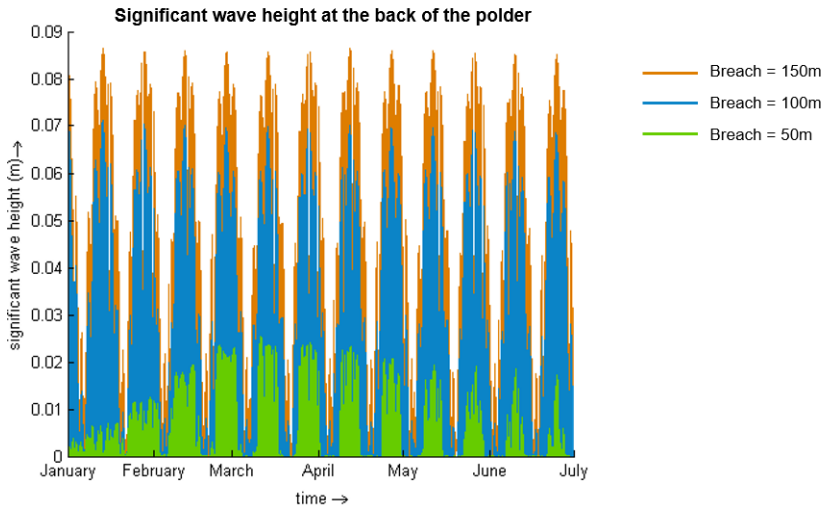

Figure C.1: Significant wave height observed at the back of the polder linear behind the middle of the breach for different dimensional breach widths

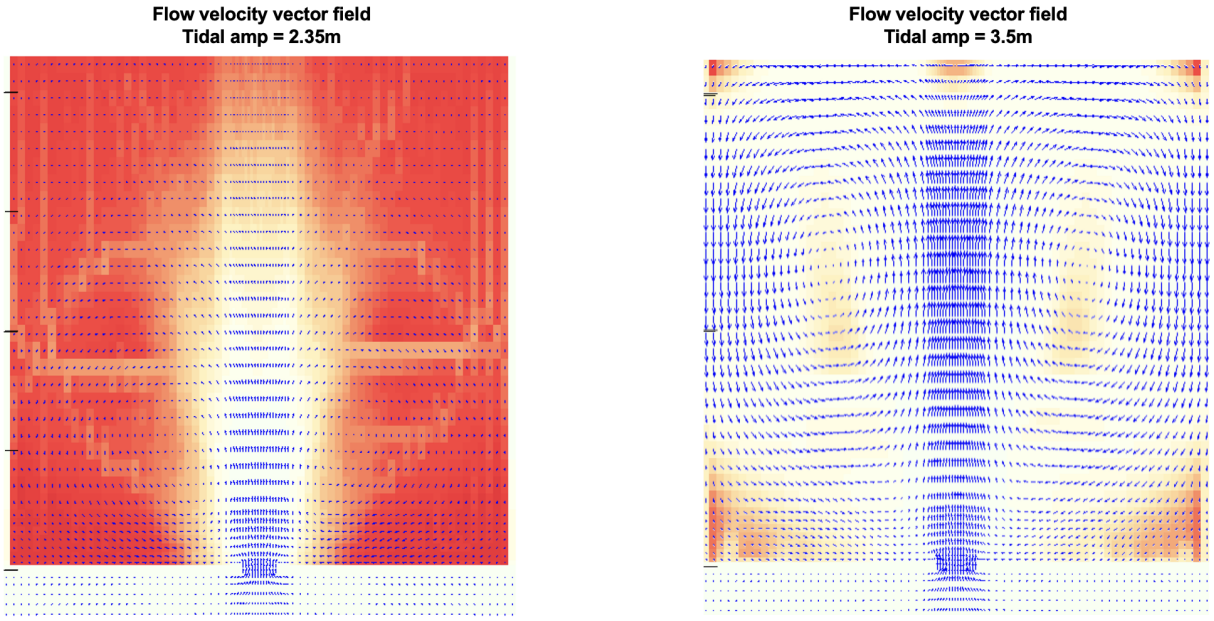

Figure C.2: Depth averaged flow velocity vector field during incoming tide for the scenarios with a tidal amplitude of 2.35m and 3.5m

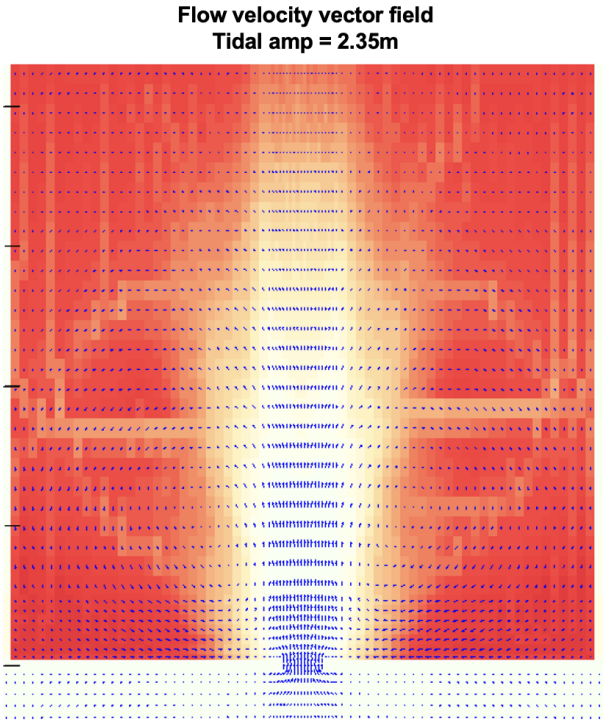

Figure C.3: Depth averaged flow velocity vector field during incoming tide for the scenario with a tidal amplitude of 2.35m

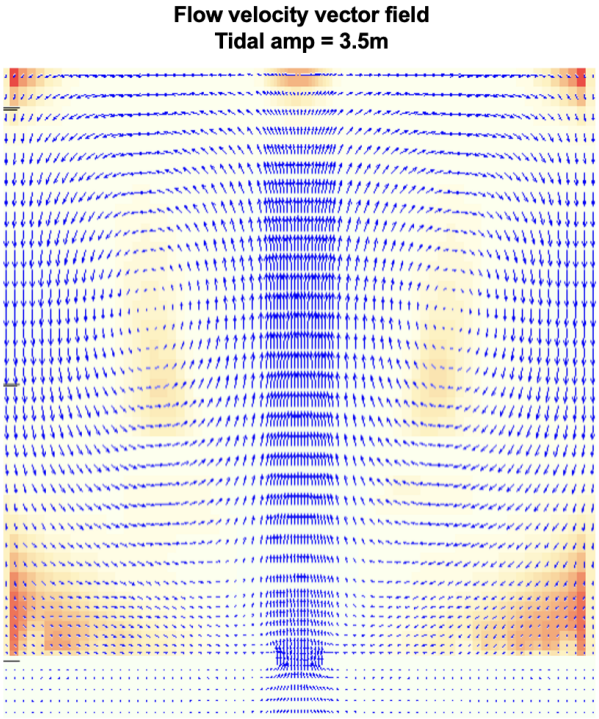

Figure C.4: Depth averaged flow velocity vector field during incoming tide for the scenario with a tidal amplitude of 3.5m

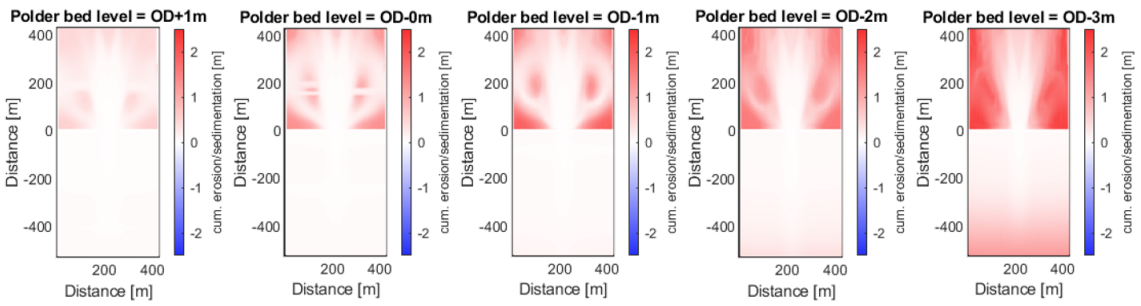

Figure C.5: The cumulative sedimentation and erosion for different values of initial polder bed levels after a real-time period of 8 years.

C.1. Scenario results: Initial bed level

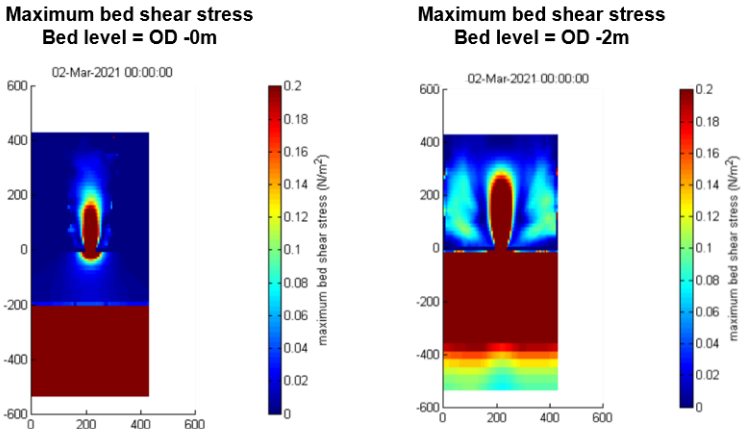

Figure C.6: The maximum bed shear stress for the scenario with an initial polder bed level of $OD-0m$ (left) and an initial bed level of $OD-2m$ (right) during high tide after 6 years of operation

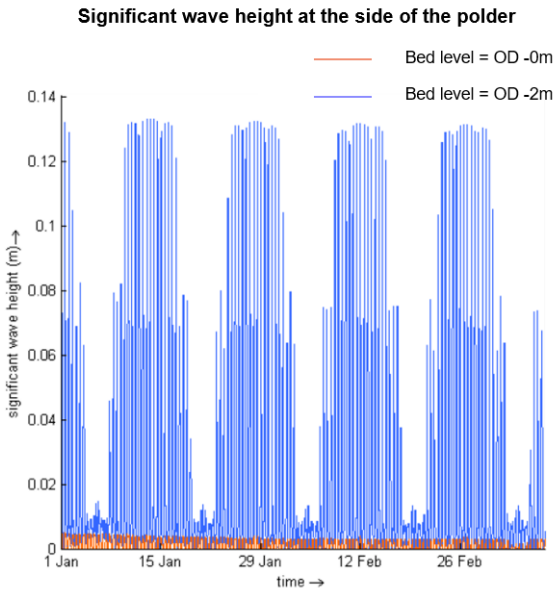

Figure C.7: The significant wave height measured at the side of the polder for both the scenarios with an initial polder bed level of $OD-0m$ and $OD-2m$

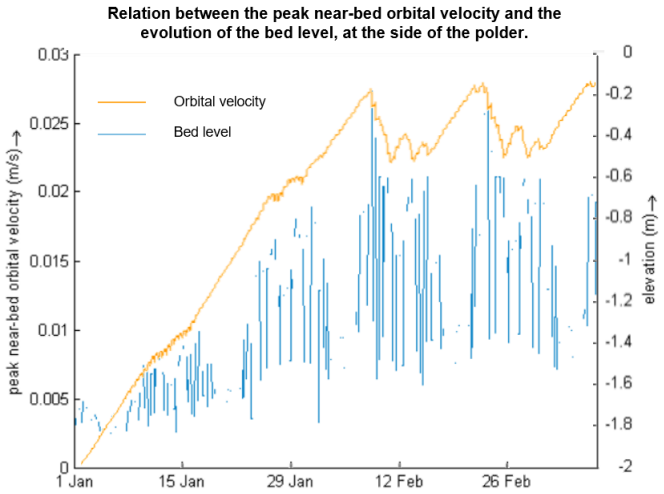

Figure C.8: The peak near-bed orbital velocity measured at the side of the polder and the local evolution in bed level at the side of the polder for the scenario with an initial polder bed level of $OD-2m$

C.2. Scenario results: Tidal Amplitude

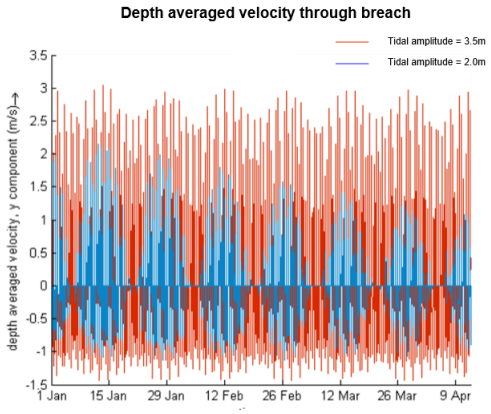

Figure C.9: The depth averaged flow velocity of the y-component through the breach for the scenario with a tidal amplitude of $2.0m$ and $3.5m$

D

Feasibility study

D.1. Parameter fit results - SSC

Table D.1: Factor results for SSC

	Absolute			Dimensionless		
SSC	a-factor [-]	b-factor [-]	Initial sed rate after 4 years [m/4y]	a-factor [-]	b-factor [-]	Initial sed rate after 4 years [-]
25mg/l	0.747707	0.013206	0.038471	1	0.213873	0.235106
50mg/l	0.747707	0.026242	0.074506	1	0.424995	0.455322
100mg/l	0.747707	0.061746	0.163634	1	1	1
150mg/l	0.747707	0.099167	0.24483	1	1.606028	1.496203
200mg/l	0.747707	0.141623	0.323374	1	2.293619	1.976195

Dimensionless a-factor

$$f(x) = a \cdot e^{-b \cdot x} + c$$

With:

$$a = -1 \quad (D.1)$$
$$b = 0.5176$$
$$c = 1$$

Dimensionless initial sed rate after 4 years

$$f(x) = p_1 \cdot x + p_2$$

With:

$$p_1 = 0.0099 \quad (D.2)$$
$$p_2 = -0.01362$$

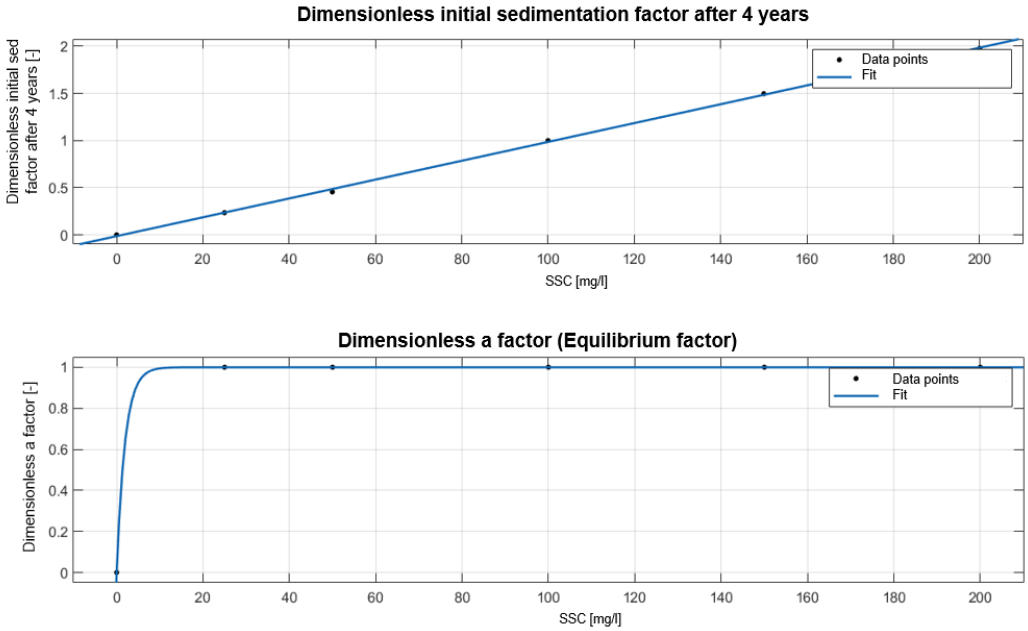

Figure D.1: Top figure: fitted formula for determining the dimensionless initial sedimentation factor for arbitrary levels of SSC. Bottom figure: fitted formula for determining the dimensionless a-factor (dimensionless equilibrium factor) for arbitrary levels of SSC.

D.2. Parameter fit results - Breach width

Table D.2: Factor results for breach width

Breach width	Absolute			Dimensionless		
	a-factor [-]	b-factor [-]	Initial sed rate after 4 years [m/4y]	a-factor [-]	b-factor [-]	Initial sed rate after 4 years [-]
25m	0.789743	0.058222	0.164075	1.05622	0.942922	1.002696
50m	0.747707	0.061746	0.163634	1	1	1
100m	0.539856	0.083507	0.153301	0.722015	1.352415	0.936849
150m	0.483754	0.088642	0.144412	0.646983	1.435582	0.882529

Dimensionless a-factor

$$f(x) = \frac{p_1}{x + q_1}$$

With:

$$p_1 = 193.4$$
$$q_1 = 154$$

(D.3)

Dimensionless initial sed rate after 4 years

$$f(x) = a \cdot x^b + c$$

With:

$$a = -7.422e^{-05}$$
$$b = 1.5$$
$$c = 1.017$$

(D.4)

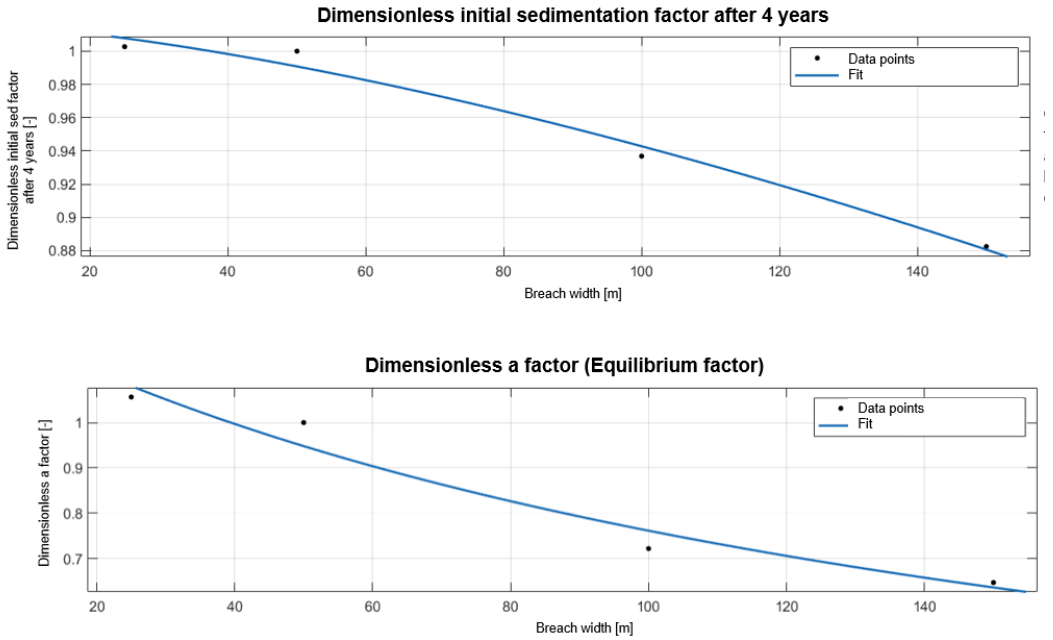

Figure D.2: Top figure: fitted formula for determining the dimensionless initial sedimentation factor for arbitrary dimensions for the breach width. Bottom figure: fitted formula for determining the dimensionless a-factor (dimensionless equilibrium factor) for arbitrary dimensions for the breach width.

D.3. Parameter fit results - Tidal amplitude

Table D.3: Results for the a- and b-factor for each scenario which represent the exponential fit and the deducted initial sedimentation rate (during 4 years) for the tidal amplitude scenarios. Both in absolute values and dimensionless values relative to the base-case scenario.

	Absolute			Dimensionless		
Tidal amplitude	a-factor [-]	b-factor [-]	Initial sed rate after 4 years [m/4y]	a-factor [-]	b-factor [-]	Initial sed rate after 4 years [-]
2.0m	0.526829	0.050533	0.096416	0.658442	1.151878	0.748719
2.35m	0.800115	0.04387	0.128774	1	1	1
2.5m	0.909472	0.043113	0.144061	1.136677	0.982747	1.118709
3.0m	0.646518	0.067732	0.153437	0.808032	1.543934	1.191519

Dimensionless a-factor

$$f(x) = p_1 \cdot x^2 + p_2 \cdot x + p_3$$

With:

$$p_1 = -1.47 \quad p_2 = 7.513 \quad p_3 = -8.494 \tag{D.5}$$

Dimensionless initial sed rate after 4 years

$$f(x) = a \cdot x^b + c$$

With:

$$a = -12.6 \quad b = -4.553 \quad c = 1.283 \tag{D.6}$$

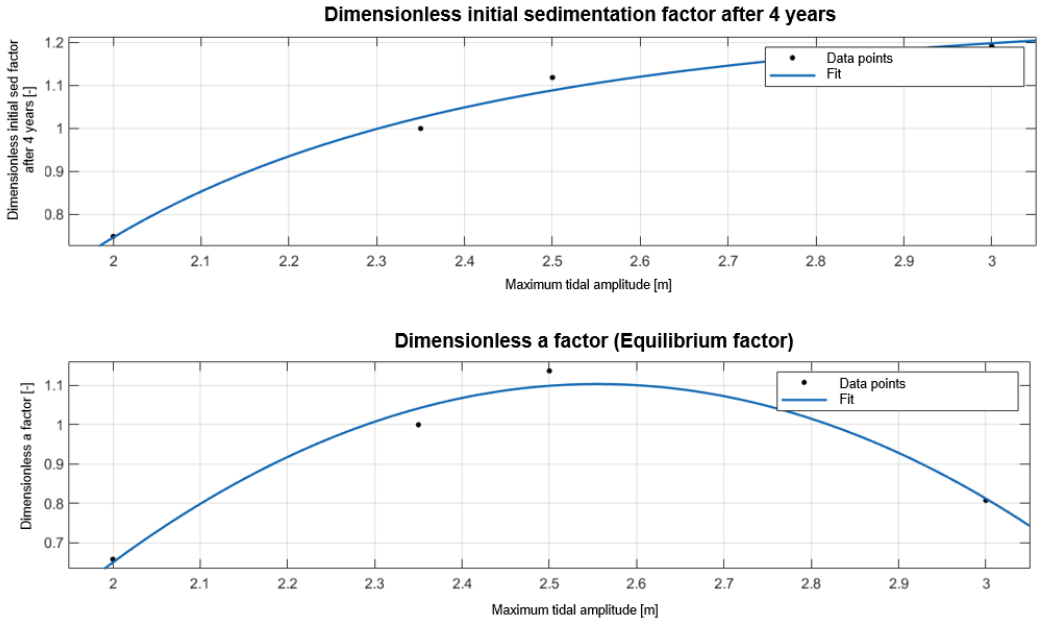

Figure D.3: Top figure: fitted formula for determining the dimensionless initial sedimentation factor for arbitrary values maximum tidal amplitude. Bottom figure: fitted formula for determining the dimensionless a-factor (dimensionless equilibrium factor) for arbitrary values maximum tidal amplitude.

D.4. Parameter fit results - initial polder bed level

Table D.4: Results for the a- and b-factor for each scenario which represent the exponential fit and the deducted initial sedimentation rate (during 4 years) for the initial polder bed level scenarios. Both in absolute values and dimensionless values relative to the base-case scenario.

	Absolute			Dimensionless		
Initial bed level	a-factor [-]	b-factor [-]	Initial sed rate after 4 years [m/4y]	a-factor [-]	b-factor [-]	Initial sed rate after 4 years [-]
OD+1m	0.72946	0.058685	0.15262	1	1	1
OD-0m	1.13985	0.072023	0.285312	1.562594	1.227279	1.869427
OD-1m	1.50643	0.081699	0.419946	2.06513	1.392163	2.751579
OD-1.5m	1.70325	0.091931	0.524078	2.334946	1.566526	3.433875
OD-2m	0.82374	0.348053	0.61902	1.129246	5.930877	4.055956
OD-3m	1.30644	0.278692	0.877939	1.790969	4.748956	5.752451
OD-4m	1.50123	0.280149	1.0117	2.058002	4.773776	6.628882

D.4.1. Shallow regime - Initial bed level higher than OD -2m

Dimensionless a-factor

$$f(x) = a \cdot e^{b \cdot x}$$

With:

$$a1 = 2.676$$
$$b1 = -3.034$$
$$c1 = 4.086 \quad \text{(D.7)}$$

Dimensionless initial sed rate after 4 years

$$f(x) = a \cdot e^{b \cdot x}$$

With:

$$a = 1.75$$
$$b = -0.4538 \quad \text{(D.8)}$$

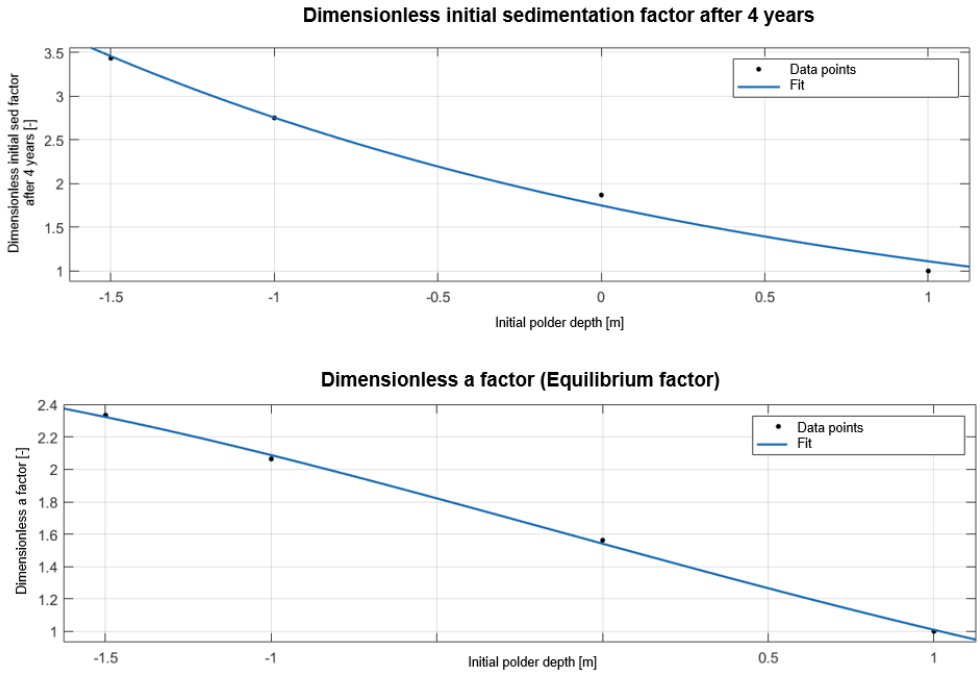

Figure D.4: Top figure: fitted formula for determining the dimensionless initial sedimentation factor for arbitrary levels of initial polder bed relative to the Ordnance Datum (OD) for the shallow polder bed regime (Initial bed level higher than OD -2m). Bottom figure: fitted formula for determining the dimensionless a-factor (dimensionless equilibrium factor) for arbitrary levels of initial polder bed level relative to the Ordnance Datum (OD).

D.4.2. Deep polder bed regime - Initial polder bed level lower than OD -2m

Dimensionless a-factor

$$f(x) = p1 \cdot x^2 + p2 \cdot x + p3$$

With:

$$p_1 = -0.1973 \quad p_2 = -1.648 \quad p_3 = -1.378 \tag{D.9}$$

Dimensionless initial sed rate after 4 years

$$f(x) = p1 \cdot x^2 + p2 \cdot x + p3$$

With:

$$p_1 = -0.41 \quad p_2 = -3.747 \quad p_3 = -1.797 \tag{D.10}$$

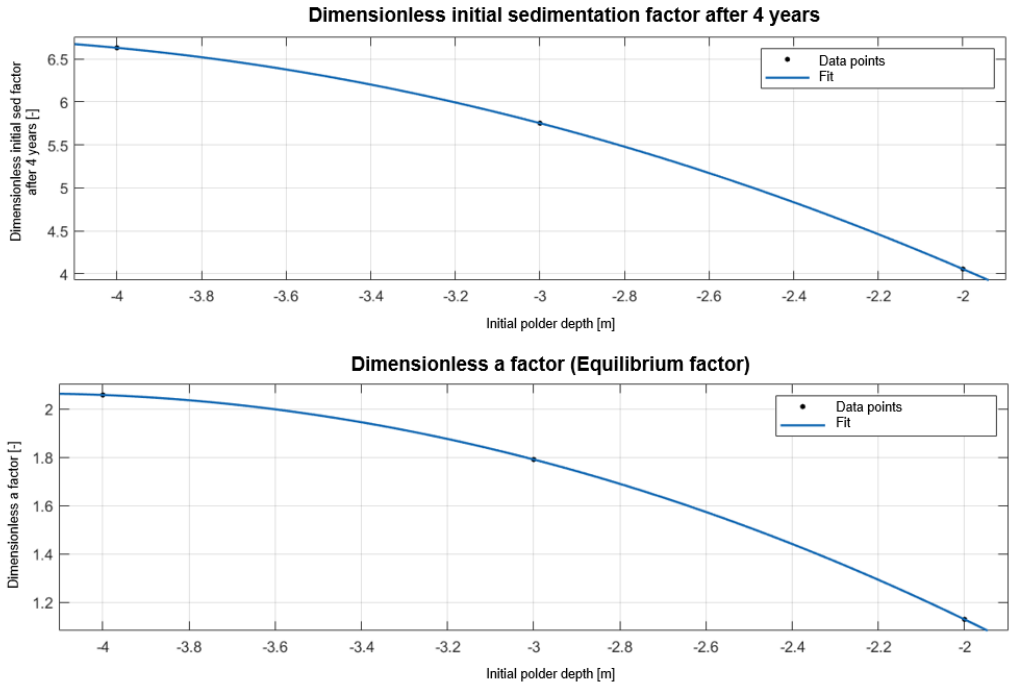

Figure D.5: Top figure: fitted formula for determining the dimensionless initial sedimentation factor for arbitrary levels of initial polder bed relative to the Ordnance Datum (OD) for the deep polder bed regime (Initial bed level lower than OD -2m). Bottom figure: fitted formula for determining the dimensionless a-factor (dimensionless equilibrium factor) for arbitrary levels of initial polder bed level relative to the Ordnance Datum (OD).

D.5. Parameter fit results - polder length

Table D.5: Results for the a- and b-factor for each scenario which represent the exponential fit and the deducted initial sedimentation rate (during 4 years) for the polder length scenarios. Both in absolute values and dimensionless values relative to the base-case scenario.

	Absolute			Dimensionless		
Polder length	a-factor [-]	b-factor [-]	Initial sed rate after 4 years [m/4y]	a-factor [-]	b-factor [-]	Initial sed rate after 4 years [-]
320m	0.042973	0.143571	1.136195	0.979553	1.114904	0.748719
430m	0.04387	0.128774	1	1	1	1
645m	0.063028	0.145902	0.818301	1.4367	1.133004	1.118709
860m	0.05914	0.119445	0.708643	1.348094	0.927553	1.191519

Dimensionless a-factor

$$f(x) = a \cdot e^{b \cdot x} + c \cdot e^{d \cdot x}$$

With:

$$a = 1.216$$
$$b = -0.0025$$
$$c = 0.6035$$
$$d = -7.281e^{-05}$$

(D.11)

Dimensionless initial sed rate after 4 years

$$f(x) = a \cdot x^{b}$$

With:

$$a = 2.055$$
$$b = -0.1083$$

(D.12)

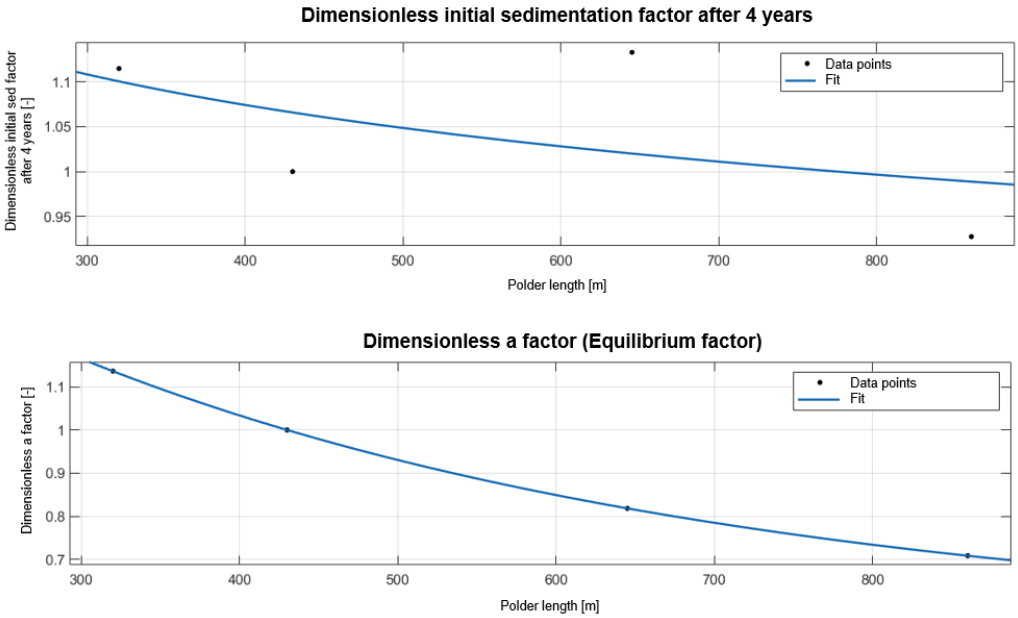

Figure D.6: Top figure: fitted formula for determining the dimensionless initial sedimentation factor for arbitrary dimensions for the polder length. Bottom figure: fitted formula for determining the dimensionless a-factor (dimensionless equilibrium factor) for arbitrary dimensions for the polder length.

D.6. Parameter fit results - Polder width

Table D.6: Results for the a- and b-factor for each scenario which represent the exponential fit and the deducted initial sedimentation rate (during 4 years) for the polder width scenarios. Both in absolute values and dimensionless values relative to the base-case scenario.

	Absolute			Dimensionless		
Polder width	a-factor [-]	b-factor [-]	Initial sed rate after 4 years [m/4y]	a-factor [-]	b-factor [-]	Initial sed rate after 4 years [-]
320m	0.967912	0.031891	0.115919	1.209716	0.726943	0.900173
430m	0.800115	0.04387	0.128774	1	1	1
645m	0.586987	0.060028	0.125299	0.733629	1.368328	0.97301
860m	0.536602	0.065554	0.123771	0.670657	1.494298	0.961145

Dimensionless a-factor

$$f(x) = a \cdot e^{b \cdot x} + c \cdot e^{d \cdot x}$$

With:

$$a = 2.174$$
$$b = -0.001883$$
$$c = 0.00436$$
$$d = 0.004661$$

(D.13)

Dimensionless initial sed rate after 4 years

$$f(x) = a \cdot x^b$$

With:

$$a = 0.725$$
$$b = 0.04455$$

(D.14)

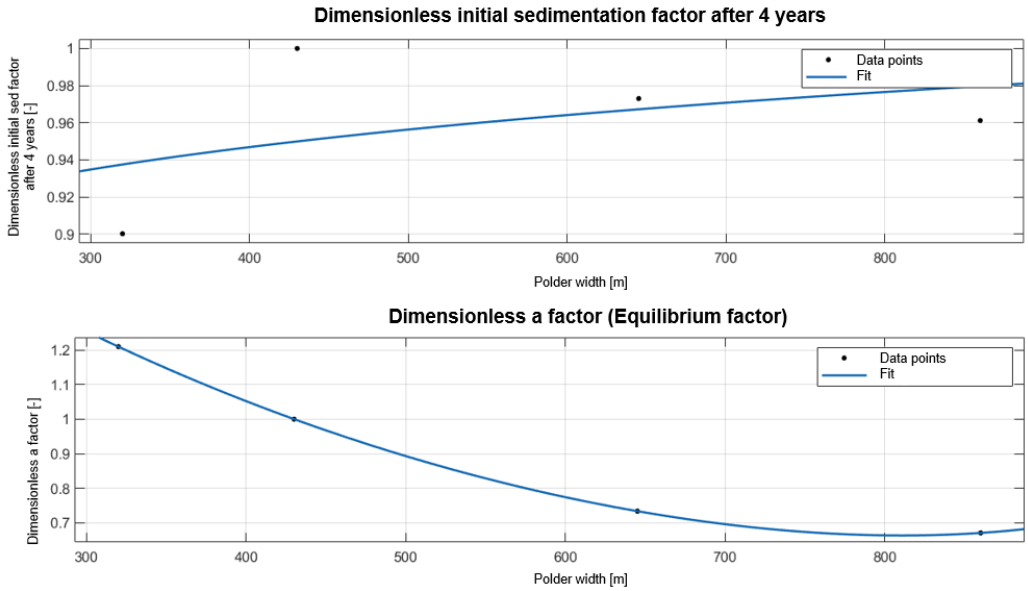

Figure D.7: Top figure: fitted formula for determining the dimensionless initial sedimentation factor for arbitrary dimensions for the polder width. Bottom figure: fitted formula for determining the dimensionless a-factor (dimensionless equilibrium factor) for arbitrary dimensions for the polder width.

E

Physical derivation of the sedimentation process within a Lease Polder

The net variation in the cumulative sediment mass within a Lease Polder can be defined by the difference in gross sediment mass input and output.

$$\frac{dM}{dt} = +S_{in} - S_{out} \tag{E.1}$$

Since the sediment mass which settles is several orders higher than in the water column, the assumption can be made that net variation in cumulative sediment mass is predominantly caused by the change in bed level z. The net variation in the cumulative sediment mass within a Lease Polder can now be rewritten to a variation in bed level multiplied by the dimensional length L and width W of the polder, and the dry bulk density of the soil ρ_d. The right-hand side can be simplified and defined as an incoming discharge Q times the incoming concentration c_{in} and an efficiency factor α. The factor α describes the trapping efficiency and would in reality be depended on multiple factors such as the depth of the polder, sediment characteristics and the internal wave energy.

$$\rho_d LW \frac{dz}{dt} = \alpha c_{in} Q \tag{E.2}$$

The assumption is made that the polder bed is moving from its initial level z_0 where the discharge is Q_0 to its equilibrium state z_{eq} where the discharge is zero. The relation between the bed level and the discharge is assumed to be linear. The discharge can now be rewritten to a dependency of the initial discharge Q_0 on the normalized ratio of the bed level relative to the equilibrium. The variation in bed level on the left-hand side can be expressed as the variation in bed level relative to the equilibrium bed level z_{eq}.

$$\rho_d LW \frac{d\left(z - z_{eq}\right)}{dt} = \alpha c_{in} Q_0 \left(\frac{z - z_{eq}}{z_0 - z_{eq}}\right) \tag{E.3}$$

With $\tilde{z}$ being the normalized bed level factor written as:

$$\tilde{z} = \frac{z - z_{eq}}{z_0 - z_{eq}} \tag{E.4}$$

Equation E.3 can now be rewritten as:

$$\frac{d\tilde{z}}{dt} = \frac{\alpha c_{in} Q_0}{\rho_d LW\left(z_0 - z_{eq}\right)}\tilde{z} = \frac{-\alpha c_{in} Q_0}{\rho_d LW\left(z_{eq} - z_0\right)}\tilde{z} \tag{E.5}$$

Setting up the integral gives:

$$\int \left(\frac{1}{\tilde{z}}\right) d\tilde{z} = \int \left(\frac{-\alpha c_{in} Q_0}{\rho_d LW\left(z_{eq} - z_0\right)}\right) dt \tag{E.6}$$

Solving the integrals results in:

$$\ln(\tilde{z}) = -t\frac{\alpha c_{in} Q_0}{\rho_d LW\left(z_{eq} - z_0\right)} \tag{E.7}$$

Rewriting to $\tilde{z}$:

$$\tilde{z} = \exp\left(-t\frac{\alpha c_{in} Q_0}{\rho_d LW\left(z_{eq} - z_0\right)}\right) \tag{E.8}$$

$\tilde{z}$ can now be expressed as the following exponential function:

$$\tilde{z} = \exp(-t/T) \tag{E.9}$$

With the time scale factor T:

$$T = \frac{\rho_d LW\left(z_{eq} - z_0\right)}{\alpha c_{in} Q_0} \tag{E.10}$$

Rewriting equation E.9 to the bed level z with $\tilde{z}$ in its original form gives:

$$z = z_{eq} + \left(z_0 - z_{eq}\right)\exp(-t/T) \tag{E.11}$$

Q_0 can now be defined as an initial average discharge relative to the initial tidal prism:

$$Q_0 = \beta\frac{LW\Delta\eta}{T_t} \tag{E.12}$$

With $\Delta\eta$ as the tidal water level range measured in the polder, T_t as the tidal time scale depending on a diurnal or semi-diurnal tide and β as a calibration factor.

Filling in the new defined Q_0 into equation E.10 gives:

$$T = \frac{\rho_d LW\left(z_{eq} - z_0\right)}{\alpha c_{in} Q_0} = \frac{1}{\alpha\beta}\frac{\left(z_{eq} - z_0\right)}{\Delta\eta}\frac{\rho_d}{c_{in}}T_t \tag{E.13}$$

Here, the timescale T is depended on the bed level difference, tidal range, tidal period and the ratio between the dry bed density and the SSC at the boundary. The α and β are the factors that are dependent on external factors.

Bibliography

Allison, S., Hardy, M., Hayward, K., Cameron, T. C., & Underwood, G. J. (2020). Strongholds of ostrea edulis populations in estuaries in essex, se england and their association with traditional oyster aquaculture: Evidence to support a mpa designation. *Journal of the Marine Biological Association of the United Kingdom*, *100*(1), 27–36.

Bakker. (2003). Een brede waterkering: van concept naar praktijk.

Bakker, J., Esselink, P., Dijkema, K., van Duin, W., & de Jong, D. (2002, 6). Restoration of salt marshes in the Netherlands. *Hydrobiologia 2002 478:1*, *478*(1), 29–51. Retrieved from `https://link.springer.com/article/10.1023/A:1021066311728` doi: 10.1023/A:1021066311728

Belzen, J. V., Bouma, T. J., & Ysebaert, T. (2020). Blue Carbon in het Verdronken Land van Zuid-Beveland. *NIOZ report*. Retrieved from `https://doi.org/10.25850/nioz/7b.b.zdoi:10.25850/nioz/7b.b.z` doi: 10.25850/nioz/7b.b.z

Boerema, A., Van Passel, S., & Meire, P. (2018, 10). Cost-Effectiveness Analysis of Ecosystem Management With Ecosystem Services: From Theory to Practice. *Ecological Economics*, *152*, 207–218. doi: 10.1016/j.ecolecon.2018.06.005

Boo, M. D. (2007). Zoetwatergetijdenatuur keert terug op Tiengemeten. *De Levende Natuur*(1), 22–26.

Bosboom, J., & Stive, M. J. (2012). *Coastal dynamics i: lectures notes cie4305*.

Camhis, M., & Coccossis, H. (1984). European maritime regions: Opportunities and dangers: A review article. *The Town Planning Review*, *55*(4), 499–505.

Chang, Y.-H., Scrimshaw, M., MacLeod, C., & Lester, J. (2001). Flood defence in the blackwater estuary, essex, uk: the impact of sedimentological and geochemical changes on salt marsh development in the tollesbury managed realignment site. *Marine pollution bulletin*, *42*(6), 469–480.

Charlier, R. H. (2002). Impact on the coastal environment of marine aggregates mining. *International journal of environmental studies*, *59*(3), 297–322.

Chauhan, P. P. S. (2009). Autocyclic erosion in tidal marshes. *Geomorphology*, *110*(3-4), 45–57.

Cheng, N.-S. (1997). Simplified settling velocity formula for sediment particle. *Journal of hydraulic engineering*, *123*(2), 149–152.

Cooper, N. J., Cooper, T., & Burd, F. (2001). 25 years of salt marsh erosion in essex: Implications for coastal defence and nature conservation. *Journal of coastal conservation*, *7*(1), 31–40.

Crowell, M., Edelman, S., Coulton, K., & McAfee, S. (2007). How many people live in coastal areas? *Journal of Coastal Research*, *23*(5), iii–vi.

Deltares. (2014). Delft3D-WAVE User Manual. *Deltares*, 1–226.

Demerbilek, Z. (2008). Water wave mechanics. *Coastal engineering manual*, *1*.

De Vriend, H., & Van Koningsveld, M. (2012). Building with nature. *Ecoshape Building with nature*.

Dillenburg, S. R., & Hesp, P. A. (2009). Coastal barriers–an introduction. In *Geology and geomorphology of holocene coastal barriers of brazil* (pp. 1–15). Springer.

Dodet, G. (2013). *Morphodynamic modelling of a wave-dominated tidal inlet: the albufeira lagoon* (Unpublished doctoral dissertation).

Elsner, P. (2009). Multi-temporal airborne remote sensing of intertidal sediment dynamics. *Remote Sensing for Environmental Monitoring, GIS Applications, and Geology IX*, *7478*(1), 74781R. doi: 10.1117/12.830672

Emmerson, R., O'Reilly-Wiese, S., Macleod, C., & Lester, J. (1997). A multivariate assessment of metal distribution in inter-tidal sediments of the blackwater estuary, uk. *Marine Pollution Bulletin*, *34*(11), 960–968.

Emmerson, R. H. C., Manatunge, J. M. A., Macleod, C. L., Lester, J. N., & Fellow, D. (1997). T i d a l Exchanges B e t w e e n Orplands M a n a g e d R e t r e a t S i t e a n d the B l a c k w a t e r Estuary , Essex. (4), 363–372.

Escoffier, F. F. (1977). *Hydraulics and stability of tidal inlets.* (Tech. Rep.). ESCOFFIER (FRANCIS F) FORT BELVOIR VA.

Esteves, L. S. (2019). *Managed Realignment : A Viable Long-Term Coastal Management Strategy?* (Vol. 53) (No. 9).

French, P. W. (1999, 1). Managed retreat: A natural analogue from the Medway estuary, UK. *Ocean and Coastal Management*, *42*(1), 49–62. doi: 10.1016/S0964-5691(98)00079-9

Fu, X., & Song, J. (2017). Assessing the economic costs of sea level rise and benefits of coastal protection: A spatiotemporal approach. *Sustainability*, *9*(8), 1495.

Ghermandi, A., & Nunes, P. A. (2013). A global map of coastal recreation values: Results from a spatially explicit meta-analysis. *Ecological economics*, *86*, 1–15.

Goudie, J. (2008). Risk Assessment of Coastal Erosion Joint Defra / EA Flood and Coastal Erosion Risk Management R & D programme. (February 2016). doi: 10.13140/RG.2.1.4240.1042

Hall, O. (2001). 4. RESULTS 4.1 Point-by-point analysis. (November 1996).

Haltiner, J., Zedler, J., Boyer, K., Williams, G., & Callaway, J. (1996). Influence of physical processes on the design, functioning and evolution of restored tidal wetlands in california (usa). *Wetlands ecology and management*, *4*(2), 73–91.

Hazelden, J., & Boorman, L. (2001). Soils and 'managed retreat'in south east england. *Soil Use and Management*, *17*(3), 150–154.

Henderson, V., Storeygard, A., & Weil, D. N. (2011). A bright idea for measuring economic growth. *American Economic Review*, *101*(3), 194–99.

Herrera-García, G., Ezquerro, P., Tomás, R., Béjar-Pizarro, M., López-Vinielles, J., Rossi, M., ... others (2021). Mapping the global threat of land subsidence. *Science*, *371*(6524), 34–36.

Huiskes, A. (1996). *Saline crops. a contribution to the diversification of the production of vegetable crops by research on the cultivation methods and selection of halophytes. ec-air-project* (Tech. Rep.). Periodic report 1/1/1996–30/6.

Huitema, T. (1947). Dijken langs zee, rivieren en kanalen. kaden om polders, droogmakerijen, enz. samenstelling, aanleg, onderhoud. *Private collection*.

Jarrett, J. T. (1976). *Tidal Prism - Inlet Area Relationships - James T. Jarrett - Google Books.* Re-trieved from `https://books.google.nl/books?=nl&lr=&id=VSycRZlMszAC&oi=fnd&pg=PA6&dq=tidal+prism&ots=zQNRZ11LdE&sig=h2icWuZtak3fAS4jJ5gRculdnZ0&redir_esc=y#v=onepage&q=tidalprism&f=falsehttps://books.google.ca/books?hl=en&lr=&id=VSycRZlMszAC&oi=fnd&pg=PA6&ots=zPTZX`

Kaneko, S., & Toyota, T. (2011). Long-term urbanization and land subsidence in asian megacities: an indicators system approach. In *Groundwater and subsurface environments* (pp. 249–270). Springer.

Kanoğlu, U., Titov, V., Bernard, E., & Synolakis, C. (2015). Tsunamis: bridging science, engineering and society. *Philosophical Transactions of the Royal Society A: Mathematical, Physical and Engineering Sciences*, *373*(2053), 20140369.

Khan, I., Hou, F., & Le, H. P. (2021). The impact of natural resources, energy consumption, and population growth on environmental quality: Fresh evidence from the united states of america. *Science of the Total Environment*, *754*, 142222.

Kiesel, J., Schuerch, M., Christie, E. K., Möller, I., Spencer, T., & Vafeidis, A. T. (2020, 9). Effective design of managed realignment schemes can reduce coastal flood risks. *Estuarine, Coastal and Shelf Science*, *242*, 106844. doi: 10.1016/j.ecss.2020.106844

Kornman, B. (2000). *Het Sieperdaschor, Tien jaar morfologische ontwikkeling.*

Kornman, B. A., & Van Doorn, K. (1997). De morfologische ontwikkeling van het Sieperdaschor tussen 1990 en 1997. , 42 pp.

Lakhan, V. C. (2003). *Advances in coastal modeling*. Elsevier.

Ledoux, L., Cornell, S., O'Riordan, T., Harvey, R., & Banyard, L. (2005). Towards sustainable flood and coastal management: identifying drivers of, and obstacles to, managed realignment. *Land use policy*, *22*(2), 129–144.

Macreadie, P. I., Anton, A., Raven, J. A., Beaumont, N., Connolly, R. M., Friess, D. A., ... others (2019). The future of blue carbon science. *Nature communications*, *10*(1), 1–13.

Marani, M., D'Alpaos, A., Lanzoni, S., & Santalucia, M. (2011). Understanding and predicting wave erosion of marsh edges. *Geophysical Research Letters*, *38*(21).

Mariotti, G., Fagherazzi, S., Wiberg, P., McGlathery, K., Carniello, L., & Defina, A. (2010). Influence of storm surges and sea level on shallow tidal basin erosive processes. *Journal of Geophysical Research: Oceans*, *115*(C11).

Masria, A., Iskander, M., & Negm, A. (2015). Coastal protection measures, case study (mediterranean zone, egypt). *Journal of coastal conservation*, *19*(3), 281–294.

McGranahan, G., Balk, D., & Anderson, B. (2007). The rising tide: assessing the risks of climate change and human settlements in low elevation coastal zones. *Environment and urbanization*, *19*(1), 17–37.

Meadowcroft, I., Morris, M., Allsop, N., & McConnell, K. (1996). *Tollesbury managed set back experiment: Breach design and construction, and embankment failure experiment*. HR Wallingford. Firm.

Miller, R. L., Fram, M., Fujii, R., & Wheeler, G. (2008). Subsidence reversal in a re-established wetland in the sacramento-san joaquin delta, california, usa. *San Francisco Estuary and Watershed Science*, *6*(3).

Moermond, C., et al. (1994). Van selenapolder naar sieperdaschor: over de ontwikkeling van een ondergelopen polder in de westerschelde. *Werkdocument RIKZ*.

Moermond, C. T. A. (1994). Van Selenapolder naar Sieperdaschor.

Neumann, B., Vafeidis, A. T., Zimmermann, J., & Nicholls, R. J. (2015). Future coastal population growth and exposure to sea-level rise and coastal flooding-a global assessment. *PloS one*, *10*(3), e0118571.

Nicholls, R. J., & Cazenave, A. (2010). Sea-level rise and its impact on coastal zones. *science*, *328*(5985), 1517–1520.

Nicholls, R. J., Hinkel, J., Lincke, D., & van der Pol, T. (2019). Global investment costs for coastal defense through the 21st century. *World Bank Policy Research Working Paper*(8745).

Nicholls, R. J., Wong, P. P., Burkett, V., Codignotto, J., Hay, J., McLean, R., ... others (2007). Coastal systems and low-lying areas.

Oevelen, D. V., Bergh, E. V. D., Ysebaert, T., & Meire, P. (2000). Literatuuronderzoek naar ontpolderingen. *Instituut voor Natuuronderzoek*.

Olsthoorn, X., van der Werff, P., Bouwer, L. M., & Huitema, D. (2008). Neo-atlantis: The netherlands under a 5-m sea level rise. *Climatic Change*, *91*(1), 103–122.

Onaindia, M., Albizu, I., & Amezaga, I. (2001, 12). Effect of time on the natural regeneration of salt marsh. *Applied Vegetation Science*, *4* (2), 247–256. Retrieved from `https://onlinelibrary.wiley.com/doi/full/10.1111/j.1654-109X.2001.tb00493.xhttps://onlinelibrary.wiley.com/doi/abs/10.1111/j.1654-109X.2001.tb00493.xhttps://onlinelibrary.wiley.com/doi/10.1111/j.1654-109X.2001.tb00493.x` doi: 10.1111/J.1654-109X.2001.TB00493.X

Price, D. C. (2016). Influence of vegetation on sediment accumulation in tidal saltmarshes : An integrated field and modelling study A thesis submitted for the degree of Doctor of Philosophy October 2016 Declaration. (October), 400.

Pye, K., French, P., Cambridge Environmental Research Consultants Ltd.(United Kingdom); Ministry of Agriculture, F., & Food, L. U. K. (1993). *Erosion and accretion processes on british saltmarshes: Volume 3-national survey of accretion and erosion status*. Cambridge Environmental Research Consultants.

Rijkswaterstaat, L. T. (1999). Technische adviescommissie voor de waterkeringen. *Delft augustus*.

Rohweder, J. J., Rogala, J. T., Johnson, B. L., Anderson, D., Clark, S., Chamberlin, F., & Runyon, K. (2008). Application of wind fetch and wave models for habitat rehabilitation and enhancement projects.

Roser, M., Ritchie, H., & Ortiz-Ospina, E. (2013). World population growth. *Our World in Data*.

Sánchez Leal, R. F., Storm, K., & Verbeek, H. (1998). Wetland Restoration: from Polder to Tidal Marsh. Hydrodynamical and morphological changes in the Sierpdaschor (SW Netherlands) after breaching of the sea wall in 1990. , 85.

Schelling, T., van der Steeg, L. J., & Leopold, M. F. (2014). Klimaatbestendige dijken, Het concept wisselpolders. *IMARES Wageningen UR*, *011*(September), 11–12.

Schjønning, P., McBride, R., Keller, T., & Obour, P. (2017). Predicting soil particle density from clay and soil organic matter contents. *Geoderma*, *286*, 83–87.

Schuttelaars, H. (2002). Vorming van estuariene troebelheidsmaxima in gedeeltelijk gemengde estuaria. *Utrecht, Universiteit Utrecht, Projectnummer DG*, *543*, 33.

Scott, C. (n.d.). *Abp marine environmental research ltd.* Retrieved from `https://www.omreg.net/query-database/226-the-saltings/`

Sheldon, R. (1968). Sedimentation in the estuary of the river crouch, essex, england. *Limnology and Oceanography*, *13*(1), 72–83.

Shepherd, D., Burgess, D., Jickells, T., Andrews, J., Cave, R., Turner, R., ... Young, E. (2007). Modelling the effects and economics of managed realignment on the cycling and storage of nutrients, carbon and sediments in the blackwater estuary uk. *Estuarine, Coastal and Shelf Science*, *73*(3-4), 355–367.

Simon, J. L. (2019). *The economics of population growth*. Princeton university press.

Small, C., & Nicholls, R. J. (2003). A global analysis of human settlement in coastal zones. *Journal of coastal research*, 584–599.

Sovacool, B. K., D'Agostino, A. L., Meenawat, H., & Rawlani, A. (2012). Expert views of climate change adaptation in least developed asia. *Journal of Environmental management*, *97*, 78–88.

Spash, C. L., & Simpson, I. A. (1993). Protecting sites of special scientific interest: intrinsic and utilitarian values. *Journal of environmental management*, *39*(3), 213–227.

Tamis, J., & Foekema, E. (2015). A review of blue carbon in the Netherlands. , 29.

Temmerman, S., Govers, G., Meire, P., & Wartel, S. (2003). Modelling long-term tidal marsh growth under changing tidal conditions and suspended sediment concentrations, scheldt estuary, belgium. *Marine Geology*, *193*(1-2), 151–169.

van Belzen. (2021). *Dubbele dijken als robuuste waterkerende landschappen voor een welvarende zuidwestelijke delta*. NIOZ Koninklijk Nederlands Instituut voor Onderzoek der Zee.

van Belzen, J., Rienstra, G., & Bouma, T. (2021). Dubbele dijken als robuuste waterkerende landschappen voor een welvarende Zuidwestelijke Delta. *NIOZ Report 2021-01* (01), 99. Retrieved from `https://doi.org/10.25850/nioz/7b.b.kb`. doi: 10.25850/nioz/7b.b.kb

Van Rijn, L. (2020). Critical bed-shear stress for mud-sand beds. (August), 1–56. Retrieved from `https://www.leovanrijn-sediment.com/papers/Threshsandmud2020.pdf`

Van Slobbe, E., de Vriend, H. J., Aarninkhof, S., Lulofs, K., de Vries, M., & Dircke, P. (2013). Building with nature: in search of resilient storm surge protection strategies. *Natural hazards*, *66*(3), 1461–1480.

Verbeek, H., & Storm, C. (2001). Tidal wetland restoration in the netherlands. *Journal of Coastal Research*, 192–202.

Verhagen, H., et al. (2005). Overtopping resistant dike, sandy dike.

Watson, S., Kritharas, P., & Hodgson, G. (2015). Wind speed variability across the uk between 1957 and 2011. *Wind Energy*, *18*(1), 21–42.

Watts, C. W., Tolhurst, T. J., Black, K. S., & Whitmore, A. P. (2003, 11). In situ measurements of erosion shear stress and geotechnical shear strength of the intertidal sediments of the experimental managed realignment scheme at Tollesbury, Essex, UK. *Estuarine, Coastal and Shelf Science*, *58*(3), 611–620. doi: 10.1016/S0272-7714(03)00139-2

Williams, P., Associates, L., & Faber, P. M. (2004). *DESIGN GUIDELINES FOR TIDAL WETLAND RESTORATION IN SAN FRANCISCO BAY.* (Tech. Rep.). Retrieved from `http://www.wrmp.org.`

Winterwerp, J., Van Kesteren, W., Van Prooijen, B., & Jacobs, W. (2012). A conceptual framework for shear flow–induced erosion of soft cohesive sediment beds. *Journal of Geophysical Research: Oceans*, *117*(C10).

Winterwerp, J. C., & Kranenburg, C. (2002). *Fine sediment dynamics in the marine environment.* elsevier.

Wolters, M., Garbutt, A., & Bakker, J. P. (2005, 5). Salt-marsh restoration: Evaluating the success of de-embankments in north-west Europe. *Biological Conservation*, *123*(2), 249–268. doi: 10.1016/j.biocon.2004.11.013

Wong, P. P. (1993). *Tourism vs environment: the case for coastal areas* (Vol. 26). Springer Science & Business Media.

Wong, P. P. (1998). Coastal tourism development in southeast asia: relevance and lessons for coastal zone management. *Ocean & Coastal Management*, *38*(2), 89–109.

Zedler, J. B., & Callaway, J. C. (1999). Tracking wetland restoration: do mitigation sites follow desired trajectories? *Restoration ecology*, *7*(1), 69–73.

Zhu, Z., Vuik, V., Visser, P. J., Soens, T., van Wesenbeeck, B., van de Koppel, J., ... Bouma, T. J. (2020, 6). Historic storms and the hidden value of coastal wetlands for nature-based flood defence. *Nature Sustainability*, *3*(10), 853–862. Retrieved from `https://www.nature.com/articles/s41893-020-0556-z` doi: 10.1038/s41893-020-0556-z